



DEGREE PROJECT IN COMPUTER SCIENCE AND ENGINEERING,  
SECOND CYCLE, 30 CREDITS  
*STOCKHOLM, SWEDEN 2017*

# **Study of neural correlates of attention in mice with spectro- spatio-temporal approaches**

**CANTIN ORTIZ**



# **Study of neural correlates of attention in mice with spectro-spatio-temporal approaches**

CANTIN ORTIZ

Master in Computer Science

Date: January 8, 2018

Supervisor: Pawel Herman

Examiner: Erik Fransén

Swedish title: En studie om neurala korrelater av uppmärksamhet hos möss med spektro-spatio-temporala tillvägagångssätt

School of Computer Science and Communication

## Abstract

While signatures of attention can be observed in widespread areas within and outside of cortex, the control of attention is thought to be regulated by higher cognitive brain areas, such as the prefrontal cortex. In their recent study on mice Kim et al. [1] could show that successful allocation of attention is characterized by increased spiking of a specific type of inhibitory interneurons, the parvalbumin neurons, and higher oscillatory activity in the gamma band in the local prefrontal network.

It was recently demonstrated that encoding of working memory in prefrontal areas is linked to bursts of gamma oscillations, a discontinuous network process characterized by short periods of intense power in the gamma band. The relationship between attention and working memory is unclear, and it is possible that these two cognitive processes share encoding principles. To address this gap, the electrophysiological data collected in the Carlén Lab have been analyzed with advanced spatio-temporal approaches.

In particular, we have analyzed bursting gamma activity in medial prefrontal cortex during attentional processing and investigated the similarities to gamma bursting observed during working memory. Gamma-band bursts during attention were reliably detected with several methods. We have characterized several features of the bursts, including the occurrence, duration and amplitude. The neuronal firing rates during and outside of bursts have also been computed. We investigated the correlation between different criteria characterizing the gamma burst and successful vs failed allocation of attention. Control data were generated to discuss the obtained results. The aim of the study was to explore the hypothesis that the medial prefrontal cortex encodes attention through gamma bursts, which could reveal some similarities and differences in coding of central cognitive processes.

No clear difference was found in the characterization between successful and failed allocation of attention. In addition, results were very similar in control set and original data. No underlying mechanism could be identified from this analysis. Therefore, as the bursts occurring in the gamma band in the prefrontal cortex (PFC) were not discriminative with respect to the different tested conditions, they do not seem to encode information related to attention.

## Sammanfattning

Även fast flera olika hjärnområdets aktivitet kan korreleras med uppmärksamhet, anses kontrollen av uppmärksamhet regleras av högre kognitiva hjärnområden, såsom främre hjärnbarken. I en nyligen publicerad artikel studerade Kim et al. [1] hjärnaktiviteten hos möss och kunde visa att en framgångsrik uppmärksamhet kännetecknas av en ökad aktivitet av en specifik typ av inhiberande nervceller, parvalbumin celler, och högre oscillerande aktivitet i gammafrekvens i främre hjärnbarkens lokala nätverk.

Det har nyligen visats att kodning av arbetsminne i främre hjärnbarken är kopplat till utbrott av gamma-oscillationer, en diskontinuerlig nätverksprocess som kännetecknas av korta perioder av intensiva oscillationer av det lokala nätverket i gammafrekvens. Relationen mellan uppmärksamhet och arbetsminne är oklar, och det är möjligt att dessa två kognitiva processer delar kodningsprinciper. För att minska detta gap av kunskap har den elektrofysiologiska datan som samlats in i Carlén Lab analyserats med avancerade spatio-temporala tillvägagångssätt.

I synnerhet har vi analyserat utbrott i gammaaktivitet i främre hjärnbarken under uppmärksamhet och undersökt likheterna med gamma- utbrott observerade under arbetsminne. Gamma-bandutbrott under uppmärksamhet påvisades på ett tillförlitligt sätt med flera metoder. Vi har karakteriserat flera funktioner hos utbroten, inklusive förekomsten, varaktigheten och amplituden. De enskilda cellernas aktivitet undersöktes även under och utanför utproten av gamma-oscillationer.

Vi undersökte sambandet mellan de olika kriterier som karakteriserar gamma-utbrott under framgångsrik mot misslyckad allokering av uppmärksamhet. Kontrolldata genererades för att diskutera de erhållna resultaten. Syftet med studien var att utforska hypotesen att den främre hjärnbarken kodar uppmärksamhet genom gamma-utbrott, vilket kan avslöja vissa likheter och skillnader i kodning av centrala kognitiva processer. Ingen klar skillnad hittades i karakteriseringen mellan framgångsrik och misslyckad allokering av uppmärksamhet. Dessutom var resultaten mycket likartade i kontrolluppsättningen och den ursprungliga datan. Ingen underliggande mekanism kunde identifieras ur denna analys. Eftersom de utbrott som uppstod i gamma-bandet i främre hjärnbarken inte var unika med hänsyn till de olika testade förhållandena, tycks de därför inte koda information relaterad till uppmärksamhet.

## Acknowledgements

Most of the work was conducted in the Carlén lab, at the Karolinska Institutet. I would therefore like to start by thanking Marie Carlén for offering me this project and for her global supervision all along the study.

As regards the day-to-day supervision, Hoseok Kim from the Carlén Lab made himself very available. I want to thank him for the time, the efforts and all the knowledge he shared with me. The project is based on the data he collected in a previous experiment and that he kindly provided to me.

From KTH, I am very grateful to Pawel Herman for his supervision, relevant advice and the feedback he provided all along this study.

I also would like to thank Erik Fransén, my examiner, who took time to discuss the project and to propose new approaches from a different perspective.

Among PhD students of the Carlén Lab, Sofie Ährlund-Richter nicely helped me to translate the abstract in Swedish, tack så mycket för det.

And then on the overall, a big thank you to the rest of the DMC crew. They really gave me a warm welcome when I joined, and from students to principal investigators, they made this work not only a formative scientific training but also a very nice human experience. Merci à Nicolas et Pierre, helping me to bring the Frenchness into the lab. Thanks to the barbecue and meme master Leonardo for initiating me to the picanha. Cheers to Janos and Moritz for the foosball games, everything is about randomness and power. I owe a lot to Iakovos, Mikael and Hans, always there to help me to fix my bike after my adventures, and to Muhad who has proven himself to handle power tools like a pro. I want to apologize to Eleana, Erianna and Michał for all the French rap you had to endure, maybe you will appreciate it someday. Toda Maya for the chocolatinas, I am sure we will find the best French bakery in Stockholm. Dank je Josina and xiexie Yang, I managed to accomplish sort of progress in Dutch and Chinese thanks to you. Skål to Naz, Chase and Chrysiida, my fellow students for the first semester. Rania, I am glad that you enlightened me on how great caretta caretta are. Dinos and Antje, I am looking forward to working with you. Thank you also to all the others that I have not quoted yet but I had the chance to meet during this work: Marc, Laura, Xinming, Daniel and Caro. Finally, thanks to my girlfriend for her moral support all along this work.

## Acronyms

**3-CSRTT** three-choice serial reaction time task.

**5-CSRTT** five-choice serial reaction time task.

**ADHD** attention deficit hyperactivity disorder.

**ANOVA** analysis of variance.

**CV<sub>2</sub>** coefficient of variance.

**EEG** electroencephalography.

**FFT** fast Fourier transform.

**fMRI** functional magnetic resonance imaging.

**FS-PV** fast-spiking parvalbumin.

**KW** Kruskal–Wallis.

**LFP** local field potential.

**MAD** median absolute deviation.

**MWW** Mann–Whitney–Wilcoxon.

**NHP** non-human primates.

**p-value** probability value.

**PET** positron emission tomography.

**PFC** prefrontal cortex.

**RMS** root mean square.

**SEM** standard error of the mean.

**SPECT** single-photon emission computed tomography.

**STD** standard deviation.

**TMS** transcranial magnetic stimulation.

**VNS** vagus nerve stimulation.

# Contents

<b>Contents</b>	<b>v</b>
<b>1 Introduction</b>	<b>1</b>
1.1 Current knowledge and related studies . . . . .	1
1.2 The project . . . . .	2
1.2.1 Problem identification and formulation . . . . .	2
1.2.2 Goals and delimitations . . . . .	3
<b>2 Background</b>	<b>4</b>
2.1 Attention in neuroscience . . . . .	4
2.2 Gamma activity during attention tasks . . . . .	6
2.3 Bursts analysis during working memory tasks . . . . .	7
<b>3 Methods</b>	<b>9</b>
3.1 Electrophysiological data . . . . .	9
3.1.1 Experimental protocol . . . . .	9
3.1.1.1 Study presentation . . . . .	9
3.1.1.2 Experimenting on animals . . . . .	9
3.1.1.3 Attention task . . . . .	11
3.1.1.4 Tetrodes recordings . . . . .	12
3.1.2 Signals . . . . .	12
3.1.2.1 Splitting local field potential (LFP) and spiking activity . . . . .	12
3.1.2.2 Dataset summary . . . . .	13
3.2 Extracting gamma activity . . . . .	13
3.2.1 Selecting signals . . . . .	14
3.2.1.1 Time period . . . . .	14
3.2.1.2 Frequency band . . . . .	15
3.2.1.3 Quality of signals . . . . .	16
3.2.1.4 Recap of selection process . . . . .	16
3.2.2 Band-pass filtering approach . . . . .	17
3.2.2.1 Filter choice . . . . .	17
3.2.2.2 Hilbert transform . . . . .	18
3.2.2.3 Edge margin . . . . .	19
3.2.3 Alternative methods . . . . .	20
3.2.3.1 RMS . . . . .	21
3.2.3.2 Spectrogram . . . . .	22
3.3 Burst detection . . . . .	23

3.3.1	Variation of signal in time . . . . .	23
3.3.1.1	During the attention period . . . . .	24
3.3.1.2	Over recording time . . . . .	24
3.3.1.3	Criterion choice . . . . .	25
3.3.2	Threshold method . . . . .	26
3.3.2.1	General formula . . . . .	26
3.3.2.2	Bursts characteristics . . . . .	26
3.3.2.3	Outliers treatment . . . . .	28
3.4	Further burst analysis . . . . .	30
3.4.1	Trial to trial burst patterns . . . . .	30
3.4.1.1	Bursts as a binary process . . . . .	30
3.4.1.2	Pairwise analysis . . . . .	31
3.4.1.3	Cross-correlation . . . . .	31
3.4.1.4	Burst overlapping . . . . .	31
3.4.2	Spiking activity . . . . .	32
3.4.2.1	Neurons classification . . . . .	32
3.4.2.2	Computing instant spiking frequency . . . . .	32
3.4.3	Surrogate dataset . . . . .	33
3.4.3.1	Utility . . . . .	33
3.4.3.2	Generation . . . . .	34
<b>4</b>	<b>Results</b>	<b>36</b>
4.1	Fixing parameters . . . . .	36
4.1.1	Principle . . . . .	36
4.1.2	Characterization function of threshold coefficient . . . . .	36
4.1.2.1	Number of bursts . . . . .	36
4.1.2.2	coefficient of variance ( $CV_2$ ) . . . . .	37
4.1.2.3	Relative amplitude . . . . .	38
4.1.2.4	Duration and interburst interval . . . . .	38
4.1.2.5	Final value . . . . .	39
4.2	Characterization . . . . .	39
4.2.1	Distribution across tetrodes . . . . .	39
4.2.2	Averaged values . . . . .	39
4.3	Comparison with surrogate dataset . . . . .	40
4.4	Influence of outliers on the characterization . . . . .	42
4.5	Comparison between trial types . . . . .	43
4.6	Trial to trial burst patterns . . . . .	46
4.7	Spiking activity . . . . .	47
<b>5</b>	<b>Discussion</b>	<b>50</b>
5.1	Key findings . . . . .	50
5.2	Methodology . . . . .	51
5.3	Is it bursts that were detected? . . . . .	52
5.4	Limitations . . . . .	53
5.5	Ethics and sustainability . . . . .	54
<b>6</b>	<b>Conclusion</b>	<b>55</b>

<b>Bibliography</b>	<b>56</b>
<b>A Experimental setup</b>	<b>64</b>
<b>B Signal analysis</b>	<b>65</b>
<b>C Supplementary results</b>	<b>68</b>



# Chapter 1

## Introduction

### 1.1 Current knowledge and related studies

The brain is a complex organ about which the current scientific knowledge is still very incomplete. It is a gigantic network of neurons. The human brain is for instance estimated to be made up of 15 to 30 billion neurons [2] which are highly interconnected, 100 trillions synapses linking them together [3]. And even though each individual neuron can only accomplish quite basic computational operations, the whole network makes it possible for animals and especially humans to develop advanced capabilities.

Among our many skills, we are able to acquire and use knowledge. All the processes linked to this ability are part of cognition. It consists for instance in treating accessible information in order to extract meaningful elements. This requires to make a selection to focus only on what is relevant. This cognitive mechanism is referred to as attention: if a stimulus is considered useful, then it is emphasized; otherwise, if it is either distracting either irrelevant, it is suppressed [4]. A deficit in attention is observed in several diseases such as schizophrenia [5, 6, 7] or autism spectrum disorder [8]. It makes attention particularly interesting, as understanding the underlying mechanisms might lead to new treatments in the future.

Several methods have been used in science in order to correlate behavior with brain activity. When a macroscopic overview is sufficient, neuroimaging is an effective and non-invasive way to correlate brain areas with a cognitive task. In the literature, positron emission tomography (PET) [9], functional magnetic resonance imaging (fMRI) [10] or single-photon emission computed tomography (SPECT) [11] are widely used. Another approach consists in observing the brain at the mesoscopic scale. In that case, the focus is put on networks and neuron level correlates of behavior. This typically involves electrophysiology, which is based on measuring the electrical properties of neural cells and tissues. Indeed, electric fields are generated in the cortex because of the electrical activity occurring in neurons and synapses. They can be recorded by placing an electrode on the scalp in the case of electroencephalography (EEG), or in the brain for recording local field potential (LFP). The recorded voltage usually presents oscillatory patterns at different frequency scales.

While signatures of attention can be observed with many methods in widespread areas within and outside of cortex, the control of attention is thought to be regulated by higher cognitive brain areas such as the PFC [12, 13]. Studies also linked attention to oscillatory activity of the LFP in the gamma band [14, 15, 16, 17, 18, 19, 20] (30-100 Hz). In

the recent study on mice by Kim et al. [1], the Carlén group showed that successful allocation of attention is characterized by increased spiking of a specific type of inhibitory interneurons, the parvalbumin neurons, and a higher oscillatory activity of the local field in the gamma band in the local prefrontal network. These results are consistent with previous work [21]. However, we still lack understanding of relationship between spiking activity of individual neurons and discrete oscillatory burst events observed in the extracellular space (local fields) in processes underlying attention in the local prefrontal circuit. Therefore, further investigations need to be conducted.

It is indeed quite common to observe short periods of intense activity called bursts when studying gamma oscillations [22, 23, 24], but their functional role and dynamical interpretation are still under investigations. Lundqvist et al. [25] showed that gamma power is increasing with memory load in an attractor network model. They then went further and researched these power variations in biological recordings. In a noteworthy study [26], they established a link between the cognitive process of working memory and bursts of gamma oscillations in the PFC. Based on these elements, their study proposed a new perspective on working memory. Thanks to single neuron analysis instead of typical averaging of neural data over trials and/or electrodes, Lundqvist et al. [26] concluded that working memory would actually be a discrete process rather than being coded by sustained activity, bursts being the manifestation of discrete memory loads.

This result is very important as it goes against the most commonly adopted theory in the last decades of working memory that presumes persistent neural activity as the hallmark and mechanism of memory maintenance[27]. Working memory has been thought to result from a very sustained activity in higher-order cortical areas such as the PFC. This has been supported by numerous studies originating as early as in 1970s [28] and continuing until now [29, 30].

## 1.2 The project

### 1.2.1 Problem identification and formulation

As mentioned in section 1.1, gamma oscillations in the PFC are strongly believed to correlate with the cognitive process of attention allocation. Kim et al. [1] observed increased gamma power in successful allocation of attention, but the origin of this fast oscillatory activity is still unclear. In several studies, bursts were observed in the gamma activity [22, 23, 24]. They have recently been related to encoding and decoding of working memory [26], which has even led to proposing a new point of view on the mechanisms behind this cognitive function. Based on this knowledge, the possibility that attention allocation might be linked to bursts in the gamma band is worth an investigation. Bursting phenomenon could explain the observed increase of gamma band power in the PFC because periods of intense activity would increase the overall power, and also be a correlate of neural mechanism underlying the allocation of attention.

Therefore, this study tackles the following question: does bursting gamma oscillatory activity occur in the PFC during attention, and if so does the modulation of bursts reflect any distinct and behaviorally relevant aspect of cognition such as a reduced attention span?

### 1.2.2 Goals and delimitations

The main project goal is to re-analyze electrophysiological data which were collected in an attentional task by the co-supervisor, Dr. Hoseok Kim, in the Carlén lab, in relation to the findings in Lundqvist et al. [26]. As all the data were already collected before, there is no need for conducting any new experiment.

The first step is to develop a reliable method for detecting gamma bursts. Several possibilities are presented in the literature. They shall be investigated and adapted to the dataset in order to decide which one is the most suitable.

Then, quantitative measures should be defined in order to characterize the gamma bursts. As we are looking for an increased power, the occurrence - number of bursts per second - and duration of bursts seem to be the two most relevant characteristics. Because of the stronger activity, it is expected to find in correct trials either more bursts, either an higher duration, either both. However, other aspects such as amplitude, distribution or correlation between bursts might also give interesting results and could be analyzed.

During the initial study, a significant difference in the spiking activity of a specific type of interneurons, the Fast Spiking Parvalbumin (FS-PV), was found between correct and failed allocation of attention. Also, in Lundqvist et al. [26], bursts were linked to an increased spiking activity of specific neurons. Therefore, it seems relevant to analyze how fast-spiking parvalbumin (FS-PV) neurons behave during gamma bursts. The expected outcome is to find correlated patterns between gamma bursts and single neuron spiking during attention.

The study outcome will determine whether there is any convincing correlation between gamma bursts and attention allocation. It will also be possible to compare the bursts observed during attention with those described in literature during other tasks, especially during working memory.

# Chapter 2

## Background

### 2.1 Attention in neuroscience

Attention is a fundamental cognitive process when it comes to organizing thoughts and acting in a meaningful manner. It is the ability to focus on necessary information while ignoring anything superfluous. In everyday life, many examples can illustrate this mechanism. For instance, somebody reading a book in public transportations will not hear surrounding conversations, as otherwise he could not integrate properly the content of the text. He might even miss his stop if he is too deeply focus, as every information not related to the reading would be suppressed, including visual or audio hints about the proximity of the station. Two main functions of attention are usually distinguished in neuroscience. The top-down attention is goal-driven and under direct control of the individual who decides to focus on specific stimuli. The bottom-up attention, also known as stimuli-driven, is induced by an intense stimulus such as a loud noise or a flash and attract the attention without anticipating it [31, 32].

Because attention is a central component for cognition, an improper functioning of this process can strongly decrease the quality of life. Attention deficit is the main symptom of attention deficit hyperactivity disorder (ADHD) [33], a mental disorder which can be a real impairment in modern society and is characterized by difficulties to pay attention, impulsive behavior and excessive activity. Attention impairment is also observed in many common diseases such as Alzheimer [34], Parkinson [35], schizophrenia [5, 6, 7] or autism spectrum disorder [8]. Identifying the mechanisms underlying attention would be of great use for developing new treatments. This knowledge could be applied in psychopharmacology, in order to design drugs with very specific targeting [36, 37]. It would also improve therapies based on directly stimulating the brain, such as vagus nerve stimulation (VNS) therapy and transcranial magnetic stimulation (TMS) [38].

Attention can be studied through many approaches. For this work, a neuroscience perspective was chosen. It consists in studying the process by analyzing the nervous system, which is the network formed by all nerves and nervous tissues together. In brief, the nervous system is split in two parts. The peripheral nervous system essentially relays information, while the central nervous system integrates and commands most of the body. It contains the majority of the nervous system and especially the brain, which can be split into different areas (lobes, Brodmann, etc.) based both on anatomical and functional properties. Among other, the prefrontal cortex (PFC) is a well studied area. It is the cerebral cortex covering the front part of the front lobe (figure 2.1). It is well known

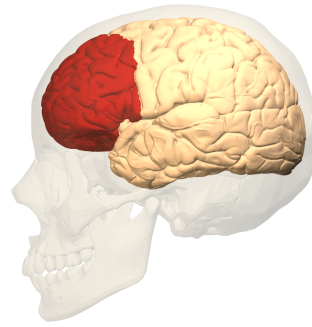


Figure 2.1: Schematic view of the PFC in human, in red (mid-sagittal section). Taken from Database Center for Life Science (DBCLS), under the license CC BY-SA 2.1 JP

for being involved in decision making [39], planning [40], execution of complex cognitive tasks [41], social behavior [42] and personality [43]. On the overall, it is essential for goal-oriented behavior [44], and in particular the PFC seems to have a crucial role for regulating the control of attention [45, 46]. Therefore, this study focuses only on the neural manifestations of attention in the PFC, omitting activity occurring in other part of the nervous system.

In order to study a cognitive process such as attention, the common practice in neuroscience is to design a test requiring attention and in which the quality of attention allocation can be evaluated or quantified from the compartment. This can be for instance by looking at a reaction time, the success or failure of a task, the time spent doing a specific behavior [47, 48], etc. Several experiments can be done based on this test. First, it is possible to look for a correlation between the activity of the nervous system and the attention level. The activity can be captured through several techniques including neuroimaging or signal recording. When doing electroencephalography, tetrodes are placed on the scalp to record voltage. Electrocorticography is more invasive and consists in recording inside the brain by inserting electrodes under the skull, but it usually provides more accurate data such as the local field potential (LFP). When several electrodes are placed very close to each other, it is possible to isolate the activity of single neurons (see 3.1.1.4 for more details about this procedure). A second approach consists in altering the functioning of some specific elements of the cortex which are believed to play a role in attention, and then observe the influence on task execution. This can be accomplished in many ways, including pharmacology when injecting drugs [49], optogenetics for targeting specific group of neurons [50] or surgery for whole brain parts [51].

The neuroscience knowledge of attention is still sparse. Desimone and Duncan [4] proposed that when it comes to sensory inputs, different pathways with different information compete using mutual inhibitory interactions. Attention would be a way to select one of these pathways according to what we decide to focus on. Thanks to a top-down control believed to mainly occur in the PFC, excitatory signals introduce a bias toward neurons representing to-be-attended features. This makes them more likely to win and remain active, establishing a pathway where information expected to be important is transmitted.

Miller and Cohen [12] went deeper and presented an integrative theory of the PFC function. The PFC would exert cognitive control by maintaining actively patterns of ac-

tivity representing goals and means to achieve them. These patterns would be used to introduce a bias in neural pathway, in order to establish the proper mapping in the neural net between input, internal functions and outputs required to achieve a specific task. This can be any sensory input, but also response execution, memory retrieval, emotional evaluation etc. Attention would only correspond to the case where the bias is relative to information, exactly as in Desimone and Duncan [4]. But with this theory, it becomes only one facet of a more global mechanism.

Several processes could explain the change of connectivity in the whole network. Because of the quickness with which changes appear, this is most likely not linked to any anatomical evolution. The main mechanism at the network level seems to be synchrony. It was shown that increasing inputs synchrony to a single neurons does not influence the output in a linear way, but has instead a super-additive effect [52]. Therefore, increasing synchrony in a group of neurons would strongly change their downstream impact. A study by Fries et al. [53] corroborates this hypothesis. They put in evidence that during visual attention, neural synchrony increases in the gamma band while decreasing in lower frequencies such as delta and theta band, in a specific neural population coding for the attended visual location. Synchrony was also observed across region in various studies [54, 55]. It puts the neurons in these regions into co-excitabile state, which boosts connectivity [56].

On the neural level, other mechanisms are involved. During spatial attention, neurons present an increased response to stimulus if their receptive fields are in attention focus [57]. Attention can also increase the sensitivity of neurons to stimulus [58], which improves behavior performance [59]. Other effects of attention on neurons were also put in evidence, such as decreasing noise correlation to increase the information capacity of a population [60] or resolving competition between stimuli [61].

## 2.2 Gamma activity during attention tasks

Electrophysiology is an effective way when it comes to understanding neural activity. The local field potential (LFP) is a measure, at a specific spatial location in the tissue, of the voltage related to neighboring electric current flows from neurons firing. It gives a representation of the overall activity in the neurons surrounding the electrode. The LFP is a continuous signal from which different frequency components can easily be extracted. LFP dynamics normally range from 0.1 to 100 Hz. This means that at the LFP time scale, single neuron recordings can be simplified as a binary process "firing or non-firing". Indeed, the basic dynamic of a single unit is the action potential whose duration is around a few milliseconds, making it instantaneous when compared with LFP fluctuations.

The different frequency components from a LFP signal are commonly split in bands, each band being associated with a specific kind of activity. However, the boundaries are arbitrary and the band delimitations are based on an usual agreement, often depending on the studied species. The gamma band corresponds to frequencies ranging from 25 Hz to 100 Hz, typically around 40 Hz, and is particularly interesting when it comes to attention.

Several studies proved that the gamma band is involved in sensory inputs. Stimulus-specific gamma oscillatory activity was observed in both anesthetized [62] and awake animals [63]. However, it was also observed in more advanced functions. Tallon-Baudry

and Bertrand [64] demonstrated that gamma oscillations have a crucial role in object representations, which is based on sensory information. Gamma role in cognitive processes was underlined at several occasions, in particular for working memory [65, 66] and attention [67, 20].

More precisely, Gregoriou et al. [68] showed that attentional processing leads to an increase activity in the gamma band of the prefrontal areas. Kim et al. [1] made further investigations and found that not only gamma oscillations are essential in the control of attention, but also that the signal power is slightly but significantly stronger when allocation of attention is successful than when it is failed.

## 2.3 Bursts analysis during working memory tasks

The central nervous system generates neural oscillations both at neuron and network levels. As regards neurons, they can fire rhythmic patterns of action potentials [69] and membrane can follow oscillatory variations [70]. When observing the network, synchronized activity of large number of neurons can induce oscillations at macroscopic scale [71]. These oscillations can be captured by extracellular recordings such as EEG or LFP.

Sometimes, oscillations get higher amplitudes and frequencies, which gives raise to periods of short but intense activity known as bursts. They can be observed in some frequency bands of the LFP during cognitive processes such as attention, as presented in section 1.1. This phenomenon, was deeply studied by Lundqvist et al. [26] for working memory, a cognitive process that makes it possible to temporarily hold information before its use. In that case, the bursts analysis led to proposing a new point of view about how working memory works.

Until now, there was a strong consensus in favor of working memory being based on sustained neurons spiking. The mechanism was supposed to be very simple: some event that needs to be remembered starts a spiking activity that is maintained until the information is needed [72]. This can be modeled by an attractor network, in which the information is held in a persistent state corresponding to a dynamic attractor. The state is supported by recurrent connections which sustain the pattern of activity. Therefore the information is lost if activity is interrupted [73]. Several studies in the last years underlined problems with this theory, especially as regards the behavior of individual neurons. Most of them show brief bouts of activity [74], which is not coherent with the sustained spiking theory but suggests instead an highly dynamic activity [75].

Alternative attractor models based on changing the synaptic plasticity of recurrent connections offer interesting features. In this simulation, states correspond to expression of the information instead of being the information itself. Spiking activity is only required during the short lifetime of state, i.e. when replaying stored information [76]. This method is more energy efficient because it requires less spikes. In addition, it is very effective for storing multiple items without perturbations. The relevance of these networks for modeling working memory is supported by analysis in which known biological constraints were added to it [25]. The model predicted that memory load would correlate with bursts of gamma oscillations. These bursts were indeed observed in monkeys [26], giving strong support in favor of the intermittent replay theory.

When it comes to attention, the continuous or discrete nature of this process is still very unclear. When studied as a behavior, it seems to be a continuous focus on something. However, when looked at in terms of neural activity, several studies [77, 78] present

evidence in favor of a discrete model. Busch and VanRullen [79] revealed for instance that performance for attended stimuli fluctuated around 7 Hz (theta band) while for unattended stimuli it does not, thereby supporting the idea of periodic attention.

Even though no direct link can be established at the moment between working memory and attention, these abilities share some similarities. Both of them are important cognitive processes when integrating sensory inputs, attention being linked to selection while working memory makes storage possible. Moreover, working memory was also related to sustained activity in the PFC [80], the same specific brain area as attention. Finally, the discrete or continuous nature is still in debate for both of them. The possibility that they are based on the same underlying mechanisms such as bursts is therefore worth investigating.

# Chapter 3

## Methods

### 3.1 Electrophysiological data

All the data used in this thesis were retrieved during the study presented in Kim et al. [1]. I did not personally gather the data, I only did analysis and did not take part in the work presented in section 3.1. However, understanding the project requires to know the methods and the reasons of this data collection.

#### 3.1.1 Experimental protocol

##### 3.1.1.1 Study presentation

This study focuses on the control of attention. Two main results are presented. First, it confirms the importance of gamma oscillations in the control of attention. But mostly, it reveals the central role of a particular type of inhibitory interneuron in the PFC, the FS-PV neurons.

During this study, two main methods were applied. As regards data collection, electrophysiology was used to gather information about neural activity. To control and modulate the activity of specific neuron groups, optogenetic manipulations were practiced.

For detection and characterization of gamma bursts, only data relative to natural neural activity was analyzed. Therefore, despite the very broad possibilities it offers, optogenetics will not be treated in this paper. Interested reader might refer to Fenno et al. [81] for a proper introduction about this recent technology.

##### 3.1.1.2 Experimenting on animals

In neuroscience, experimenting is extremely difficult. Because of the complexity and very incomplete understanding of the nervous system, there is usually no effective alternative to conducting experiments on living organisms at the moment in neuroscience.

Even though the human brain is by far the most advanced brain known to exist, and the most interesting one to understand as regards medical treatment, it is unacceptable to conduct invasive experiments on humans for obvious ethical reasons. Therefore, most of experiments are done on animals according to a very strict ethical code.

A lot of animal species can be used in neuroscience according to the experiment requirements. A very important group is called non-human primates (NHP). The main interest of working with monkeys is that they share a lot of similarities with humans,

especially when it comes to brain functions and anatomy. They are able to accomplish advanced tasks and to understand more complex protocols than any other animals. A lot of studies about social behavior, face recognition, mental illness or language can exclusively be conducted on NHP. They usually produce brain signals of very high quality.

However, NHP present a lot of cons. It can be difficult to handle them, making it necessary to use some physical and chemicals restraining methods [82]. They are also among the most expensive animals for experimenting, both in buying and maintenance costs. This reduces substantially the number of subjects that laboratories can afford. Usually, only one female and one male animals are used in order to avoid a potential sexual bias. Training is longer compared with most of other animals and NHP can be very sensitive to a change of carer. Also, breeding lineage of genetically modified animals is a very common practice in neuroscience to specifically identify and manipulate neurons and circuit types. But the current knowledge about NHP genomes is incomplete. Combined with the fact that monkeys reproduce slowly, it makes it almost impossible to work with genetically modified primates. Most of all, there are very big ethical concerns in the use of NHP. Even though the strong brain similarities that monkeys share with human "has scientific advantages, it poses some difficult ethical problems, because of an increased likelihood that primates experience pain and suffering in ways that are similar to humans." [83]

An opposite approach is to experiment on more basic organisms such as the lamprey, fruit fly or the zebra fish. They present several interesting properties such as rapid development, easy genetic manipulations or cheap prices and easy maintenance. The zebra fish has a high physiological and genetic homology to mammals. In addition, embryos are transparent, which is extremely convenient for observations [84]. The small size of its brain enables exhaustive measurements of neuronal activity patterns [85], which is very useful to understand the neural mechanisms underlying higher brain functions. Because of their basic brain capabilities, using them in experiments raises fewer ethical concerns than with more advanced animals. However, brain abilities limitation is also the main problem with these organisms. Even though training is possible through conditioning [86], it cannot go further than basic tasks. Only extremely simple brain functions such as motor behavior can be studied with these animals.

Finally, some intermediate strategy is to work on rodents, especially on mice and rats. They are mammals which are relatively close to humans. Most of human brain areas have their equivalent in both species. Rodents exhibit many of the brain functions that exist in humans, including social skills. They can be trained to accomplish behaviors that quantify the effectiveness of these functions such as attention, working memory, aggressiveness, etc. They are cheap, easy to breed and genetically well known which make them very convenient for creating genetically modified lineage. However, they cannot accomplish as advanced functions as monkeys. Recordings of brain signals are also usually not of the same quality as the one you could obtain with NHP.

Effective tests exist on rodents for quantifying attention which makes resorting to monkeys unnecessary. However, there is no satisfying method to study this cognitive process on basic organisms. Therefore rodents were used in Kim et al. [1]. Mice were preferred to rats. The main reason is that the genetic toolbox is more developed for mice, even though rats tend to catch up since a few years [87]. Other arguments are that mice are smaller, easier to handle and more adapted to optogenetics. They are usually more active, therefore it is possible to record more trials. They are also stronger and re-

cover quickly from implant surgery.

All animal handling was done according to the Guidelines of the Stockholm municipal committee for animal experiments.

### 3.1.1.3 Attention task

An important part of the experiment consists in designing a task for testing attention. Various tests have been proposed in literature. They offer different approaches which range from observing unconditioned behavior to cue detection of visual targets [47]. On rodents, the five-choice serial reaction time task (5-CSRTT) is a widely used cue based test for sustained attention [88, 89] with a high construct validity [90]. The 5-CSRTT is commonly declined in different versions with two to nine choices.

In Kim et al. [1], it was decided to use a variant of the 5-CSRTT. Mice usually learn slower than rats, making the conditioning for 5-CSRTT long, while it does not seem to improve significantly the test quality. An odd number of choices being more popular and supported by literature, the three-choice serial reaction time task (3-CSRTT) was chosen.

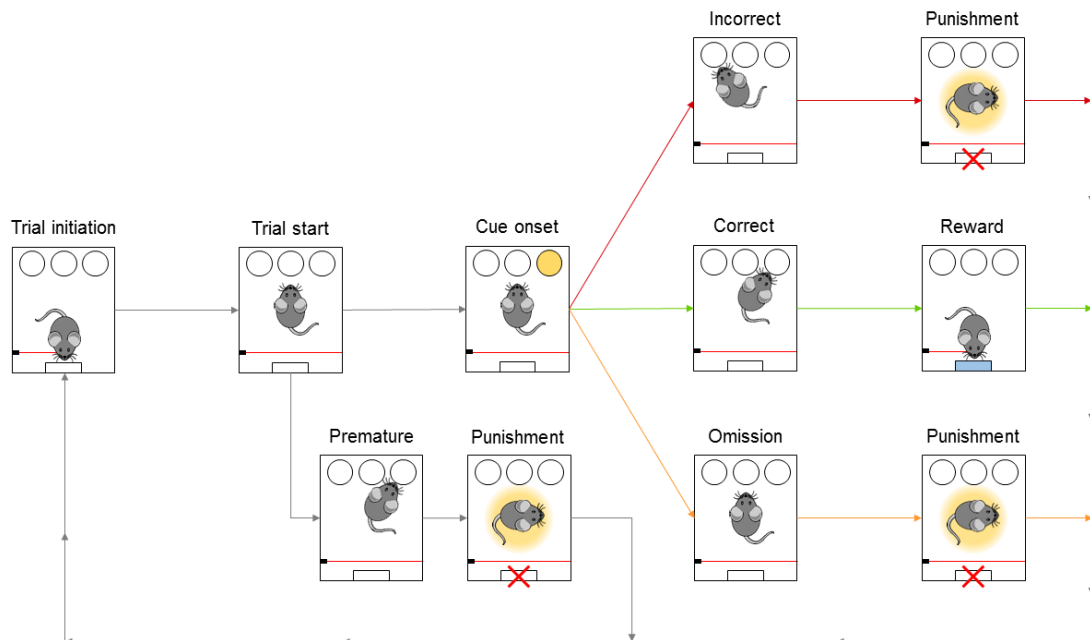


Figure 3.1: Schematic representation of the 3-CSRTT for fully trained animals; inspired by Kim et al. [1]. After trial start, if the animal pokes a hole before cue onset, the trial is considered premature which leads to punishment. If the animal waits for the cue, it can either poke the proper hole (correct in green, lead to reward), the wrong one (incorrect in red, lead to punishment) or not push any hole in the 5 seconds period (omission in orange, lead to punishment). New trial is then initiated.

The mouse is placed in an operant chamber with nine holes in the front wall, out of which three are used. The whole process is automatized and does not require any human interaction except for starting and ending the experiment. The animal interacts with these three holes by nose poking into them. This is captured by infrared sensors. The animal also interacts with a reward port from which it gathers its reward. An infrared photobeam captures both entrance and exit of the animal from the port.

Trial is initiated by the animal approaching the reward port, breaking the photobeam. Trial starts when the animal turns back to watch holes, reconnecting the photobeam. After a random delay of 3,4 or 5 seconds, the cue is briefly presented for one second through lightning of a diode inside one of three holes randomly picked. The animal then has 5 seconds to nose poke the correct hole. If it manages, it gets a reward (15% sucrose solution) and can initiate a new trial. If it fails by nose poking the wrong hole, omitting to nose poke a hole during these 5 seconds or nose poking before cue onset, the trial is failed. A strong light is emitted for 5 seconds as a punishment before a new trial can be started (figure 3.1).

Animals were conditioned for this task by going through six different levels of increasing difficulty (figure A.1). They were considered fully trained when reaching at least 80% accuracy for the final task. With this setup, attention is sustained in the period between the trial start and the cue onset.

#### 3.1.1.4 Tetrodes recordings

Neural signals were recorded using tetrodes that were inserted into mice brains. Each tetrode is made of four fine wires (12  $\mu\text{m}$ ) which are twisted together. The point of using four individual electrodes combined together as one tetrode is to identify single neurons from their firing activity. Indeed, each electrode is at a different spatial location, but still very close to the three others. Therefore, surrounding action potentials are usually detected in the four channels of the tetrode but with different amplitudes because of the slightly different position. Proper analysis then makes it possible to identify the firing activity of several individual neurons.

In order to keep tetrodes inside the brain, the flexDrive was used [91]. It is a small (about 2 cm high for a 1.5 cm diameter) and light (2 g) device in which four tetrodes are loaded before being fixed on the skull during a surgery. This is a long term setup that normally end-up being integrated by the rodent (see appendix figure A.2). Therefore, recordings can be performed on a long period. Also, this system allows to move tetrodes deeper each day, making it possible to record from slightly different spatial locations in the brain every time. During experiments, the flexDrive was connected to the Digital Lynx 4SX acquisition system and data was retrieved with the Cheetah data acquisition software at a 32 kHz sampling frequency.

### 3.1.2 Signals

#### 3.1.2.1 Splitting LFP and spiking activity

For each tetrode, the Cheetah acquisition provides a signal for every four electrodes. This signal is mixing several phenomena happening at different time scales. While action potential occurs at high frequency, the LFP dynamics are much slower.

The first step is to split these two distinct activities through filtering. Because the four electrodes of a tetrode are very close to each other, the LFP is almost identical in the four of them. Therefore, the LFP is extracted only from one electrode for the whole tetrode. It is obtained by applying a band-pass filter to select low frequencies, between 0.1 Hz and 500 Hz. As its dynamics are relatively slow, it is down sampled by a factor 32 at 1 kHz.

The individual neuron spiking trains are extracted by first band-pass filtering the high frequencies of the signal, between 600 Hz and 6000 Hz (figure 3.2). Then, single units

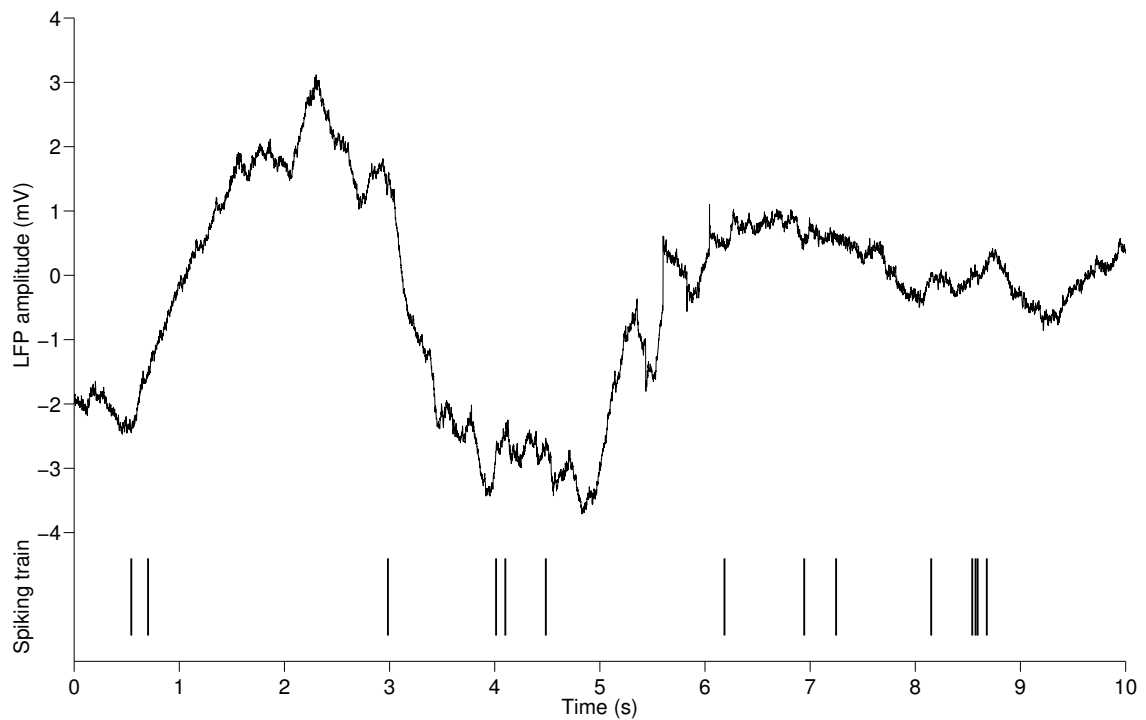


Figure 3.2: Example of LFP and spiking train during 10 s of recording. On the top, the LFP. On the bottom, the spiking train of a single neuron. Firing action potential is considered as a binary process.

are identified by using the MClust offline sorter from A.D. Redish on the four signals of a tetrode.

### 3.1.2.2 Dataset summary

Three fully trained implanted animals were used for the experiment. During each recording session, about 64 to 100 trials of the 3-CSRTT were performed by an animal. The same animal could only go through a recording session once a day. On total 54 sessions were recorded: 25 with animal *A5G1*, 23 with *A1G2* and 6 with *A3G2*.

For each session, 4 tetrodes recordings are available. Each recording is made of 4 signals from the electrodes. One LFP is extracted per tetrode, meaning that on the overall there are  $54 * 4 = 256$  LFP available. One high frequency signals is extracted per electrode, resulting in  $54 * 4 * 4 = 864$  signals. After units sorting, 476 single neurons in 148 tetrodes are identified from these signals. In 68 tetrodes, the signal was not good enough to identify any neuron (figure 3.3).

## 3.2 Extracting gamma activity

As explained in the previous section, two types of data are available after preliminary treatments: LFP and spike trains. However, bursts are studied specifically during attention and in the gamma band. Thus, it is first required to process the data into a represen-

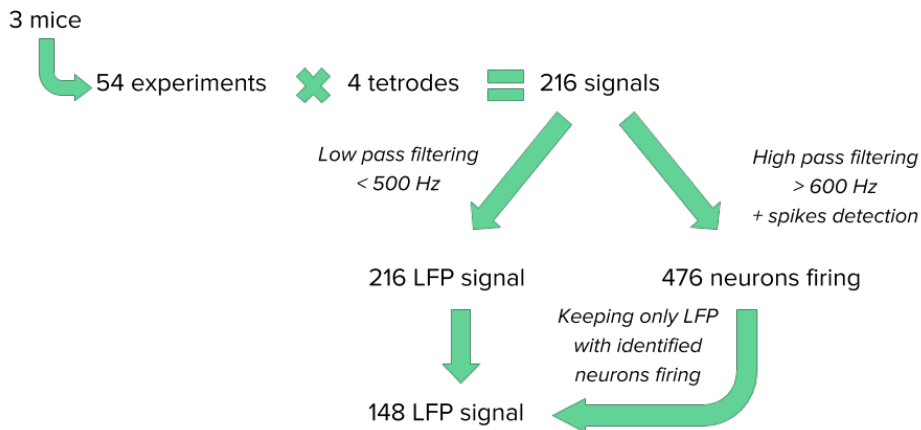


Figure 3.3: Summary of the dataset. Band-passing of low and high frequencies is simplified as low-pass and high-pass filters.

tation of the gamma activity during the proper time period.

### 3.2.1 Selecting signals

#### 3.2.1.1 Time period

During a trial, attention is sustained in a period ranging from the start of the trial, when the mouse starts watching the holes, until the cue onset. During the rest of the trial, different behaviors such as motor activity or reward collection are occurring.

Because of the random delay, this period can be 3, 4 or 5 seconds long. This random delay in the 3-CSRTT increases on the overall the attentional load and prevents any strategy for predicting the cue occurrence. However, it raises problems when it comes to analysis, as the period of attention varies in duration across trials which can introduce a bias.

Analysis from Kim et al. [1] suggests that there is a short transient period of increasing activity after trial start. It is followed by a stationary state of sustained activity at its maximum level before cue onset. Any difference in bursting activity according to allocation of attention seems more likely to be observed in the intense stationary state, therefore, it was decided to focus on this period.

The shortest delay being of 3 seconds, looking at the 2 seconds before cue seems reasonable. This 2 seconds duration was also applied for trials with 4 and 5 seconds delay, as using constant time window reduces the risk of biasing data. In this thesis, the 2-second period before cue is referred to as attention period (figure 3.4). If the assumption of stationarity of the activity is correct, then there is no problem in aligning all periods on the cue instead of trial start.

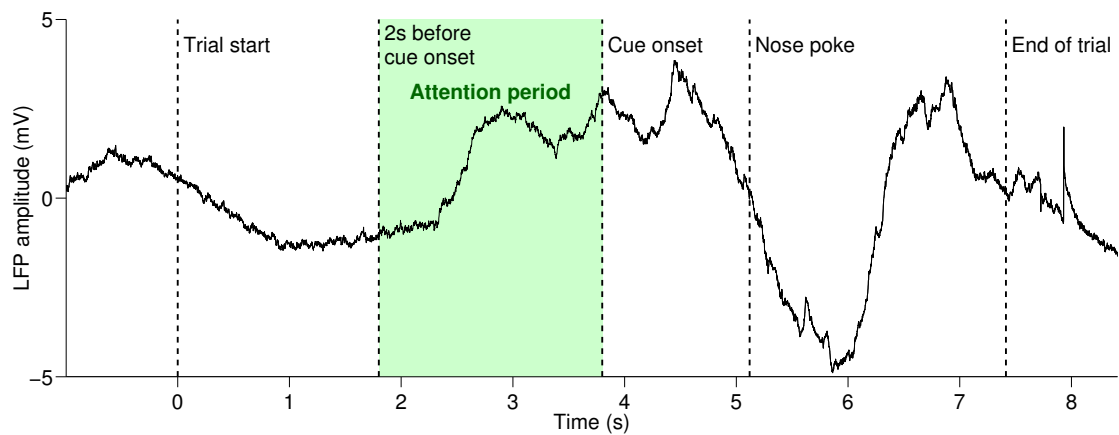


Figure 3.4: Succession of events in a correct trial. Time is relative to the start of the trial. The period of maximum attention is ranging from two seconds before cue to cue onset. Trial starts when the mouse turns from reward port to face holes. In that example, the cue onset occurs approximately 4 seconds later (3.8 s, small difference being due to some setup inaccuracy). The animals nose pokes correctly 1.3 s after cue onset (5.1 s after trial start) and waits 2.3 s to push the reward collection port, ending the trial (7.4 s after trial start).

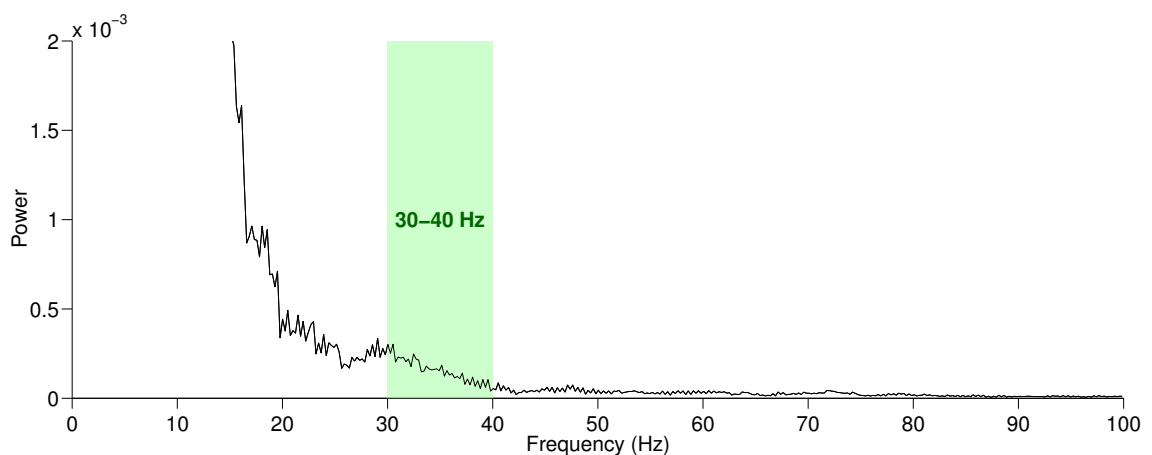


Figure 3.5: Periodogram of the LFP from one trial during the 2-second attention period. Computed with multitapers (TW = 5; 9 tapers). Power in the lower frequencies is very strong and therefore not in the plotting range. For frequencies higher than 40 Hz, power is almost null. The gamma power is mostly focused between 30 Hz and 40 Hz.

### 3.2.1.2 Frequency band

The gamma band is commonly defined by ranging from 30 Hz until higher frequencies up to 100 Hz. However, the activity in rodents is usually weak in very high frequencies. In our recordings, almost no power can be observed after 40 Hz (figure 3.5). Therefore, the analysis was limited to the band between 30 Hz and 40 Hz.

### 3.2.1.3 Quality of signals

Recordings are performed on moving animals, which results in very noisy signals. It can be linked to pure motor activity, but also to the mouse bumping its head on the box borders. This leads to contaminated signals that are sometimes not exploitable. In particular, it can happen that the signal saturates at a constant value if it gets out of recording range, as illustrated in figure 3.6. During the saturation, there is absolutely no information encoded, which makes it impossible to deduce the gamma activity.

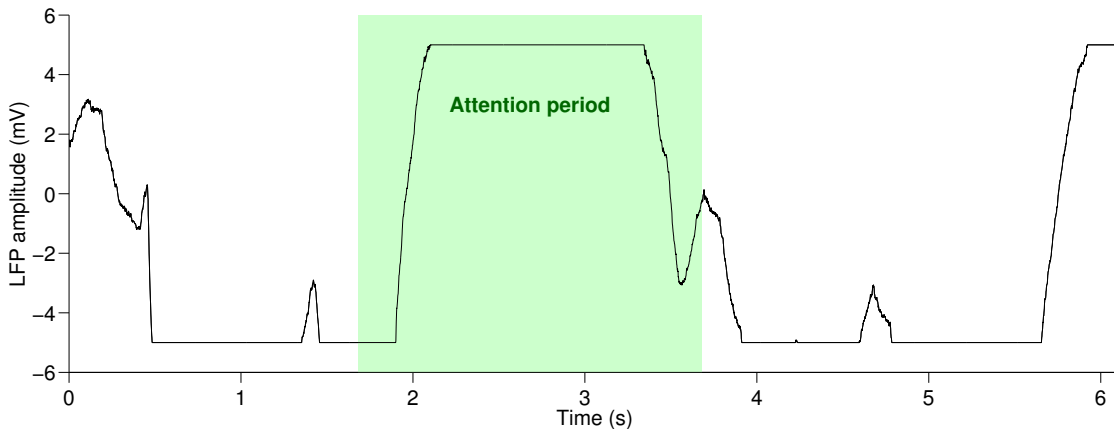


Figure 3.6: Example of an extremely bad recording, not representative of an average signal. It saturates at a constant value for almost the whole attention period.

The signal quality changes a lot from one trial to another. Therefore, this problem should be addressed with a trial by trial approach. An algorithm was developed in order to extract an exploitable signal from a contaminated one. First, all periods of saturation are detected. After trying several set of parameters, it seemed optimal to define saturation as having a constant value for three data points in a row (3 ms at 1 kHz). These detected constant periods are used to split the signal into several sub-signals that never saturate. Only the longest signal is selected (figure 3.7). The original LFP is returned in the case that it never saturates. In the end, a test is applied on the signal length. If it lasts for 1 s or less, it is considered to be too short for further analysis and the whole trial is discarded. Otherwise, the trial is kept, either completely either in a cut version.

When the signal saturates, several periods of non-saturation can usually be extracted. However, the previous method only uses the longest period while it might be possible to exploit the shorter ones. Even if this would increase the amount of data available, it would require to artificially reconnect or combine together these signals in the end of the process. This calls for strong assumptions and presents the risk of biasing the data and decreasing the dataset quality instead of improving it. Thus this solution was non implemented.

### 3.2.1.4 Recap of selection process

The selection process for ensuring signals quality reduces progressively the size of the dataset. The first step consists in working only with tetrodes from which single neuron activity was identified. Indeed, it can be assumed that if no neuron can be detected around the tetrode, either the signal quality is insufficient either the spatial location of

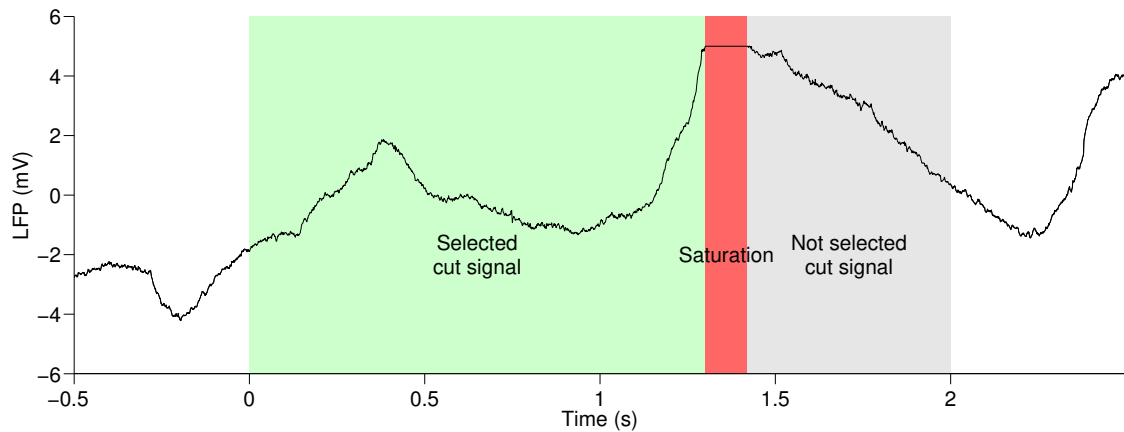


Figure 3.7: Illustration of the cutting process. Time is relative to the start of attention period, ranging from 0 to 2 s. The signal saturates for 121 ms (in red). Two proper signals are extracted, of 1300 ms (in green) and 579 ms (in grey). Only the longest signal is selected for further computations.

the tetrode is not optimal. In both cases, it is safer to avoid using these signals. This selection reduces the number of tetrodes by 68 out of 216 (-31.5%).

In the 148 tetrodes, not all trials are interesting. It can happen that the animal does not try to accomplish the trial even though it initiated it. It can be for instance scratching itself, sniffing or exploring. This lack of motivation and investment in the task obviously leads to a failed trial. However, the failure is not due to a bad allocation of attention but related to a lack of will. These trials are referred to as unfocused trials in this thesis. It is not relevant to analyze them, and they were manually detected and discarded (2,307 trials out of 10,123; -22.8%) by watching video recordings of the experiments (figure 3.8A). I did not have to sort the trials myself as this had already been done for the previous analysis.

The last step consists in the treatment presented previously, cutting or discarding signals that saturate. This reduce the dataset by 13.1% compared with the previous state.

In the end, considering the whole selection process, about 46% of recorded trials are kept, not taking into account information lost by cutting part of the signals. This represents 7,816 trials. This seems to be a reasonable number of samples for running a statistically relevant analysis.

## 3.2.2 Band-pass filtering approach

### 3.2.2.1 Filter choice

This study focusing only on the gamma activity, a simple approach is to filter the LFP in order to look only at the information in that range. A band-pass filter suits perfectly to the situation: it cuts the frequencies that are too low (<30 Hz) or too high (>40 Hz). In this thesis, an order 5 Butterworth filter was applied in the forward and reverse directions to obtain the effect of zero-phase filtering. The implementation in MATLAB was done thanks to the FieldTrip toolbox [92], which includes effective functions for filtering.

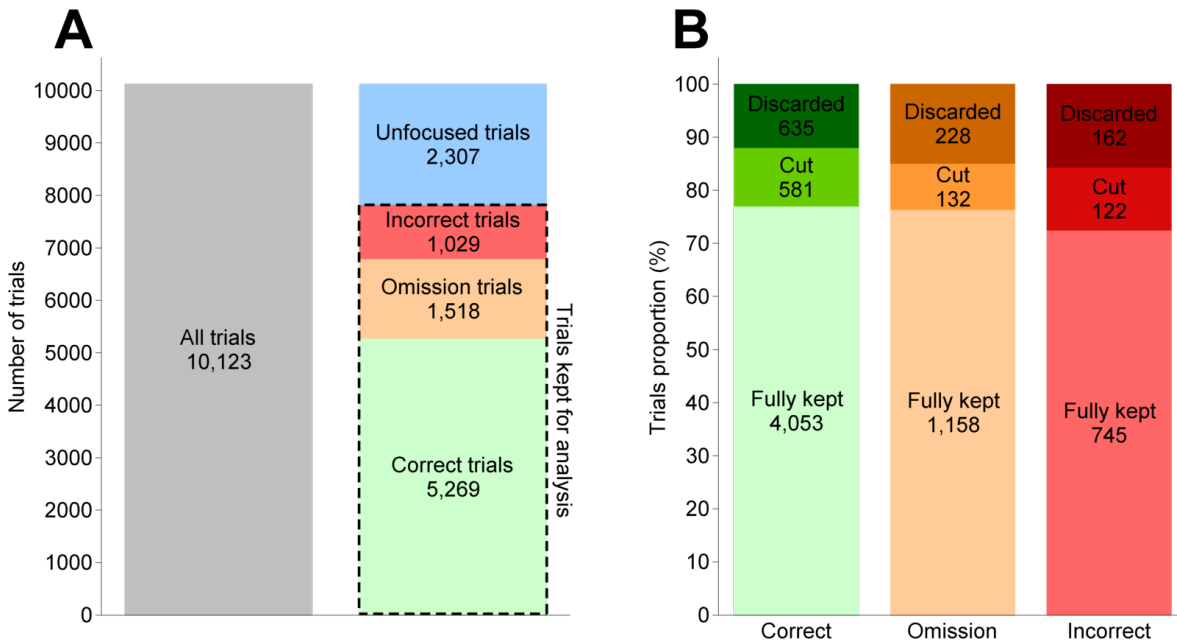


Figure 3.8: **(A.)** Repartition of trials in the 148 selected tetrodes. After discarding unfocused trials, most common output is correct (67.4%). Most common error is omission (19.4%). Incorrect is the rarest situation (13.2%). **(B.)** Repartition of trials after the selection process. Most of them are kept in their original form (72 to 77%). Cut signals lasting between 1 s and 1.99 s represents 8 to 12% of trials; discarded 12 to 16%. No obvious difference can be observed in signal quality according to the trial result.

### 3.2.2.2 Hilbert transform

After band-pass filtering, it is possible to observe gamma oscillations. However, the oscillatory activity has to be analyzed in order to extract the signal intensity. A good approximation of the power can be obtained by computing the envelope of the gamma signal, a smooth curve outlining its extremes.

The Hilbert transform is a linear operator that can be used for extracting an envelope. It returns the analytic representation of the signal, which is simply another representation of the real-valuated signal but in complex values. This is based on the fast Fourier transform (FFT) algorithm which converts a  $N$  points signal sampled at  $F_s$  in its original domain (in that case time) to a  $N$  points signal in the frequency domain, the point  $k$  corresponding to a frequency of  $(k - 1) * (F_s/N)$ . This frequencies are bounded between  $-F_s/2$  and  $F_s/2$ . Therefore, when the frequency is higher than  $F_s/2$ , data points represent negative frequencies which are computed by subtracting  $F_s$  (see appendix figure B.1 for more details).

An important property of the FFT is that the transformed sequence presents an Hermitian symmetry about the  $f = 0$  axis if and only if the input signal is real. If  $\bar{f}$  is the conjugate of  $f$ , then it means that  $\bar{f}(x) = f(-x)$ . Thus negative frequencies can be recomputed from the positive ones; they can be discarded without information loss and simply be replaced by null values.

The Hilbert transform is simply defined as the result obtained after inverting the signal without negative frequencies back into time domain. However, because the Fourier transform is not Hermitian anymore, its inverse is now complex. It makes some manipu-

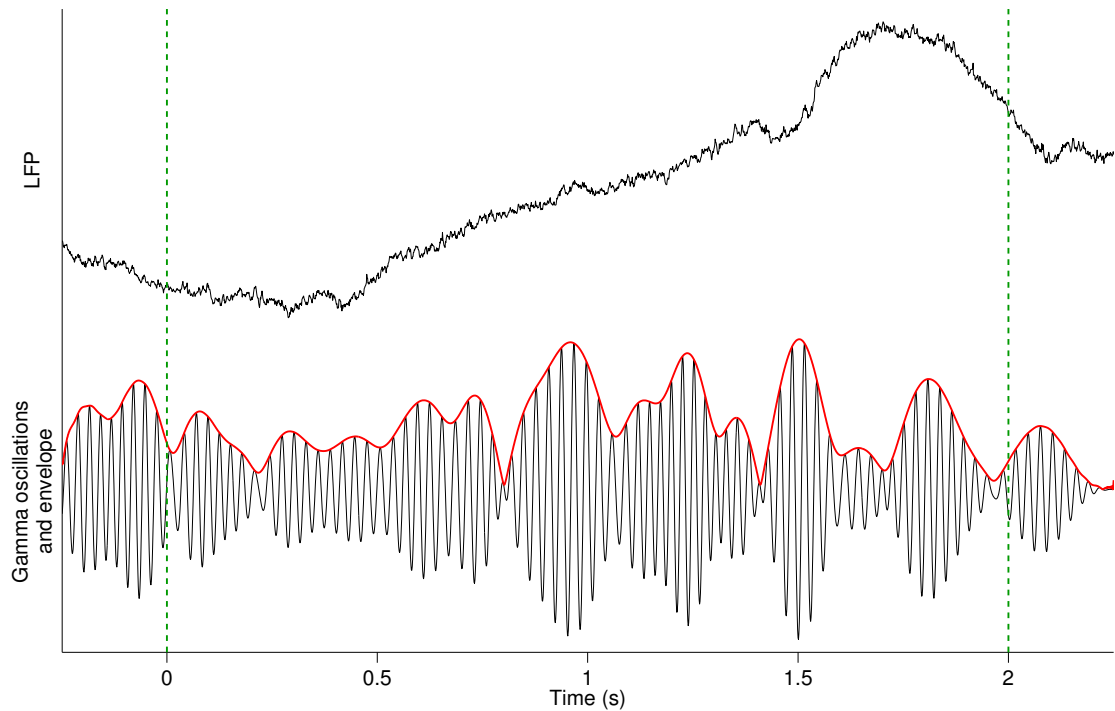


Figure 3.9: Envelope extraction. On the top, the raw LFP signal. On the bottom, gamma oscillations obtained after filtering (black) and the envelope extracted with the Hilbert transform method (red). Green dashed lines represents the attention period limits. Time is relative to the beginning of attention period. Amplitude is in different arbitrary units for LFP and gamma activity.

lation on the signal easier. In particular, the envelope can be simply accessed at any time point by computing the complex magnitude of the Hilbert transform (figure 3.9).

### 3.2.2.3 Edge margin

Some irrelevant behavior can happen at the edges of the signal. This is due to the two transformations that are applied.

First, filtering is only done on a finite-time sequence. However, side effects can appear when filtering because selecting a window leads to an information loss. It means that at the edges, the signal can be different than if it was observed in a wider window in which these surrounding information would not have been lost. This phenomenon attenuates quickly when moving away from the extremities. Previous empirical testing of this dataset has shown that it usually disappears after 250 ms.

Then, the Hilbert transform envelope can also present an erratic behavior at the last data points before the sequence limits, such as a strong increase or decrease of amplitude.

The combination of these two side effects might lead to computing very irrelevant gamma activities. In order to avoid this, a margin of 250 ms is applied to both sides of the sequence (figure 3.10). The original 2-seconds attention period is extended to 2.5 sec-

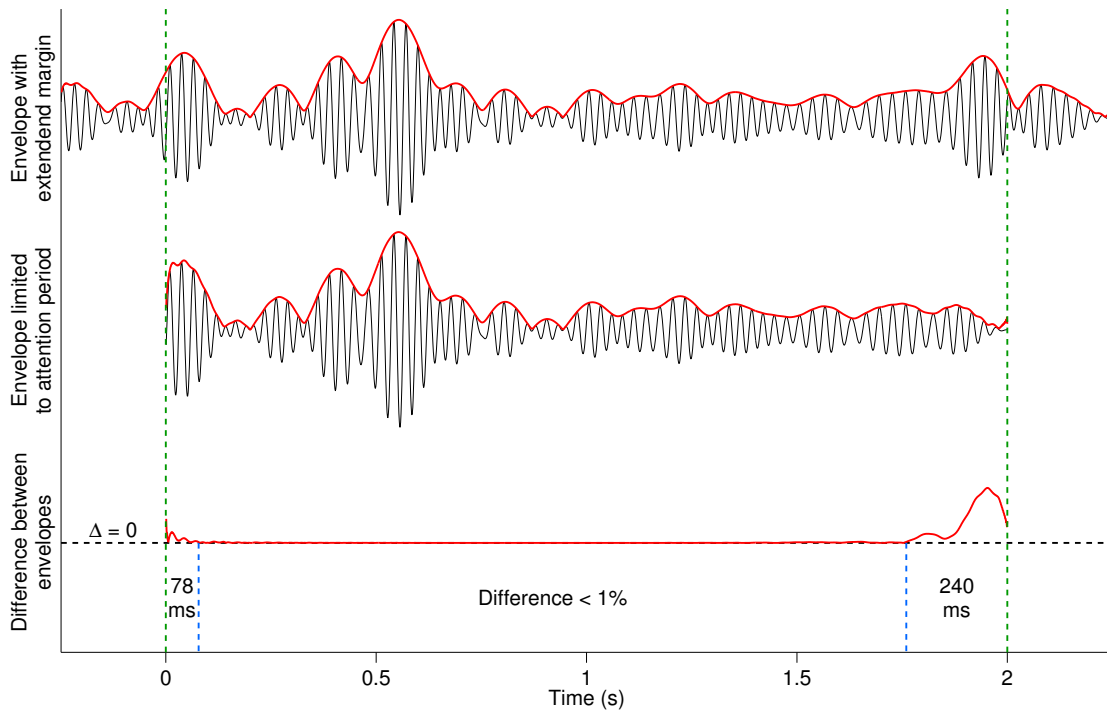


Figure 3.10: Interest of edges cutting. On top, signal is computed during the 2-second attention period extended by two 250 ms margin windows (delimited by green vertical dashed lines). On the middle, signal is just computed during 2-second attention period. On the bottom, the difference in absolute value between the two computed envelopes. Envelopes are identical (difference < 1%, delimited by blue vertical dashed lines) except at the edges (strong difference for 78 ms after beginning and 240 ms before ending). An important difference can be observed between the two filtered signal at the end of attention period. On the same way, Hilbert envelope has an inappropriate tendency to increase (end of both signals) or decrease (start of the 2-seconds signal).

onds. Then the usual algorithm is applied, first finding non saturating signal and then filtering and computing envelope. At the end, 250 ms are cut at both extremities of the envelope. The sequence length after cutting is checked, and the trial is discarded if the cut envelope is shorter than 1 second. The whole signal extraction process is summarized in figure 3.11.

### 3.2.3 Alternative methods

Other methods were also tried to extract gamma activity. Preliminary results were very similar in all cases, which led to focusing only on one of them. The band-passing followed by Hilbert transform being quite common in literature and computationally efficient, it was kept in the end.

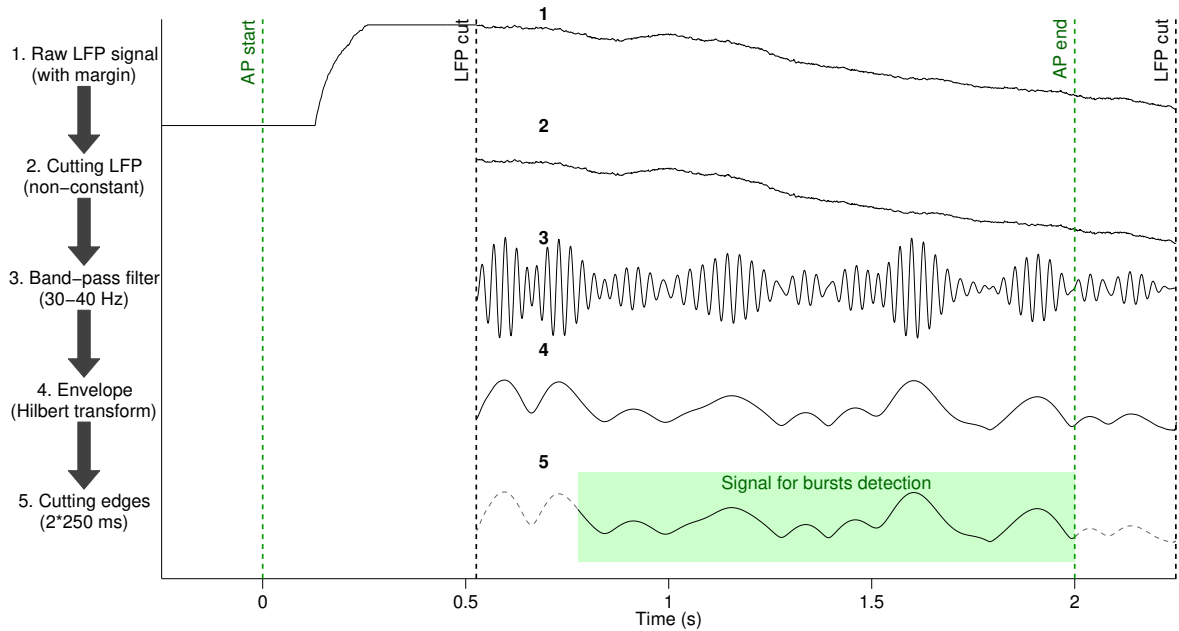


Figure 3.11: Whole process of envelope extraction. **(1.)** As 250 ms of the signal will be cut at both edges in the end to avoid side effects, the period of maximum attention (abbreviated as AP, 2 s before cue, delimited by green dashed lines) is extended with a 250 ms margin before and after. **(2.)** Non-constant LFP is extracted from this 2.5 s signal. Kept signal is delimited by the black dashed lines (1725 ms duration). **(3.)** Band-pass filtering is done between 30 Hz and 40 Hz. **(4.)** Envelope is the complex magnitude of Hilbert transform of filtered LFP. **(5.)** When filtering and doing Hilbert transform, the signal can be irrelevant at the edges. 250 ms are cut at both sides to avoid this. After cutting, the final signal is 1225 ms long. This is longer than 1 second, therefore the whole trial is not discarded.

### 3.2.3.1 RMS

After band-pass filtering, an alternative to Hilbert transform for representing signal intensity is to use the root mean square (RMS), also known as quadratic mean.

With digital recordings, it is computed across the signal in a moving window of an odd size of  $m$  data points. If  $x_1, x_2, \dots, x_N$  are the  $N$  samples of the sequence and  $R$  the RMS sequence, then:

$$R_k = \sqrt{\frac{1}{m} \sum_{i=k-\frac{m-1}{2}}^{k+\frac{m-1}{2}} x_i^2} \quad \frac{m-1}{2} < k \leq N - \frac{m-1}{2}$$

The RMS signal cannot be defined on half of the moving window length at both beginning and ending of signal because of the lack of data (see appendix figure B.2). While testing this method, a 61 ms window gave satisfying results.

As RMS fluctuates a lot, it is necessary to smooth it. This was simply done by applying a moving window averaging, which means that every data point is the average value of the surrounding data points in the original sequence. A 41 ms window was used.

Even though the Hilbert envelope and the RMS look different at first sight, they are

almost identical after a standard score (Z-score) normalization. For a signal made of  $N$  samples, the first step is to compute the mean value and standard deviation of the distribution of these  $N$  samples. Then, each value is expressed as the signed number of standard deviations to the mean instead of using the original value. For instance, a Z-scored value of 1 means that the original value is equal to  $\text{mean} + 1 * \text{std}$ . With this normalization, the focus is put on signal variations instead of values.

The burst detection algorithm used in this thesis is based on detecting period of high activity compared to the mean. Therefore, similar signals after Z-scoring should produce quite similar bursts characterization. As Z-scored RMS and Z-scored envelope are very similar (figure 3.12), detected bursts were logically consistent with the two methods.

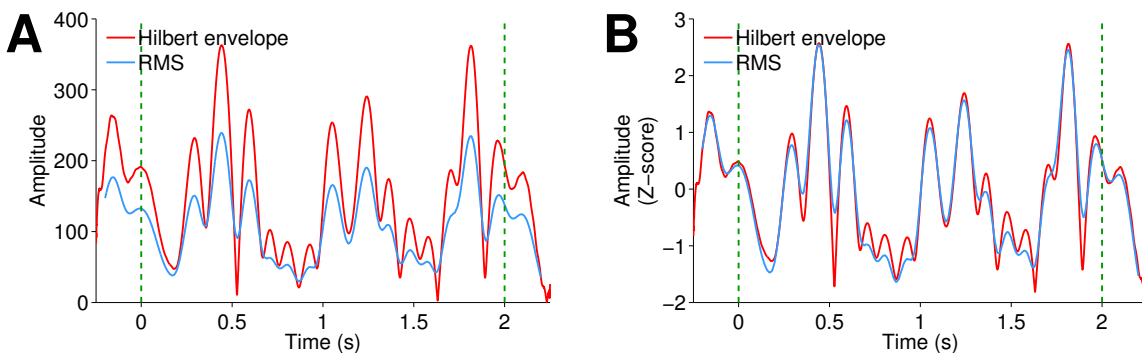


Figure 3.12: Comparison between RMS and Hilbert envelope for one trial. **(A.)** Original envelope and original filtered RMS. Envelope is more fluctuating as it follows peak values while RMS is less varying as it is a mean value. **(B.)** Z-scored envelope and RMS. The two signals are very similar, even though RMS is slightly smoother.

### 3.2.3.2 Spectrogram

A different approach can be to work with spectrograms. Instead of getting the power as a simple function of time, it is more accurately defined as function of time and frequency range.

Normally, one of the main interest of using spectrograms is to avoid filtering, as the power of different frequencies can be observed distinctly. However, because of the noise in the recordings and more specifically of lower frequencies contaminating the higher ones, it was not possible to extract proper spectrograms without filtering the data. Therefore, the spectrogram approach only consisted into analyzing in a different way the same 30 to 40 Hz band-passed signal already used for RMS and envelope.

Instead of computing simple spectrograms, multi-tapers estimation was applied in order to reduce the estimation bias. The idea is to chose a set of functions for windowing, known as tapers, with some specific properties. The signal is then multiplied to all of theses window functions, leading to several estimations of the signal. In the end, the spectrogram is obtained by averaging all the estimations.

The Chronux package proposes a nice implementation of multi-tapers for MATLAB [93] [94] and was used for these computations. It runs with Slepian functions as tapers. After experimenting with different values, the final set of parameters was fixed at 5 tapers with a time-bandwidth product of 3, a time window between 150 and 250 ms de-

pending on the case and a time bin of  $1/15$  of the time window. In order to increase the frequency resolution for plotting, padding parameter was sometimes set to 1 or 2.

However, when detecting period of intense activity, having a simple function of time is simpler. Therefore, the mapping of signal intensity on the time-frequency plane was converted into an amplitude signal function of time. This can be simply achieved by averaging over all frequency bins, for every time bin (see appendix figure B.3). As for every methods including a moving window, the signal cannot be computed on half of the window length and a margin is required to compensate.

As the spectrogram represents power, it cannot be directly compared with an amplitude such as the envelope or the RMS. The two signals were rescaled into the same range of values for plotting. After Z-score normalization, it can be noticed that the spectrogram power is less fluctuating than the other methods. This is probably due to the wider moving window (figure 3.13).

On the overall, preliminary results were similar for envelope and spectrogram approaches. The values were different, as the smoother variations of spectrogram lead to detect less bursts of higher durations, but the same properties were observed.

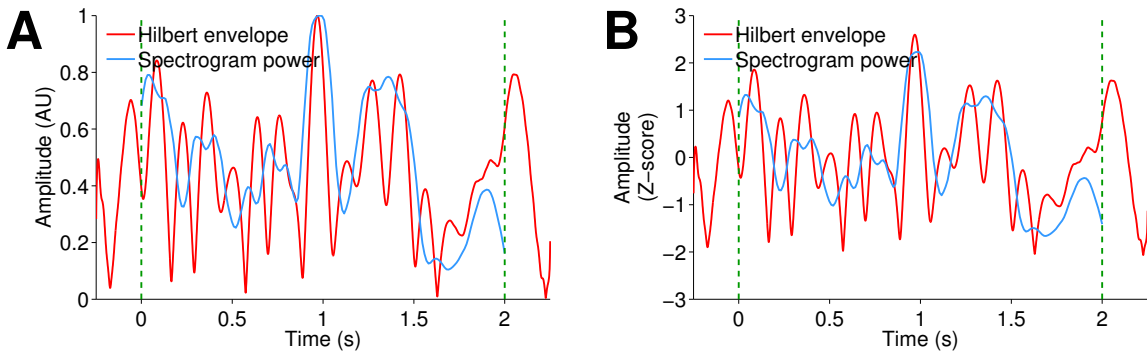


Figure 3.13: Comparison between spectrogram power and Hilbert envelope for one trial. **(A.)** Original envelope and spectrogram power, divided by max value in order to rescale them in the  $[0, 1]$  interval. This is required because the spectrogram power is not at all in the same range of values as the envelope. **(B.)** Z-scored spectrogram power and Hilbert envelope. Activity is similar, but less variations can be observed with the spectrogram approach. These results can vary a lot with the set of parameters adopted (in this case: time-bandwidth product = 3, tapers = 5, time window = 175 ms, time bin = 11.66 ms).

### 3.3 Burst detection

#### 3.3.1 Variation of signal in time

Bursts can be defined as period of short but intense activity. A representation of the power was extracted in the previous section through the Hilbert envelope, therefore it is now necessary to define formally what can be considered as an intense activity. This concept makes sense only when compared to a baseline level used as reference. This reference can be a global or local criteria, depending on the signal characteristics. Thus the first step is to analyze the signal variations in time.

Two different time scales shall be investigated. The first one is short and corresponds

to the variations that could be observed during the two seconds of attention period. The second one is much longer and would be linked to the modulation happening during the whole recording, which lasts from 45 minutes to one hour.

### 3.3.1.1 During the attention period

During the two seconds before the cue onset, the signal power might not be evenly spread in time. There could be a tendency to get stronger power at some specific timing. To investigate this possibility, the amplitude of gamma envelope during the attention period was averaged across the dataset (figure 3.14).

No clear tendency over time can be observed, supporting the idea that power is uniformly split. Therefore, the analysis was made with the assumption that power baseline is the same during the whole attention period.

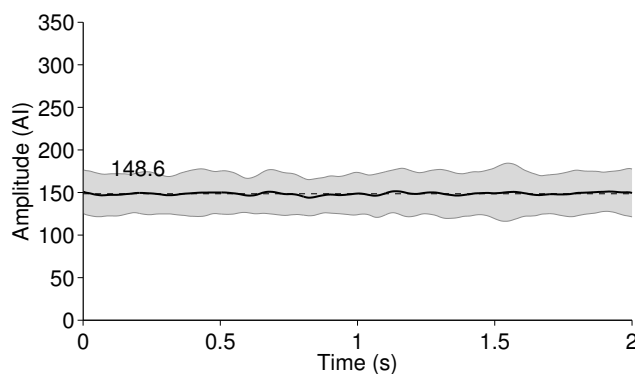


Figure 3.14: Amplitude averaged across tetrodes during attention period. In each tetrode, an average amplitude across trials is first computed. Only full 2-seconds trials were used. Then, these 148 trial-averaged amplitudes are averaged across the 148 tetrodes. Dashed lines is the mean amplitude (148.6 AI). Error is the standard deviation over tetrodes.

### 3.3.1.2 Over recording time

Another possibility is to have variations of power between the first and the last trial of a tetrode during the recording of an experiment (about 50-70 trials in one hour). A simple way to address this problem is to analyze in every tetrode the mean power of trials, ordered chronologically, and see if a trend can be extracted.

A first analysis by looking at the behavior in a few tetrodes suggests an overall loss of power trough time (annex B.4). In order to check if this can be observed more generally, the mean amplitude of each trial in every tetrodes was computed and sorted by the order in which trials were recorded. Then the correlation between mean amplitude and trial number was estimated trough Pearson correlation coefficient and linear regression computed in all tetrodes.

The Pearson correlation coefficient quantifies how linear correlation is the correlation. It is bounded between -1 and +1. An absolute value close to 1 means that the linearity is very strong while a value close to zero indicates an absence of correlation. The sign informs about the correlation positiveness or negativeness. For each coefficient, a probability value (p-value) can be computed to indicate the significance of the observation. It depends on the coefficient value and on the sample size.

The distribution of correlation coefficients across tetrodes is presented in figure 3.15 A. Individually, 45 tetrodes out of 148 present a negative correlation with a 95 % confidence. This is 30 %, which is much more than the expected proportion of type I error. No tetrode presents a significant positive correlation.

The distribution of Pearson coefficients is centered on  $-0.24$ . This is a strong bias toward negative values. Student's *t*-test (assumption of normality seems reasonable from plotting) supports this, the p-value for a zero-centered distribution being inferior to  $1 \times 10^{-35}$ . It can therefore be concluded that there is tendency to lose power over time in a non negligible number of tetrodes.

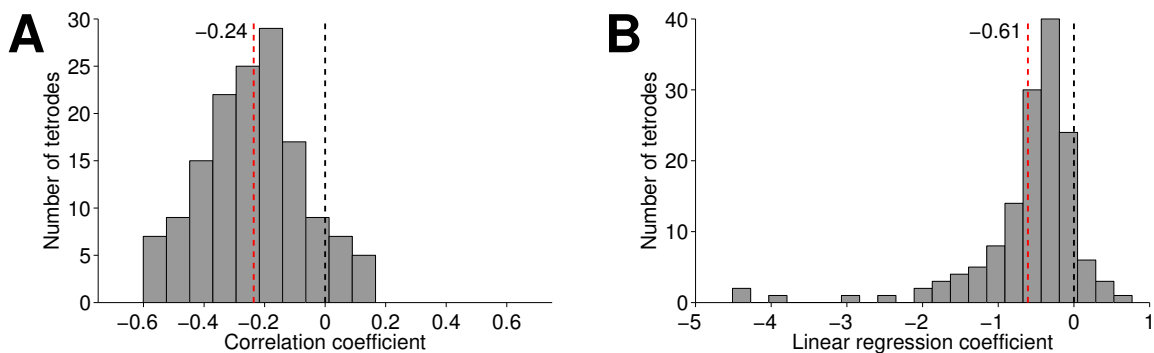


Figure 3.15: **(A.)** Distribution of correlation coefficients among tetrodes. Student's *t*-test p-value:  $5.62 \times 10^{-36}$  **(B.)** Distribution of linear regression coefficients among tetrodes. Student's *t*-test p-value:  $1.39 \times 10^{-17}$

This only proves that a power decrease happen in many tetrodes but this does not quantify how strong it is. However, applying a linear regression can provide an estimation. The results of this second approach are consistent with the previous observations of decreasing power as presented in figure 3.15B. Distribution is centered around  $-0.61$  (p-value from *t*-test for zero-centered distribution inferior to  $1 \times 10^{-17}$ , assumption of almost normality is acceptable).

After doing linear regression, power loss can simply be defined by the variation of power between first and last trial normalized by initial power, power being estimated from the linear model (see appendix figure B.5). Even if this model fits badly to the data, the point is not to get a proper modeling but to appreciate the phenomenon as a first approach. According to this method, the mean loss of power in a tetrode is approximately 12 % during recording ( $-12.2 \pm 0.91$  standard error of the mean (SEM)). It cannot be neglect.

### 3.3.1.3 Criterion choice

Some conclusions can be extracted from this quick analysis. First, as power is evenly split in the two seconds attention period, it seems reasonable that the chosen criteria is kept the same during these two seconds.

However, it was shown in the previous section that the loss of power on longer time periods cannot be neglected. Therefore, using a global criterion would require to introduce a normalization, which is always delicate as it can bias the data. The simplest way is to pick a local criterion for each trial.

### 3.3.2 Threshold method

As the method for extracting gamma power was presented before, it is now necessary to decide how to detect bursts from this signal. A common method in literature for bursts detection is based on a threshold. Even though the exact modalities vary from one study to another, the general idea is that when the signal power get above the threshold, a burst is occurring. A similar method will be applied here.

#### 3.3.2.1 General formula

Bursts are periods of intense activity. The concept of "intense" can only be defined relatively to surrounding activity. Therefore, the threshold should be based on the general characteristics of gamma power in the attention period. Defining an intense activity requires both a baseline and the limits of acceptable deviation from this baseline.

This can be done with very basic statistics tool. The mean value can be used as a baseline while the standard deviation provides relevant information on signal fluctuations. Acceptable deviation from baseline is defined by multiplying the standard deviation by an arbitrary coefficient. It was shown in the previous section that the criterion has to be defined locally. Therefore, the mean value and standard deviation are computed across the trial duration. The general formula is:

$$T = \mu + k * \sigma \quad (3.1)$$

where  $T$  is the threshold value,  $G$  the envelope of the gamma filtered signal,  $k \in \mathbb{R}_+$  an arbitrary coefficient,  $\mu$  the mean value of  $G$  and  $\sigma$  the standard deviation of  $G$ .

This approach is exactly equivalent to using the coefficient  $k$  as a threshold on the z-score normalized signal:

$$\begin{aligned} G > T &\equiv G > \mu + k * \sigma \\ &\equiv \frac{G - \mu}{\sigma} > k \\ &\equiv z > k \end{aligned}$$

where  $z$  is  $G$  normalized by z-score,  $G$  positive not constant.

The coefficient applied to the standard deviation in the general formula is arbitrary and depends on the desired selectivity for bursts. The higher it gets, the less bursts are found (figure 3.16).

Several values were proposed in literature according to the signal properties. Rosero and Aylwin [95] used a coefficient of 1.5 on awake rats during olfactory related tasks. Lundqvist et al. [26] preferred applying a coefficient of 2 on monkeys during working memory task. In this study, the coefficient value was fixed based on a preliminary analysis presented in section 4.1.

#### 3.3.2.2 Bursts characteristics

Several characteristics can be defined for bursts detected with this threshold method (figure 3.17).

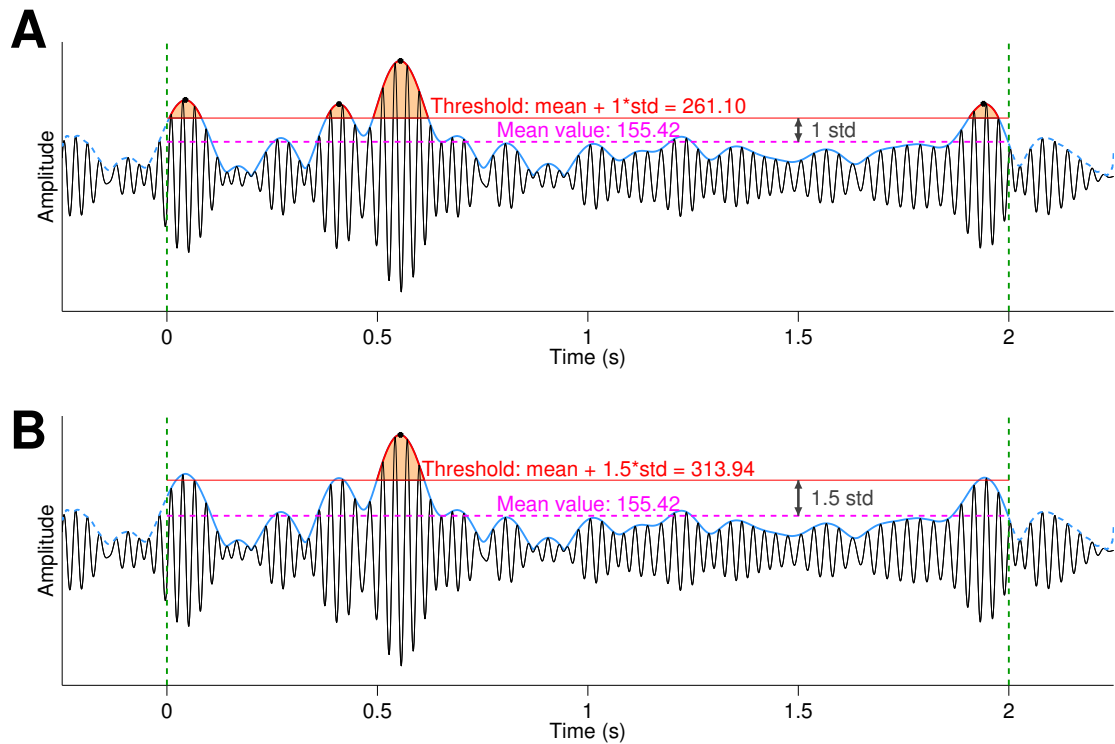


Figure 3.16: Burst detection on gamma-filtered signal. Detected bursts are represented by red envelope and orange background. **(A.)** Case with 1 as coefficient. 4 different bursts are found. **(B.)** Case with 1.5 as coefficient. Only one burst is found as threshold is higher. Even if the envelope goes above the threshold at other points, this is not long enough to be considered as a burst (duration smaller than 50 ms).

**Occurrence.** The first characteristic is the occurrence of a burst. The simple definition is that a burst is occurring when the envelope amplitude is higher than the threshold. In order to differentiate a burst from a simple peak activity, a minimum time spent above the threshold is commonly imposed. In this study, it was considered that a burst was made of several oscillations. Therefore, a minimum duration criterion of at least two oscillations was imposed. As the frequency band is quite narrow (30-40 Hz), one oscillation can last from 25 to 33 ms. The shortest duration was chosen, and therefore a burst is defined as an amplitude higher than the threshold for at least 50 ms.

**Duration.** The simple way to define a burst duration is to take the time spent above the threshold. An alternative method proposed in another study [96] was tried. It uses two threshold instead of one. The upper threshold is used to detect bursts, but duration is computed by the time spent above a lower threshold. It did not seem to improve in any way the characterization and therefore it was decided to rely on the basic method.

**Timing.** Even if a burst is lasting for a certain time, it can be useful to associate a specific timing to it. The middle time between begin and end of burst is defined as burst timing.

**Amplitude.** Amplitude is defined for every burst as the highest amplitude reached during the burst. It is usually very close or identical to the amplitude at the middle of the burst - burst timing - because bursts are most of the time almost symmetrical.

**Relative amplitude.** The amplitude can vary a lot between tetrodes, or from one trial to another. In addition, the peak value of a burst might not be the most accurate representation of its intensity. Therefore, a relative amplitude was also defined. It is computed per trial, as opposed to the raw amplitude that is computed per burst, and is obtained by dividing the mean power during all bursts of the trial by the mean power of the trial outside bursts. It is therefore a ratio representing how intense are the bursts relatively to the rest of the signal.

**Interburst interval** This is the time between the timings of two consecutive bursts. When the signal has  $N$  bursts,  $N - 1$  interburst intervals can be computed. If the signal has zero or one burst, no interburst interval can be extracted.

**Coefficient of variance** The  $CV_2$  is computed in order to characterize the interburst interval distribution. It is defined by:

$$CV_2 = \frac{1}{n-1} \sum_{i=1}^{n-1} \frac{2|l_i - l_{i+1}|}{l_i + l_{i+1}}$$

where  $l_1, l_2, \dots, l_n$  are  $n$  interburst intervals.

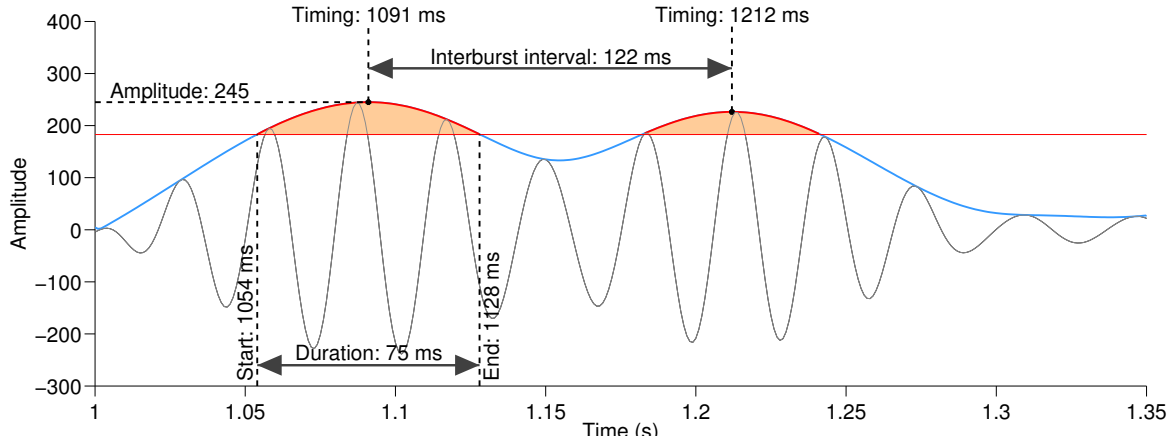


Figure 3.17: Illustration of several burst characteristics. Attention period is only represented from 1 to 1.35 s after it started. Threshold is represented by the red line. Two bursts are detected. In that example, maximum amplitude is reached exactly at burst timing.

### 3.3.2.3 Outliers treatment

Some recordings present unexpected variations. It is complicated to say with certainty if they correspond to neural activity, movement perturbation or simply external noise. Usually, it consists in peaks or high amplitude cycles in the LFP (figure 3.18). After band-pass filtering, it leads to gigantic gamma bursts. In the distribution of characteristics, these bursts appear as outliers.

They are problematic for several reasons. First, they might be totally irrelevant in terms of biology and therefore it would not make sense to study them. On the other hand, if they actually represent a neural phenomenon, discarding them would be an important loss of information. Also, they might introduce a bias in the burst characterization. As their amplitude can be up to twenty times higher than a typical burst, they would most likely strongly influence the bursts characteristics and especially the amplitude.

To address this issue, outlier detection algorithms were applied. The easiest way to recognize these undesirable bursts is their amplitude, which is much higher than in a normal burst. Therefore, the detection is done on the distribution of bursts amplitudes: bursts whose amplitude does not fit to the distribution according to the algorithm criteria are considered to be outliers. As every tetrode is assumed to generate an independent distribution of burst characteristics, outliers should be detected in the 148 distributions of amplitudes across trials that correspond to the 148 tetrodes analyzed.

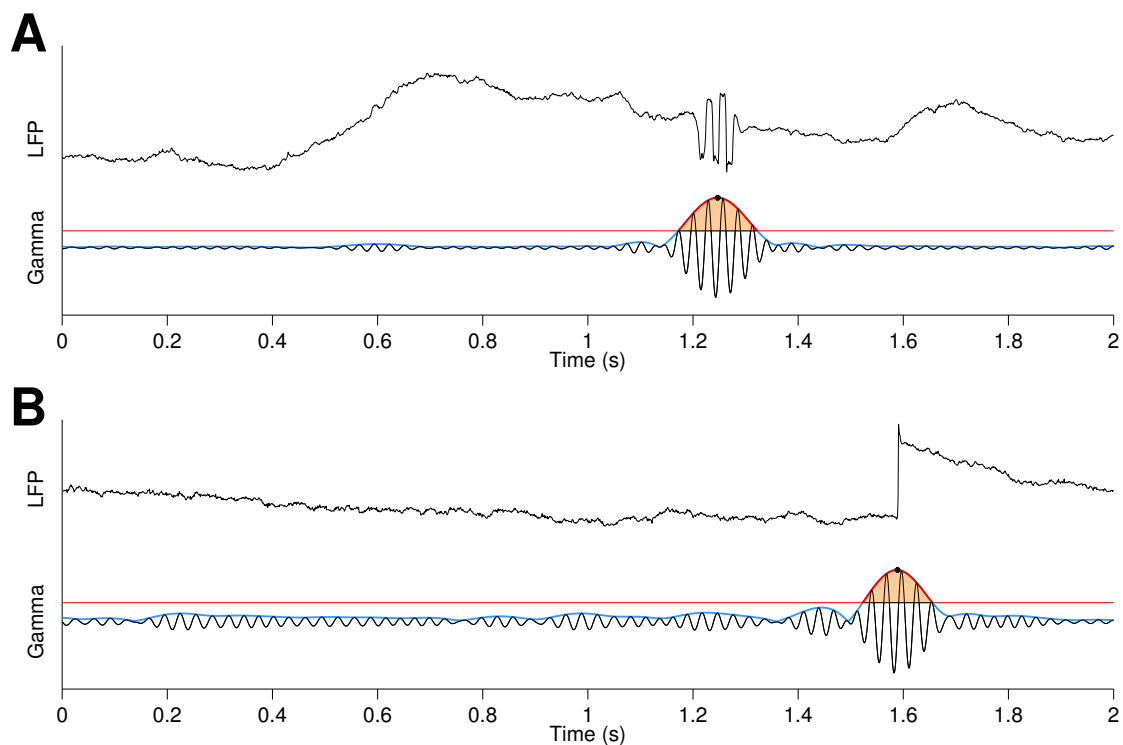


Figure 3.18: Example of two outliers. Horizontal red line is the threshold set at  $\text{mean} + 1.25 * \text{std}$  (A.) High amplitude cycles. They usually contaminate the whole LFP frequency band, from 1 to 100 Hz. After filtering, they cause an enormous peak that pushes the threshold way very high. (B.) Outliers due to fast LFP variations. It causes an enormous burst.

The first implemented algorithm is the Tukey's method. It is a very common approach, even though the classification might be unsatisfying for small sample size. It is based on the quartiles calculation [97]. Dataset is split into four equal-size groups by three values  $Q_1$ ,  $Q_2$  and  $Q_3$ . The interquartile range is defined as distance between  $Q_1$  and  $Q_3$ :  $I_{QR} = Q_3 - Q_1$

Two different criteria are used, according to the desire confidence for a point to be

an outlier. Outer fences bound the interval outside of which data points are classified as probable outliers. It is defined by  $F_{outer} = [Q_1 - 3 * I_{QR}, Q_3 + 3 * I_{QR}]$

Inner fences limit the interval in which a point cannot be considered to be an outlier:  $F_{inner} = [Q_1 - 1.5 * I_{QR}, Q_3 + 1.5 * I_{QR}]$ . Samples between inner and outer fences are possible outliers.

In order to decide which limit is the most suitable for gamma bursts, both criteria were tested and then LFP and gamma activity were plotted for some of the detected outliers. When inner fences classification was used, several signals with strong but normal activity were detected as outliers, which did not happen with outer fences. Therefore, this second criterion was chosen.

Another approach consists in using the median absolute deviation (MAD) method. In order to identify points that are not fitting into the distribution, the MAD is computed. This value, as opposed to the standard deviation, presents the advantage of being very insensitive both to the presence of outliers and to the sample size [98]. It is defined as the median of the absolute deviation from data's median, times a coefficient:

$$MAD = b * \text{median}(|X_i - \text{median}(X_j)|)$$

where  $X_j$  is the distribution of values and  $b$  a constant equal to 1.4826 linked to the assumption of normality.

Then, distance from the median is computed for all the data points and normalized by the MAD:

$$d_i = \frac{x_i - \text{median}(X_j)}{MAD}$$

where  $d_i$  is the normalized distance of data point  $x_i$  to the distribution median.

A criterion is finally fixed to decide if the point is an outlier or not. It can be in absolute value if both lower and upper outliers are expected, but in the case of gamma bursts only too intense activity is of interest. Miller [99] proposes to fix that limit at a distance greater than 3 when looking for a very conservative model. After testing different values and looking at some signals classified as outliers, this value seemed satisfying.

## 3.4 Further burst analysis

### 3.4.1 Trial to trial burst patterns

The hypothesis that specific patterns of bursts would be occurring and repeating between trials was investigated. The conjecture behind is that if the allocation of attention is not related to the number of bursts, maybe it could instead be correlated to patterns of burst timing. Indeed temporal bursting patterns are a well-known phenomenon for neurons [100] [101]. At the LFP scale, patterns of beta and gamma bursts induced by odor stimuli were observed on anesthetized rats [102].

#### 3.4.1.1 Bursts as a binary process

First, the bursting process was simplified into a binary model whom two states are "bursting" and "non-bursting" respectively coded by 1 and 0. Envelope signals ( $S_i$ ) were converted into these simple bursting signals ( $B_i$ ) of identical length.

Signals with only one burst were discarded. Indeed, the notion of timing patterns with only one timing value available is not relevant.

Signals that were shorter than 2-second due to cutting were discarded to avoid biasing the study by analyzing patterns extracted from signals with various lengths. As these signals only represent a small proportion of trials, it seemed acceptable to simply ignore them instead of trying to include them in this analysis.

### 3.4.1.2 Pairwise analysis

The similarity between burst timings patterns is analyzed by pair of trials. If there are  $N$  trials in a tetrode, this corresponds to  $N(N - 1)$  pairs of trials to analyze.

However, the measure that is defined in this section is symmetric. It means that computing the similarities of patterns between  $(S_1)$  and  $(S_2)$  is the same as computing the similarities of patterns between  $(S_2)$  and  $(S_1)$ . Therefore, only half of the pairs are meaningful for this analysis, which corresponds to  $\frac{N(N-1)}{2}$  values.

### 3.4.1.3 Cross-correlation

The potential patterns are not necessarily synchronized. Therefore, the first step consists into realigning the binary signals to maximize simultaneous bursting. A specific optimal alignment is computed for all trial pairs.

This alignment that optimizes the overlapping of the binary sequences is obtained by applying cross-correlation and selecting the lag that maximizes it. The appropriate signal is then shifted by this lag before the next step.

### 3.4.1.4 Burst overlapping

Similarity of patterns is approached by introducing a coefficient that will be called overlapping. It is bounded between 0 and 1, and defined as the number of samples with both signals bursting divided by the number of samples with at least one of the two signals bursting.

If it is equal to zero, bursting never occurs simultaneously. This is an impossible case when both signals contain at least one burst and optimum lag has been chosen. If it is equal to one, then all the bursts are perfectly synchronized.

This coefficient can be defined more formally from the binary sequences  $B_i$  and  $B_j$ . For realignment purposes, they are first extended.  $B'_i$  and  $B'_j$  are obtained by adding a sequence of zeros at one of the extremities in order to align them based on the optimal lag. Then, simultaneous bursting is simply defined by  $B'_i \wedge B'_j$  while at least one signal bursting is  $B'_i \vee B'_j$ . When  $N'$  is the length of  $B'_i$  and  $B'_j$ , overlapping is therefore simply

defined as  $\frac{\sum_{i=1}^{N'} (B'_1 \wedge B'_2)_i}{\sum_{i=1}^{N'} (B'_1 \vee B'_2)_i}$ . An illustration of this process for two signals with high pattern

repeatability can be seen in figure 3.19.

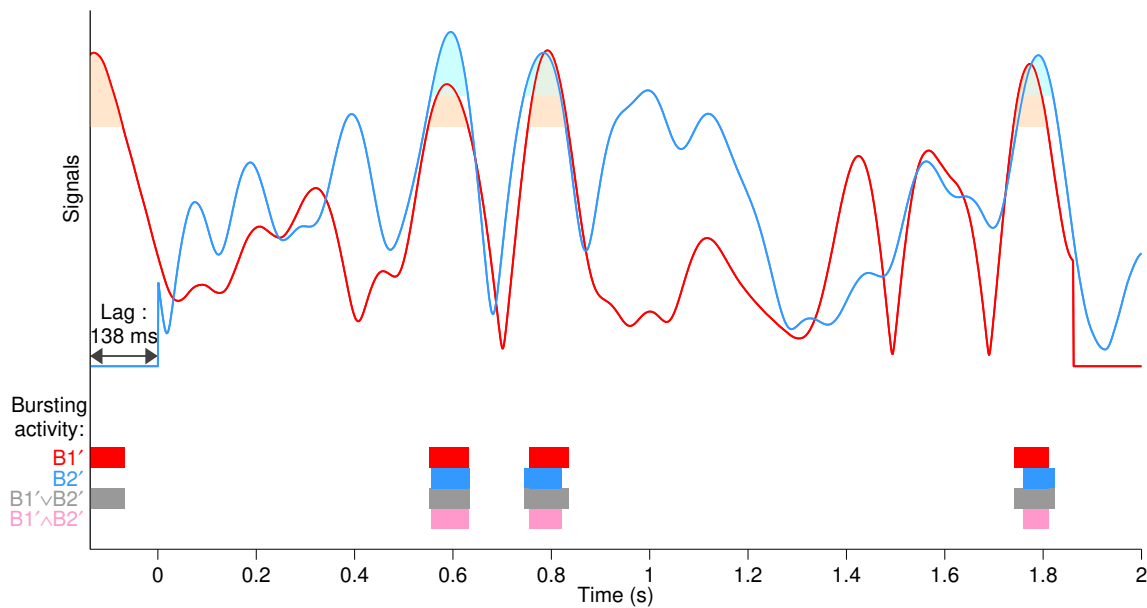


Figure 3.19: Example of high pattern repeatability between two signals  $S_1$  (red) and  $S_2$  (blue, 138 ms lag added for maximizing simultaneous bursting). Overlapping is of 59.8 % (192 ms of synchronous bursting out of 321 ms of bursts).  $B'_1$  is  $B_1$  extended by 138 zeros in the end while  $B'_2$  is  $B_2$  with a sequence of 138 zeros in the beginning.

## 3.4.2 Spiking activity

### 3.4.2.1 Neurons classification

Out of the neuron types isolated in Kim et al. [1], the focus is put on two of them: the FS-PV interneurons and the pyramidal cells. The groups proposed in this previous study were reused without running a new unit classification algorithm. This classification was based on the distribution of peak-to-valley ratio and half-valley width for each spike waveform. Firing rates were used for further separation and a gaussian mixture model was fit to the units.

### 3.4.2.2 Computing instant spiking frequency

In this study, spiking activity is modeled as a discontinuous binary process: signal is sampled at 1000 Hz and for every time point, either one action potential is being fired or the neuron is at rest. This discontinuous representation might not be the most appropriate one. For instance, spiking activity can be smoothed into a continuous representation of instant firing frequency.

An effective way to do this is to convolute the spiking train signal with a gaussian kernel. Depending on the kernel shape, the estimation will capture more effectively different ranges of frequencies.

The two main types of neurons that were identified before are firing at two different rates which lead to use two different kernels to capture them. While the activity of pyramidal cells is usually between 3 and 10 Hz, FS-PV interneurons are more commonly firing between 15 and 40 Hz. Therefore, a wider gaussian with 100 ms standard deviation

was used to capture slow firing pyramidal cells and a narrower kernel with 30 ms standard deviation fit better for fast spiking parvalbumin interneurons (see figure 3.20).

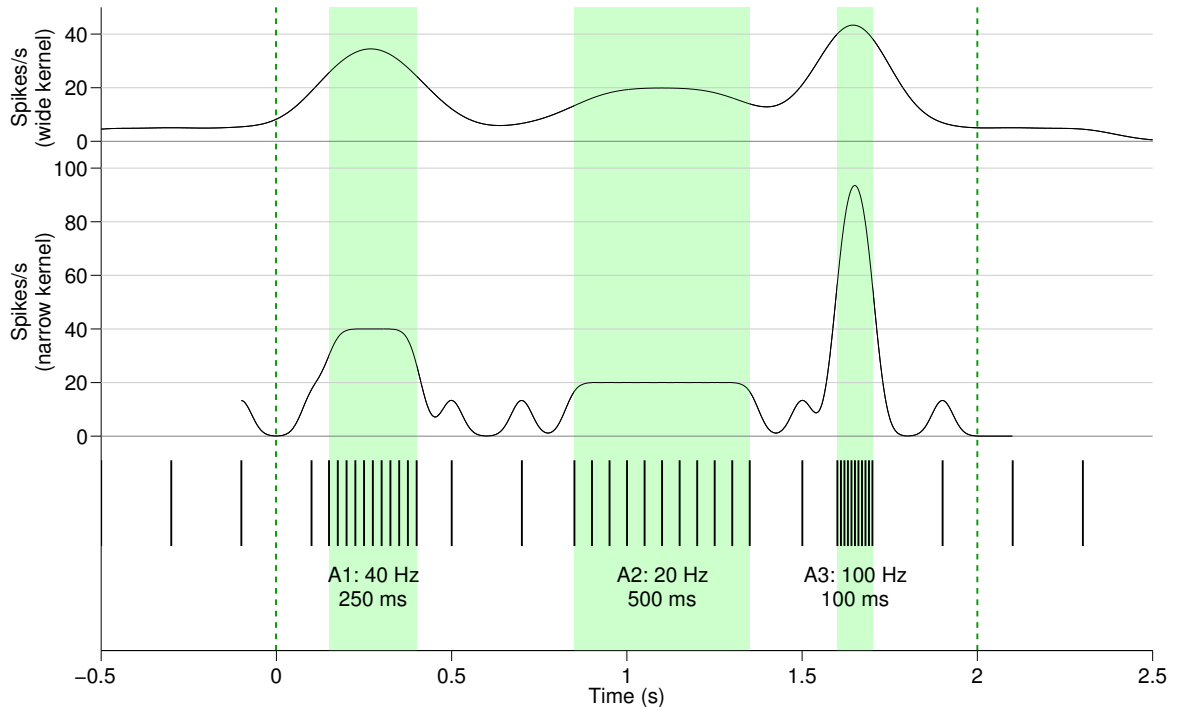


Figure 3.20: Two firing rates computed from an artificial spiking activity with different kernels. Spiking activity (on the bottom, vertical lines) is made of a 5 Hz baseline spiking over which three periods with more intense activity are added. In A1, spiking rate is 40 Hz for 250 ms. A2 corresponds to 500 ms at 20 Hz and A3 to 100 ms at 100 Hz. On the top, kernel is a gaussian of standard deviation 100 ms computed on a 1-second window (gaussian can be considered null outside). It captures well lower frequencies such as the 5 Hz baseline or A2. Estimated value for higher frequencies such as A1 or A3 is very far from reality. On the middle, kernel is narrower with a standard deviation of 30 ms computed over a 200 ms window. Low frequencies such as the baseline are badly represented while higher frequencies during A1, A2 and A3 are correct.

### 3.4.3 Surrogate dataset

#### 3.4.3.1 Utility

With this analysis, the gamma bursts from recorded LFP during attention were detected and characterized in several ways. However, it would be interesting to apply the same method to a control dataset. Indeed, nothing guarantees right now that the detected bursts correspond to a meaningful property of the LFP. They might simply be random fluctuations that could be observed in any oscillatory signal.

This control dataset can be made by generating surrogate data. The principle is to identify a property of the signal that is assumed to influence the bursting phenomenon. Then surrogate signals are generated from the original ones with this property erased,

usually through randomization. If the burst detection algorithm provides a significantly different characterization when run on the artificial signals, this would support the hypothesis that the identified property influences the bursts. It would also mean that the real bursts are more than simple random fluctuations of the signal, as a randomized signal would not be characterized the same way as the real recordings.

### 3.4.3.2 Generation

The surrogate data were generated based on the hypothesis that bursts are linked to the phase of different frequency components. The idea is that the phases would be organized in a way that make the gamma bursts appear more often, or would make them longer, or maybe more intense etc.

The phase randomization algorithm can be used to generate surrogate data in which the phase organization of the original signal is erased. It keeps the same Fourier spectrum as the original data but the phases are given new values selected randomly and uniformly in the  $[-\pi, \pi]$  interval [103].

The algorithm is applied on the gamma filtered signal in order to generate a new signal from which an envelope can be computed. The idea behind the algorithm is similar to the principle of Hilbert transform. The original signal made of  $N$  data points is converted from time domain to frequency domain through FFT. This gives a sequence of  $N$  complex-valuated samples.

Because the analysis is about the gamma band, only the phases of coefficients corresponding to frequencies in the interval [30,40] Hz are randomized. The original magnitudes are kept.

As the signal is real valuated in the time domain, the transformed signal presents an Hermitian symmetry about the  $f = 0$  axis. This property shall be kept during all transformations in order to retrieve a real valuated signal after phase randomization. Therefore, only samples corresponding to positive frequencies will get a random phase assigned. Negative frequencies [-40,-30] Hz are defined by taking the complex conjugate of the [30,40] Hz coefficients.

The modified signal is made of the original FFT coefficients, except for the [-40,-30] and [30,40] Hz frequency range in which the phase was randomized. It can be inverted back into the time domain and will be real valued as the algorithm makes sure to conserve the Hermitian symmetry (figure 3.21).

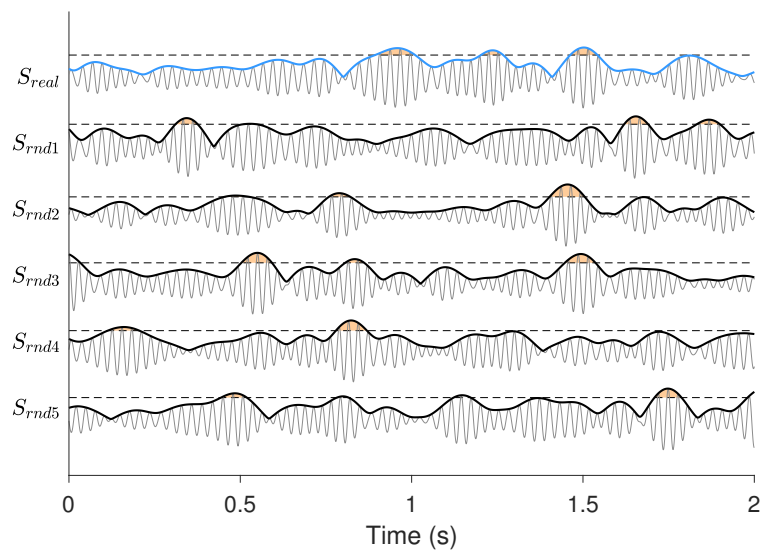


Figure 3.21: Example of phase randomization for two different signals. On the top in blue, the original signal  $S_{real}$ . Under it, five different phase-randomized signals:  $S_{rnd1}, \dots, S_{rnd5}$ .

# Chapter 4

## Results

### 4.1 Fixing parameters

#### 4.1.1 Principle

The first step of this project is to fix the parameters defined in the burst threshold formula 3.1:  $T = \mu + k * \sigma$  where  $\mu$  is the mean and  $\sigma$  the standard deviation. Choosing an optimal value requires to adapt the coefficient  $k$  to the data properties. The main factor to consider is the number of bursts detected. If too many bursts are identified, they might simply be periods of higher activity that can be observed in any oscillatory signal. If not enough bursts are found, then the model is probably too restrictive and might miss some events. In addition, it will be harder to conduct a statistically significant study with a small data set.

However, burst rate is not the only value to consider. The other characteristics can also be useful in order to decide the threshold value. Indeed, some variations can be expected when the threshold coefficient increases. Any unexpected variations might indicate that the model presents interesting properties in a specific range of coefficients.

In order to investigate this, the burst detection algorithm was applied with different threshold values ( $k \in [0, 2]$  with 0.0125 spacing, i.e. 160 different coefficients). The characterizations of bursts were then plotted function of the threshold coefficient: for each coefficient, one value was extracted per burst characterization. This is done by averaging the characterizations in each tetrode over the trials, and by then averaging across tetrodes. The rationale behind this is that each tetrode corresponds to a specific spatial location in the brain, and therefore provides one independent distribution of bursts. As the values are normally or almost normally distributed across tetrodes (see section 4.2), averaging over tetrodes gives a good and easy to read representation of the characterization.

#### 4.1.2 Characterization function of threshold coefficient

##### 4.1.2.1 Number of bursts

The burst rate follows the expected variations: when the coefficient increases, the threshold gets higher. Thus, less bursts are detected and the burst number function of the threshold coefficient is a decreasing function (see figure 4.1.A). There is no statistical evidence for linearity of this curve.

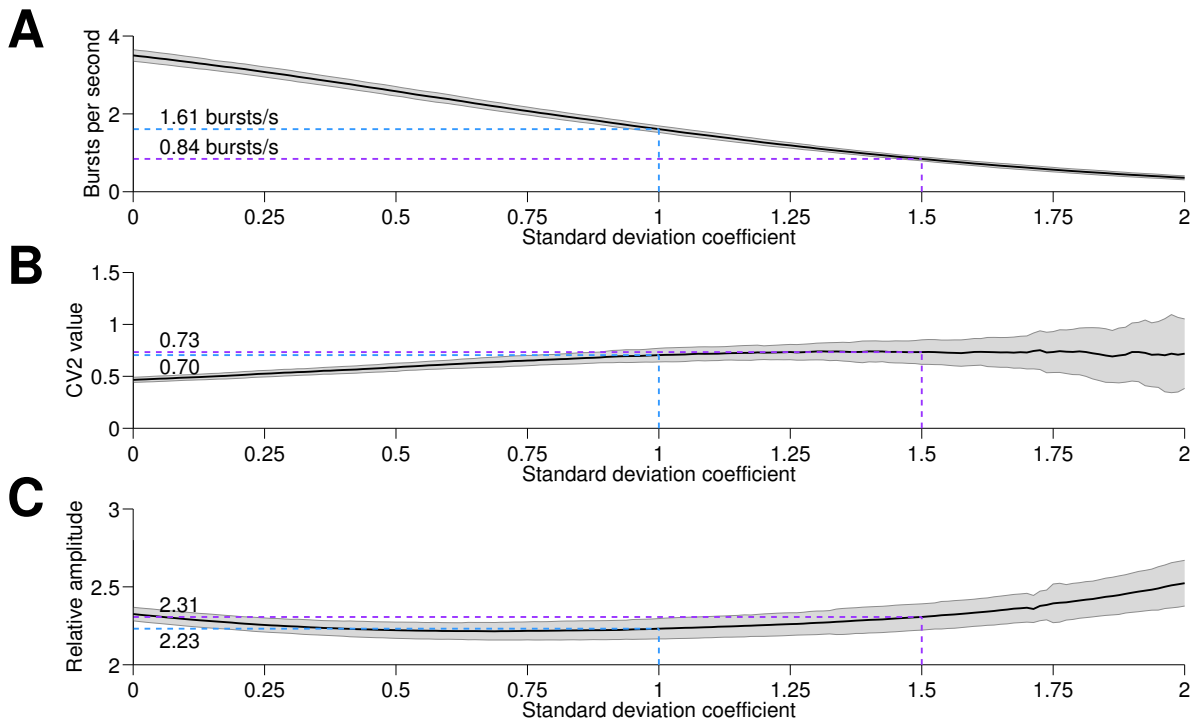


Figure 4.1: Burst characterizations relevant for deciding the threshold coefficient. Values are obtained by averaging first over trials then tetrodes. Error is standard deviation of the distribution across tetrodes.

**A. Occurrence rate**

**B.  $CV_2$**  With high coefficients, it becomes very uncommon to have 2 bursts in one signal. Therefore, few interburst intervals are computed and the  $CV_2$  value gets high deviation.

**C. Relative amplitude.**

Below a coefficient of 1, the number of bursts gets over 1.5 per second, which means an average of 3 bursts in a 2-second trial. This seems to be an acceptable lower boundary in order to avoid over-detection.

As regards the upper boundary, when the coefficient exceeds 1.5, the number of bursts drops under 0.8, which means on average less than 2 bursts in a 2-second trial. It becomes very selective and interburst intervals are hard to compute as they can only be estimated in trials with at least 2 bursts. Therefore, this will be the upper limit. This reduces the range of acceptable threshold coefficient to  $k \in [1, 1.5]$  interval.

#### 4.1.2.2 $CV_2$

The  $CV_2$  computed from interburst interval measures the variability of burst generation. When the value gets closer to 1, the generation of bursts is highly unpredictable. When the  $CV_2$  is close to 0, bursts are almost generated periodically. At first when the threshold coefficient increases,  $CV_2$  value also gets higher. When the coefficient exceeds 1.2,  $CV_2$  converges toward the constant value of 0.73 (figure 4.1.B).

The lower and increasing  $CV_2$  value at the beginning indicates that for lower thresh-

olds, burst occurrence is rather predictable. However, bursts become more and more randomly generated when the threshold increases. A hypothesis for this phenomenon is that with lower coefficients, any high activity triggers a burst. As periods of higher activity will naturally occur from randomness in the oscillatory signal, this would make the burst generation quite close to be periodic. When the threshold increases, periods of random high activity become less likely to be intense enough for triggering a burst. This would make the burst generation less predictable, resulting in an increase of  $CV_2$ .

The convergence toward a constant value at 0.73 might indicate that at some point bursts become fairly random ( $CV_2$  getting closer to 1), even though their generation is still quite far from following a perfect Poisson distribution ( $CV_2 = 1$ ). The convergence could indicate an intrinsic property of the model. In the previous paragraph, it was hypothesized that the algorithm would detect less random high activity when the threshold increases. In continuation of this assumption, the convergence could indicate that when the coefficient is higher than 1.2, only actual bursts are detected and therefore the real  $CV_2$  of bursting phenomenon is computed.

For these reasons, it seems relevant to fix the threshold coefficient in the range where  $CV_2$  is constant. Considering the previous restrictions, this means that  $k \in [1.2, 1.5]$ . Even if the previous interpretations are highly speculative, they seem worth to be formulated: if they correspond to the observed phenomenon, then they add a useful information for establishing a relevant model. If they happen to be false, they would only add a useless restriction on the coefficient range and therefore not strongly impact the study.

#### 4.1.2.3 Relative amplitude

The highest amplitude reached by the envelope during a burst was defined as the peak amplitude in section 3.3.2.2. It logically increases with the threshold coefficient: when the threshold is set at a higher value, only high amplitude bursts are detected. However, the variations of relative amplitude are more complex. As it can be seen in figure 4.1.C, it first decreases for coefficients smaller than 0.7. Only then, it starts increasing.

The mechanism behind these variations can be understood by analyzing the definition of relative amplitude: the mean amplitude during bursts divided by the mean amplitude outside bursts. When the threshold value increases, the signal samples that were barely above the previous threshold and therefore counted in the "inside bursts" part of the signal will be under the new threshold. They become classified in the "outside burst" signal, which has two consequences: the mean power inside bursts increases because the lowest values are discarded, and the mean power outside bursts also increases because new high values are added. The variations of the relative amplitude depends on which of these two mean values proportionally increases the most.

When the threshold coefficient exceeds 0.7, the relative amplitude starts increasing. This is an appreciable property of the model, as it reflects bursts becoming more and more intense compared with the baseline. Therefore, a new criterion forcing the threshold coefficient to be higher than 0.7 is added. However, this was already included in previous constraints and do not reduce the range of selection.

#### 4.1.2.4 Duration and interburst interval

Burst duration and interburst interval both presented the expected variations without providing relevant information for fixing the coefficient. There was no statistical evidence

for linearity. When the threshold increases, burst duration obviously decreases as more power is required to reach the threshold value. Furthermore, less bursts are detected, which increases the time between them. Interburst interval thus increases (see appendix figure C.1).

#### 4.1.2.5 Final value

The previous analysis showed that the most suitable range for the threshold coefficient is between 1.2 and 1.5. Several values were tested during investigations and provided very similar results. In the end, the value of 1.25 was used. When  $\mu$  is the mean value of the envelope and  $\sigma$  the standard deviation of the envelope over the trial duration, the final formula for setting the threshold  $T$  is therefore:

$$T = \mu + 1.25 * \sigma \quad (4.1)$$

## 4.2 Characterization

After doing the last adjustments on the threshold in the previous section, a detailed characterization of bursts can be run on the dataset (characteristics were defined in section 3.3.2.2). In each tetrode, the characteristics are computed for all trials. Then, they are averaged across trials in order to end up with one value per tetrode per characteristic. If there are very few values for a characteristic in a tetrode, then this tetrode is not used in order to avoid biasing the data. This limit was empirically put at a minimum of 10 values.

A tetrode can be discarded for one characteristic but not for another. For instance, the number of bursts per second (occurrence) can only be computed once per trial while there are as many duration values as bursts. Because one trial usually contains several bursts, the criterion of 10 values is more easily reached for duration than for occurrence.

### 4.2.1 Distribution across tetrodes

The distributions of characteristics across tetrodes were plotted (figure 4.2). They are either Gaussian either almost Gaussian. This was analyzed by running the Lilliefors test on the 5 distributions. It tests the null hypothesis that the distribution of a characteristics belongs to the normal family. Null hypothesis was rejected at the 5 % significance level for burst occurrence rate (p-val = 0.02) and burst relative amplitude (p-val = 0.001).

As only few tetrodes do not follow the normal distribution, an outlier detection algorithm was applied on each of the 5 distributions across tetrodes. The MAD method described in section 3.3.2.3 for discarding trials was adapted in order to detect unusual tetrodes. One outlier was detected in occurrence, duration and interburst distributions. Four outliers were detected in relative amplitude distribution. These seven outliers correspond to seven distinct tetrodes, i.e. the same tetrode is never classified as an outlier in two different characteristics.

### 4.2.2 Averaged values

The obtained results are averaged across tetrodes. If the characteristics are normally distributed, the average value combined with the error is a good and convenient repre-

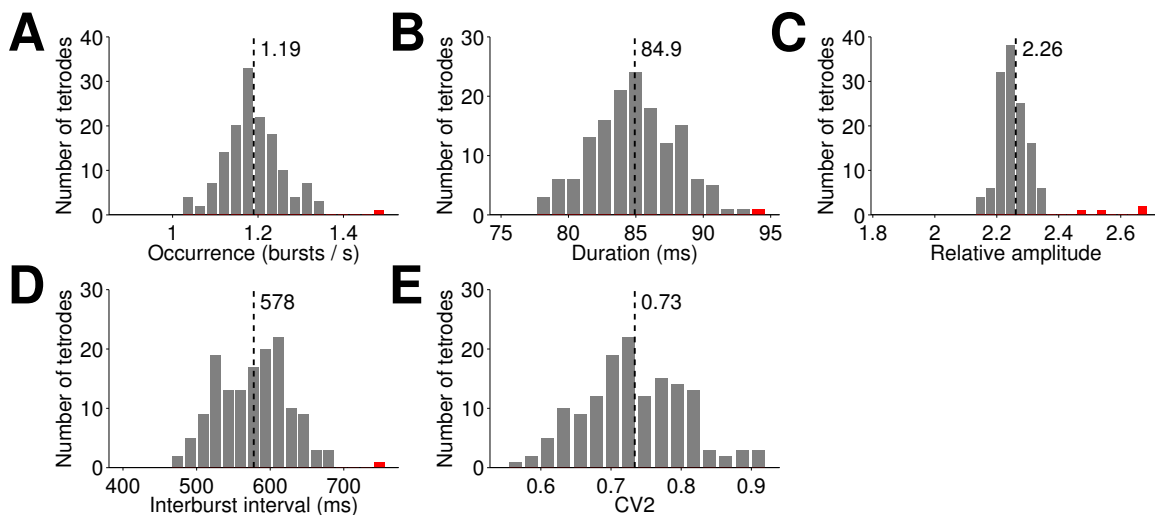


Figure 4.2: Distribution of several characteristics across tetrodes: occurrence rate (A), duration (B), relative amplitude (C), interburst interval (D) and  $CV_2$  (E). Dashed lines represent the mean value. Red bars are outliers detected in the distribution by using the MAD algorithm.

Number of tetrodes (of outliers): A-145(1)/B-148(1)/C-145(4)/D-146(1)/E-145(0)

sensation of the distribution. Therefore, tetrodes detected as outliers in the previous section were first discarded from the distribution in which they do not fit. This makes the distributions Gaussian (as expected, Lilliefors test is always negative). Only then values were averaged across tetrodes (figure 4.3).

Burst rate is  $1.19 \pm 0.005$  bursts/s. Therefore, most trials have between 2 to 3 bursts occurring. Bursts are quite shorts with an average duration of  $84.8 \pm 0.3$  ms while the minimum duration was set at 50 ms. Bursts are  $2.25 \pm 0.004$  times more intense than the rest of the signal and the average time between two bursts is  $576 \pm 4$  ms. The  $CV_2$  value at  $0.734 \pm 0.006$  indicates that the generation of bursts is fairly random, even though it does not follow a perfect Poisson distribution.

### 4.3 Comparison with surrogate dataset

A control dataset was generated using the phase-randomization method presented in section 3.4.3. For each real tetrode, 100 phase-randomized tetrodes were generated. Each of these random tetrodes contains the same number of trials as the original tetrode they are generated from. The difference is that every real signal is phase-randomized and replaced by its surrogate copy. Then, the burst detection algorithm is applied on the 100 randomized tetrodes. As usual, the characteristics are averaged across trials. Therefore, for each characteristic in each tetrode, 100 surrogate values are obtained. The last step is to average these 100 values across phase-randomized tetrodes in order to end up with one single surrogate value per characteristic per tetrode.

The real and surrogate distributions were compared for all characteristics (figure 4.4). Tetrodes identified as outliers in the previous section were discarded in both real and surrogate distributions. Surrogate characteristics are normally distributed (see appendix

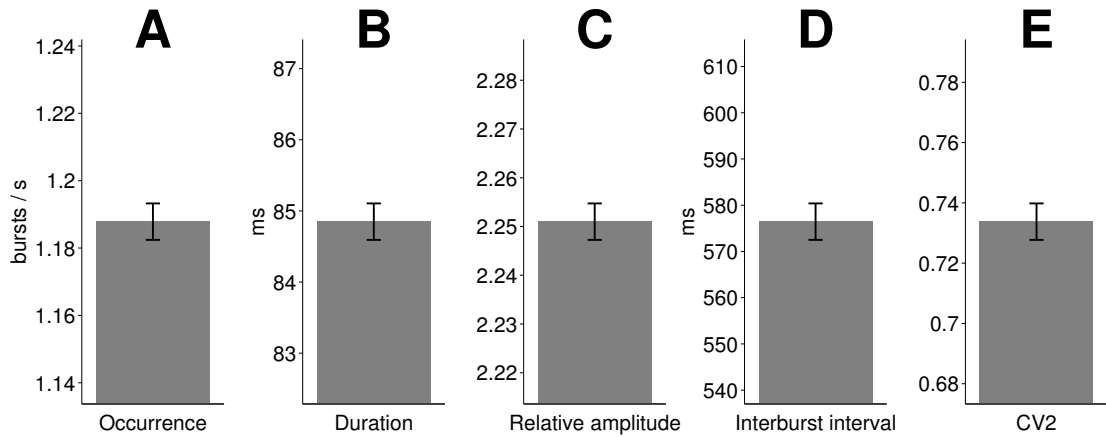


Figure 4.3: Burst characteristics averaged across tetrodes. Error in SEM. The number of tetrodes changes from one characteristic to another as tetrodes with low number of values for a characteristic are discarded as explained in section 4.2.

**A. Occurrence rate** 1.19 bursts/s  $\pm$  0.005 ( $N = 144$ )

**B. Duration** 84.8 ms  $\pm$  0.3 ( $N = 147$ )

**C. Relative amplitude** 2.25  $\pm$  0.004 ( $N = 141$ )

**D. Interburst interval** 576 ms  $\pm$  4 ( $N = 145$ )

**E. CV<sub>2</sub>** 0.734  $\pm$  0.006 ( $N = 145$ )

C.2). Variance of surrogate distributions is much smaller than the variance of real data. This is due to the final surrogate characteristics being the average of 100 intermediate values. Because of these unequal variances, two-sample  $t$ -test shall be used instead of paired  $t$ -test when testing mean equality.

No significant difference in burst occurrence can be detected between the two datasets. In the same way, the null hypothesis of equal mean cannot be rejected at the 5 % significance level neither for interburst interval nor CV<sub>2</sub> distributions.

Bursts are significantly shorter in the surrogate dataset ( $p$ -val from  $t$ -test  $< 0.01$ ) with an average duration of 84.8 ms in real signals while the mean duration is 84.2 ms in surrogate data. Even though significant, this is a very small difference. Identically, relative burst amplitude is slightly but significantly higher in real than surrogate data (2.25 vs 2.23,  $p$ -val  $< 1 \times 10^{-6}$ ). Because the effect size [104] of these variations is very small, no conclusion can be drawn from the observed differences between real and surrogate datasets.

Several factors could explain this absence of difference. As any model, the burst detection algorithm provides a limited estimation of a real phenomenon. This estimation could be insufficiently accurate to underline a difference. Another alternative is that burst generation is not related to phase values. Indeed, the surrogate dataset was generated through phase-randomization because it was assumed that phases matter for burst generation. If bursts are due to another property of the signal, randomizing the phase would not change the bursts characterization. Alternatively, there could also be no meaningful bursts occurring during attention in the PFC. If so, detected bursts would simply be in-tense activity due to random signal variations.

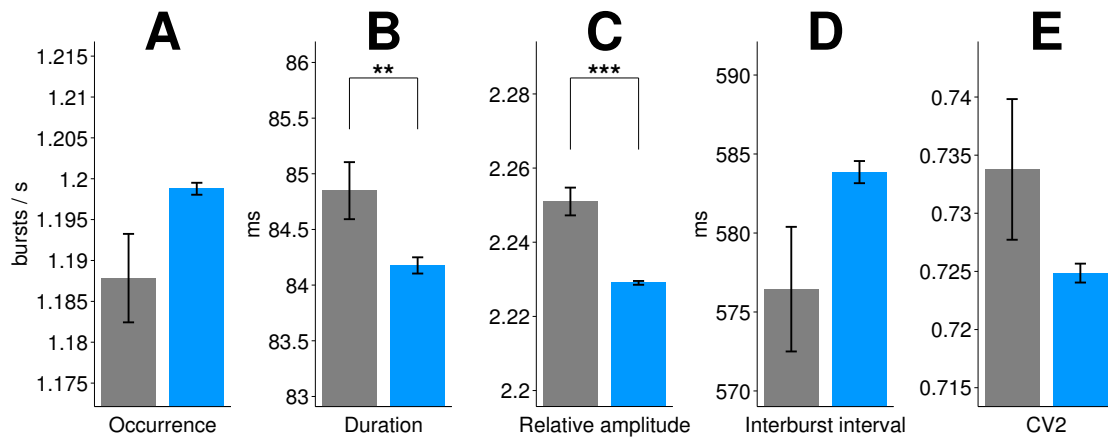


Figure 4.4: Averaged burst characteristics compared between real (grey, on the left) and surrogate (blue, on the right) datasets. Error is SEM. As data are normally distributed with different variances, two samples  $t$ -test, also known as Welch's  $t$ -test, is run for all characteristics. It tests the null hypothesis that real and surrogate data are normally distributed around the same mean value.

- A. Occurrence rate:** Real  $1.19 \text{ bursts/s} \pm 0.005$  - Surrogate  $1.20 \text{ bursts/s} \pm 0.001$ ;  $p = 0.13$   
**B. Duration:** Real  $84.8 \text{ ms} \pm 0.3$  - Surrogate  $84.2 \text{ ms} \pm 0.1$ ;  $p = 0.0068$  (\*\*)  
**C. Relative amplitude:** Real  $2.25 \pm 0.004$  - Surrogate  $2.23 \pm 0.001$ ;  $p = 4.3e - 7$  (\*\*\*)  
**D. Interburst interval:** Real  $576 \text{ ms} \pm 4$  - Surrogate  $584 \text{ ms} \pm 1$ ;  $p = 0.17$   
**E. CV<sub>2</sub>:** Real  $0.734 \pm 0.006$  - Surrogate  $0.725 \pm 0.001$ ;  $p = 0.16$

#### 4.4 Influence of outliers on the characterization

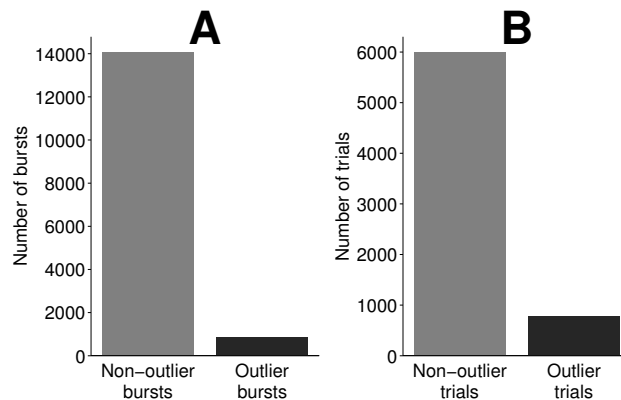


Figure 4.5: Proportion of outliers (black, right) and non-outliers (grey, left) in bursts (A) and trials (B). Trials are considered outliers if they contain at least one burst classified as an outlier.

- A. Bursts** 14,083 acceptable bursts, 850 classified as outliers (5.7 %)  
**B. Trials** 6,003 acceptable trials, 788 classified as outliers (11.6 %)

Both MAD and quantile methods described in 3.3.2.3 were tested and provided very similar results. The MAD method was chosen for further computations as it is theoretic-

cally more robust. It classified 5.7 % of bursts as outliers. Trials that contain at least one outlier are considered unusable and also classified as outlier trials. They correspond to 11.6 % of trials (see figure 4.5). Having twice as much outlier trials than bursts is due to most of outlier trials containing only one very intense burst: the 850 outliers bursts are contained in 788 trials. This corresponds to an average of 1.08 bursts per trial while non-outlier trials contain more than two bursts on average.

Discarding outliers from the distribution have the expected influence. As outliers usually contain only one very intense burst, characterizing the dataset with outliers leads to detect less (1.14 vs 1.19 burst/s) but longer (87 vs 85 ms) and more intense bursts (2.8 vs 2.2 relative amplitude). Detailed results are presented in figure 4.6.

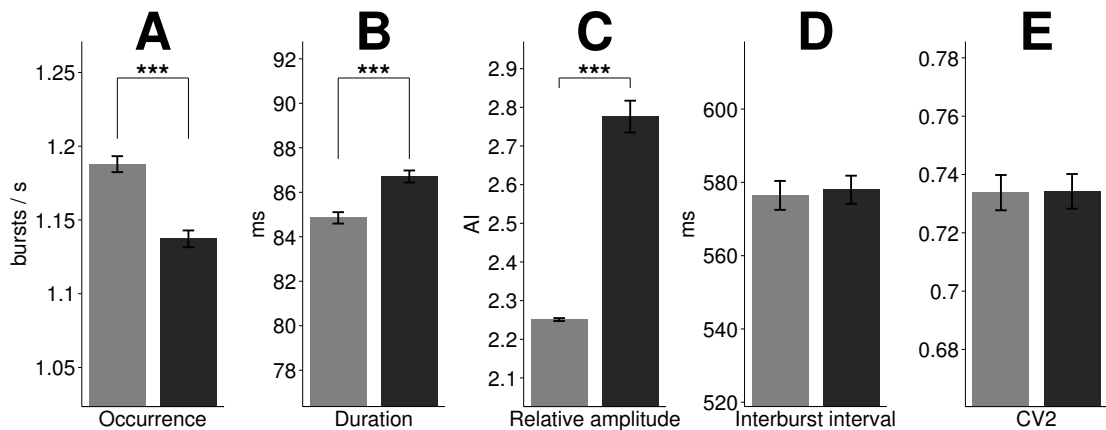


Figure 4.6: Averaged burst characteristics compared between real data after discarding outliers (grey, on the left) and real data with outliers included (black, on the right). Error is SEM. Paired-samples *t*-test is run for all characteristics with the null hypothesis that data with and without outliers are normally distributed around the same mean value. All distribution meet the assumption of normality, but the equality of variances does not hold for relative amplitude. In that case, the two-samples *t*-test was used instead.

**A. Occurrence rate:** No outliers 1.19 bursts/s  $\pm$  0.005/ - Raw 1.14 bursts/s  $\pm$  0.006;  $p = 1e - 43$  (\*\*\*)

**B. Duration:** No outliers 84.8 ms  $\pm$  0.3/ - Raw 86.7 ms  $\pm$  0.3;  $p = 3e - 39$  (\*\*\*)

**C. Relative amplitude:** No outliers 2.25  $\pm$  0.004/ - Raw 2.78  $\pm$  0.041;  $p = 3e - 29$  (\*\*\*)

**D. Interburst interval:** No outliers 576 ms  $\pm$  4/ - Raw 578 ms  $\pm$  4;  $p = 0.12$

**E. CV<sub>2</sub>:** No outliers 0.734  $\pm$  0.006/ - Raw 0.734  $\pm$  0.006;  $p = 0.79$

## 4.5 Comparison between trial types

To address the hypothesis of bursts being correlated with the allocation of attention, the characterization was computed again while regrouping trials by type: correct (C), incorrect (I) and omission (O). Instead of working with one distribution per characteristic, three distributions across the 148 tetrodes corresponding to the three trial types are now calculated. As usual, characterizations in tetrodes are obtained by averaging across trials.

For each characteristic, tetrodes previously identified as outliers (section 4.2.1) are first discarded from the three distributions. Then, tetrodes with less than 5 values for a characteristic are also discarded. This lower limit than in previous sections (limit was first set

at 10 values per tetrode in section 4.2) is due to a small number of incorrect and omission trials in many tetrodes. If the limit criterion was not adapted, only 14 tetrodes out of 148 (9 %) would be kept for the distribution of occurrence in incorrect trials. Using a slightly less restrictive criterion largely increases the number of tetrodes (77 instead of 14 tetrodes when limiting at 5 trials instead of 10).

Values are normally or at least almost normally distributed across tetrodes for every characteristics and trial types. Lilliefors test only rejects the null hypothesis of normality at the 5 % significance level for three distributions: incorrect ( $p = 0.02$ ) and omission ( $p = 0.04$ ) interburst intervals and incorrect durations ( $p = 0.04$ ). Based on these p-values being barely significant and bar plots, distributions can still be assumed to belong to the normal family.

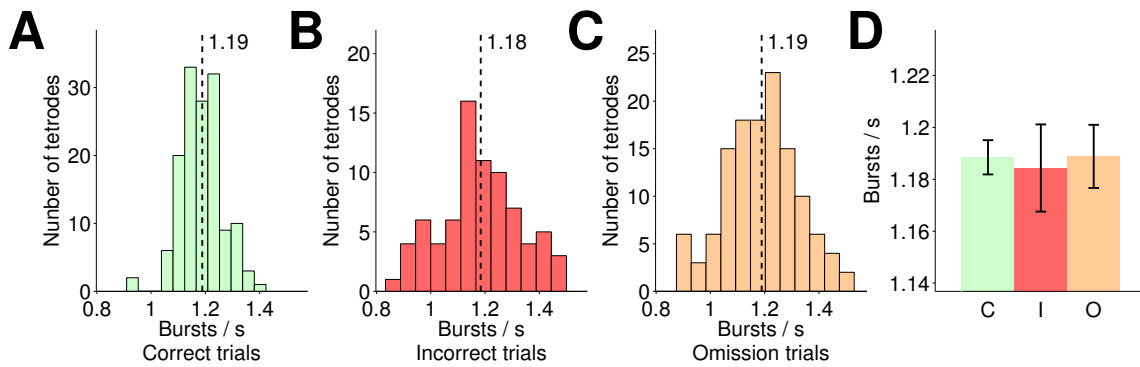


Figure 4.7: Burst occurrence rate comparison per trial type. Kruskal-Wallis p-val= 0.97

**A. Correct:** 1.19 bursts/s  $\pm$  0.007 (N = 144)

**B. Incorrect:** 1.18 bursts/s  $\pm$  0.017 (N = 77)

**C. Omission:** 1.19 bursts/s  $\pm$  0.012 (N = 126)

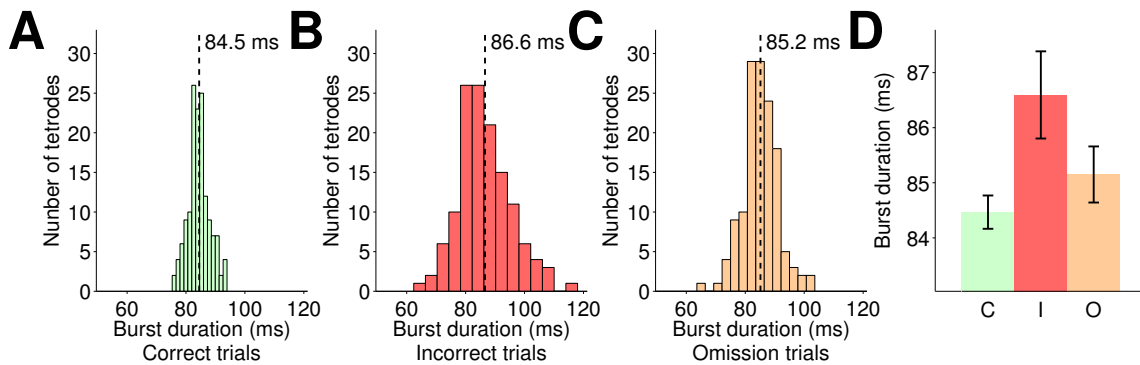


Figure 4.8: Burst duration comparison per trial type. Kruskal-Wallis p-val= 0.23

**A. Correct:** 84.5 ms  $\pm$  0.3 (N = 146)

**B. Incorrect:** 86.6 ms  $\pm$  0.8 (N = 132)

**C. Omission:** 85.2 ms  $\pm$  0.5 (N = 137)

Because correct trials are more frequent than incorrect and omission, variance in correct distributions is smaller. A non-parametric test is therefore more suitable for testing if samples originate from the same distribution than a classic one-way analysis of variance (ANOVA). The Kruskal-Wallis test was run for each characteristic in order to test if

correct, incorrect and omission trials come from the same distribution.

For burst occurrence (figure 4.7), burst duration (figure 4.8), interburst intervals (figure 4.10) and  $CV_2$  (figure 4.11), the null hypothesis of samples originating from the same distribution could not be rejected at the 5 % significance level. For burst amplitude (figure 4.9), the Kruskal-Wallis test returns a p-value of 0.008. Two-samples *t*-test can be run as post-hoc test as only three pairs of distributions should be tested, thus limiting the risk of type I error. The *t*-test is negative when testing equal means of incorrect and omission distributions ( $p = 0.78$ ) and correct with incorrect ( $p = 0.052$ ). The null hypothesis is rejected for correct and omission distribution with  $p = 0.008$ . However, even though this is a significance difference, the effect size is too small to draw any conclusion (2.24 relative amplitude in correct VS 2.21 in omission).

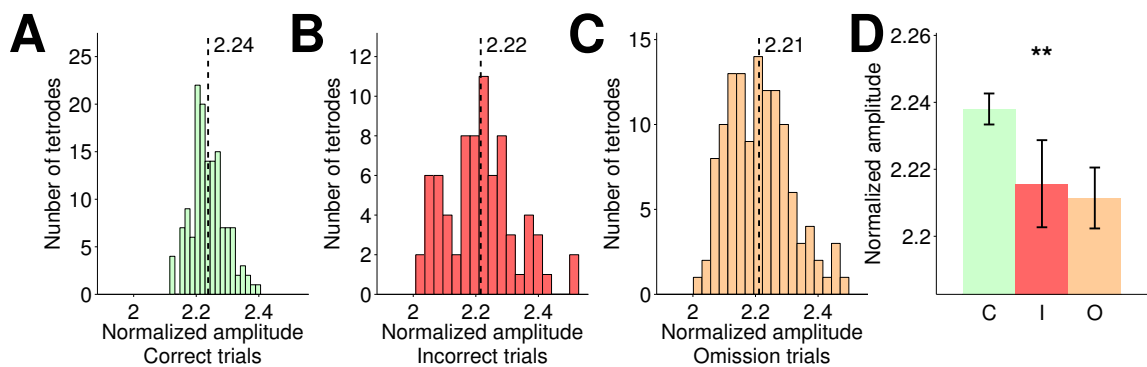


Figure 4.9: Burst amplitude comparison per trial type. Kruskal-Wallis  $p$ -val= 0.008 (\*\*)

**A. Correct:**  $2.24 \pm 0.005$  ( $N = 141$ )

**B. Incorrect:**  $2.22 \pm 0.013$  ( $N = 75$ )

**C. Omission:**  $2.21 \pm 0.009$  ( $N = 124$ )

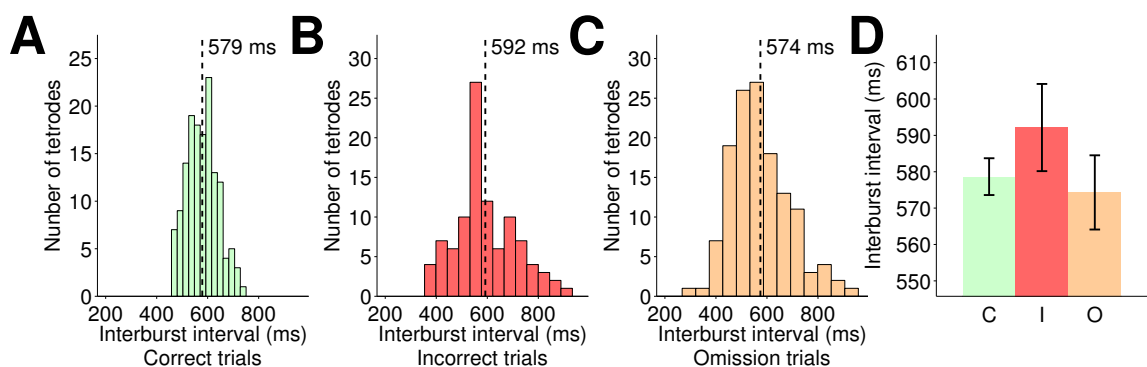


Figure 4.10: Interburst intervals comparison per trial type. Kruskal-Wallis  $p$ -val= 0.32

**A. Correct:**  $579 \text{ ms} \pm 5$  ( $N = 145$ )

**B. Incorrect:**  $592 \text{ ms} \pm 12$  ( $N = 99$ )

**C. Omission:**  $574 \text{ ms} \pm 10$  ( $N = 133$ )

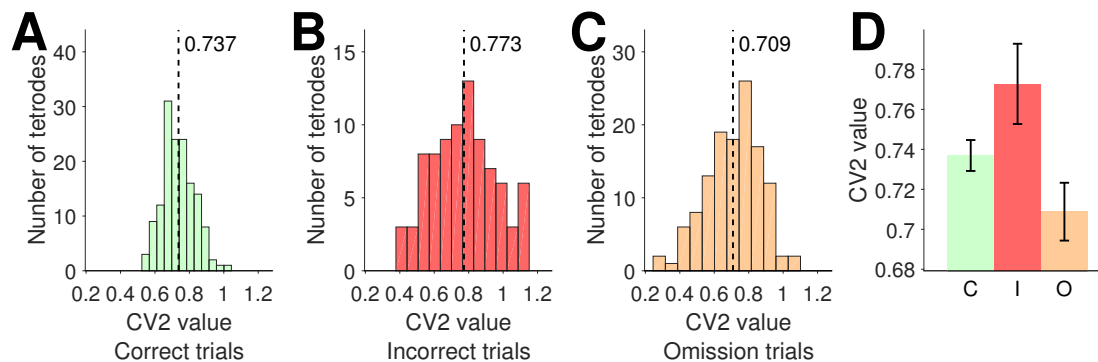


Figure 4.11:  $CV_2$  comparison per trial type. Kruskal-Wallis  $p$ -val= 0.076

**A. Correct:**  $0.737 \pm 0.008$  ( $N = 145$ )

**B. Incorrect:**  $0.773 \pm 0.020$  ( $N = 85$ )

**C. Omission:**  $0.709 \pm 0.014$  ( $N = 126$ )

## 4.6 Trial to trial burst patterns

A method was presented in section 3.4.1 in order to quantify the repeatability across trials of bursting patterns through a measure called overlapping. The idea is that if the number or duration of bursts does not depend on the trial type, maybe the temporal organization of these bursts is important. Two hypotheses were formulated. First, it is possible that bursts happen according to some temporal patterns that have a tendency to repeat themselves from one trial to another. Allocation of attention could correlate with the repeatability of these patterns. Typically, one might expect that failed allocation of attention could be due to an absence of pattern, which would result in a lower overlapping.

To investigate this, overlapping between trials of the same type was computed per tetraode. Trials with zero or one bursts were discarded because patterns are irrelevant in that case. Overlapping was averaged across trial pairs, in order to get one value per tetraode. Then distribution of overlapping across tetrodes were compared for correct, incorrect and omission trials (figure 4.12.A). The Kruskal-Wallis test was used as variance is higher in incorrect and omission distributions, due to less trials being available. No significant difference was underlined, invalidating the hypothesis that during correct trials bursts have a stronger tendency to follow specific patterns than in other trials.

The next tested hypothesis is that in each trial type, bursts would follow different patterns. The repeatability of patterns would be the same when comparing trials of the same type, as in all cases bursts would occur based on a pattern. However, overlapping should be lower when crossing types, i.e. for instance when comparing the patterns of a correct trial with an incorrect trial, as the patterns would be different.

In a first time, overlapping was computed by crossing trial types in the three possible manners: comparing correct with incorrect, comparing correct with omission and comparing incorrect with omission. As before, the overlapping value of trial pairs is averaged across tetrodes and distribution analyzed (figure 4.12.B). The Kruskal-Wallis test did not reject at the 5 % significance level the null hypothesis that the three overlapping groups come from the same distribution.

As no difference based on trial type was detected when computing overlapping in trials of same and crossed types, the study could be simplified by averaging across types in

order to look at only two distributions: the overlapping in trials of same type versus the overlapping in trials of crossed types. For each of these distributions, one value is available per tetrode, value are normally distributed (Lilliefors test  $p$ -val higher than 0.25 in both cases) and variance similar. Therefore, paired  $t$ -test can be used. It does not reject the hypothesis that both distribution have the same mean value. This invalidates the hypothesis that bursts are generated according to different patterns in different trial types.

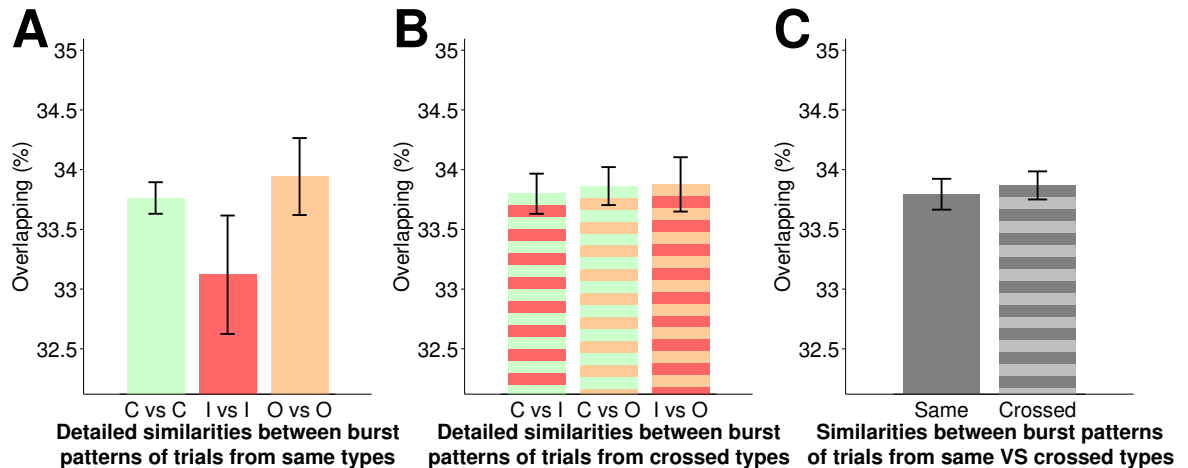


Figure 4.12: Repeatability of burst patterns.

**A. Burst pattern similarities of same type trials:** [Correct vs Correct]  $33.8\% \pm 0.1$  - [Incorrect vs Incorrect]  $33.1\% \pm 0.5$  - [Omission vs Omission]  $33.9\% \pm 0.3$  (KW  $p = 0.05$ )

**B. Burst pattern similarities of crossed type trials:** [Correct vs Incorrect]  $33.8\% \pm 0.2$  - [Correct vs Omission]  $33.9\% \pm 0.2$  - [Incorrect vs Omission]  $33.9\% \pm 0.2$  (KW  $p = 0.87$ )

**C. Burst patterns similarities of same VS crossed type trials:** [Same types]  $33.8\% \pm 0.1$  - [Crossed types]  $33.9\% \pm 0.1$  - ( $t$ -test  $p = 0.49$ )

These results can be explained in several ways. The first possibility is that gamma bursts have the same trial-to-trial repeatability of single channel patterns in all trial types. This would result into getting the same overlapping with all combinations. It is also possible that pattern exists and are different between trial types. However, the model for pattern detection is pretty basic and might actually be too simple in order to reliably detect patterns repeatability in our dataset. Another possibility is that no specific pattern actually underlie the burst generation. Further analysis could be conducted by generating a surrogate dataset in which bursts do not follow any pattern, for instance by randomizing the time at which a burst occurs. Then, the overlapping should be compared between surrogate and real data.

## 4.7 Spiking activity

The spiking activity of two well isolated neuron groups was analyzed. The first group is made of pyramidal cells and contains 329 different neurons that were identified in the whole dataset. The second group corresponds to FS-PV interneurons. They are less common, with only 30 single units detected. For each of these groups, two hypothesis were tested: is spiking activity increased during bursts? Is spiking activity different between trial types?

In order to address this question, the number of spikes was calculated inside bursts, outside bursts and during the whole attention period. As neurons are associated to one tetrode in which they were detected, firing rates of a neuron are calculated during all non-discarded trials of this tetrode, i.e. trials that are neither saturating nor outliers. If the neuron is inactive during a trial (less than 2 action potentials fired), then the trial is also discarded. The number of spikes inside and outside bursts is counted, then these values are divided by the time spent bursting and non-bursting to compute a firing rate.

However, simply counting the number of spikes occurring leads to a poor representation of instant firing activity. A more accurate estimation can be obtained by using a Gaussian kernel smoother. This transform the spiking train into a continuous process. As explained in methods, section 4.7, the estimate should be better with a narrower kernel for FS-PV (standard deviation (STD) of 30 ms), while lower firing rates observed in pyramidal cells lead to use a wider kernel (100 ms STD).

No difference could be observed in the neuronal activity inside and outside bursts with these two kernels, neither for pyramidal cells (figure 4.13.A) nor with FS-PV (figure 4.13.C). As firing rates of neuron are not normally distributed (see appendix C.3 A&B), a non-parametric test equivalent to the  $t$ -test was used for comparing the two distributions: the Mann–Whitney U test, also known as Mann–Whitney–Wilcoxon (MWW).

One could argue that smoothing the spike train by convolving it with a Gaussian kernel might bias the analysis. Indeed, smoothing spreads each spike across time instead of having it as binary process. The wider the kernel, the broader the spreading. This provides a value of firing rate at each time sample. However, when looking at a short and continuous period such as a burst, knowing this instant firing rate is unnecessary. Furthermore, a spike close to the extremities of a burst can partially be counted in the wrong category, i.e an inside spike will spread outside and vice versa. Alternative methods for estimating burst rates were therefore tested, including using a very narrow kernel (30 ms window with 6 ms standard deviation) and simply counting spikes without smoothing. All approaches were very consistent as presented in appendix C.3, which supports the result that spiking activity is the same inside and outside bursts.

Because there is no difference in firing rate inside and outside bursts, there is no need to differentiate bursting or non bursting state when comparing spiking activity for different trial types. Trial spiking rate is estimated by counting spikes occurring during the attention period, then dividing by the duration. Values are regrouped by trial types afterward and averaged. Once again, no significant difference could be observed in pyramidal cells (figure 4.13.B) and FS-PV (figure 4.13.D). Because firing rates are not normally distributed, the Kruskal-Wallis test was used for checking if the three groups correct-incorrect-omission come from the same distribution.

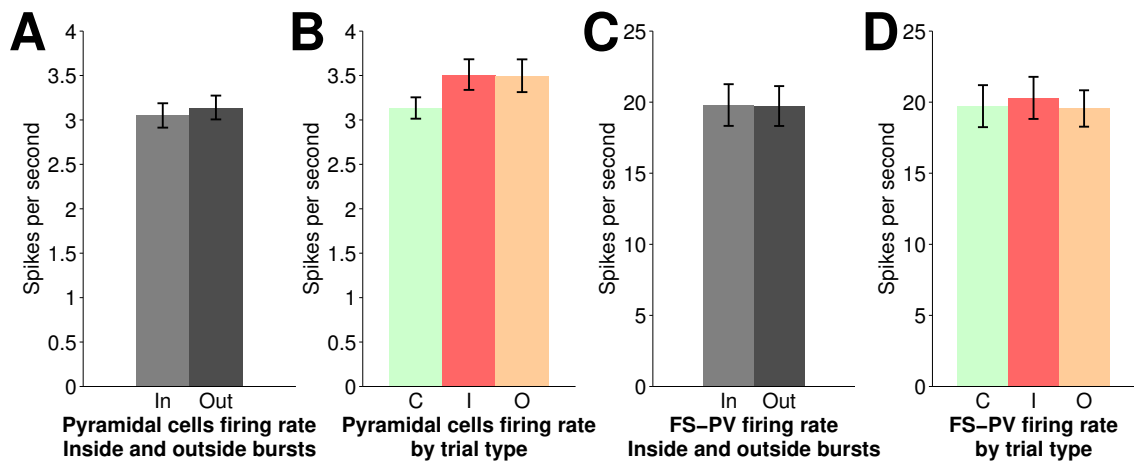


Figure 4.13: Spiking activity of pyramidal cells and FS-PV interneurons. Because mean firing rates across neurons do not follow a normal distribution, non-parametric statistical tests are used: equality of median is tested with the Mann–Whitney–Wilcoxon (MWW) test (equivalent to  $t$ -test) while the Kruskal–Wallis (KW) test is applied for the null hypothesis that samples originate from the same distribution.

**A. Pyramidal cells - inside VS outside bursts:** [IN] 3.05 spikes/s  $\pm$  0.14 - [OUT] 3.14 spikes/s  $\pm$  0.13 (MWW  $p = 0.53$ ,  $N = 320$  neurons)

**B. Pyramidal cells - trial types:** [C] 3.13 spikes/s  $\pm$  0.12 - [I] 3.51 spikes/s  $\pm$  0.17 - [O] 3.50 spikes/s  $\pm$  0.18 (KW  $p = 0.85$ ,  $N = 307/242/257$  neurons)

**C. FS-PV - inside VS outside bursts:** [IN] 19.79 spikes/s  $\pm$  1.47 - [OUT] 19.73 spikes/s  $\pm$  1.40 (MWW  $p = 0.88$ ,  $N = 30$  neurons)

**D. FS-PV - trial types:** [C] 19.72 spikes/s  $\pm$  1.48 - [I] 20.30 spikes/s  $\pm$  1.48 - [O] 19.55 spikes/s  $\pm$  1.28 (KW  $p = 0.89$ ,  $N = 30/30/30$  neurons)

# Chapter 5

## Discussion

### 5.1 Key findings

In this study, a suitable criterion for detecting gamma bursts during attention was fixed. It is adapted to our LFP recorded in the mouse medial prefrontal-cortex. From pre-analysis results, it was defined as a threshold on the envelope of gamma-filtered signal at 1.25 standard deviations upper than the mean trial envelope (section 4.1).

Using this criterion, burst were detected and characterized in terms of occurrence, duration, relative amplitude, interburst interval and  $CV_2$  value (section 4.2). Low-quality recordings and outliers trials were discarded, as it was shown that outliers can strongly bias the characterization (section 4.4).

A surrogate dataset was generated through phase-randomization of gamma signals and was then characterized. This dataset is designed to test the hypothesis that detected bursts correlate with a specific distribution of phases. However, no clear difference was detected between the characterization of the real and surrogate data. It means that either bursts are not related to the signal phases, or the burst detection algorithm is not accurate enough to underline a difference, or the signal does not actually contain gamma bursts but simply power fluctuations (section 4.3).

As burst were assumed to correlate with allocation of attention, the characterization was then split into three groups: correct, incorrect and omission trials. The rationale is that trial output would depend on the quality of attention allocation. No clear difference between the characterization of different trial types could be put in evidence. The hypothesis that bursts are a correlate of attention could not therefore be validated (section 4.5).

As no difference could be observed between trial types with a basic characterization, more advanced properties of burst were analyzed. In particular, the hypothesis that temporal organization of burst matters was formulated. To address it, the repeatability of potential burst patterns was estimated through the overlapping ratio. Trial-to-trial similarities of burst patterns were the same with all trial types, and therefore none of the results could confirm neither the presence of burst patterns nor their correlation with allocation of attention (section 4.6).

The last part of the study focuses on a potential underlying mechanism of bursts. The hypothesis is that an increased neural activity would cause the apparition of bursts. This was tested for two well isolated groups, the pyramidal cells and FS-PV interneurons. The spike rate was calculated inside and outside bursts but no difference could be de-

tected. This implies that if bursts are correlated with spiking activity of pyramidal cells or FS-PV, the process is more complex than a simple increased firing rate during bursts. The hypothesis that average neural activity would depend on the allocation of attention was tested by comparing mean firing rate in correct, incorrect and omission trials. Once again, no significant difference was detected (section 4.7).

## 5.2 Methodology

Based on the preliminary tests, it was decided to use the band-pass filtering method followed by Hilbert transform to represent the gamma power over time. However as explained in section 3.2.3, plenty of alternative methods are proposed in the literature such as spectrograms [26] and RMS [95]. These approaches keep the principle of a threshold in order to define bursts.

The threshold can be defined in many different ways. First, the choice of calculating mean and standard deviation during the current trial is debatable. In some cases it is preferred to use a broader window by computing the threshold based on the last ten trials in order to minimize a potential erasing of trial-to-trial differences [105]. In addition, the criterion does not have to be based on the mean and standard deviation. For instance, the distribution of power across time can be split into quantiles. It is then considered that a burst happens when the signal stays in the highest quantile continuously for more than a minimum duration [96]. Instead of adjusting the model selectivity through a coefficient, it can be done by extending the desired range, like to the 60<sup>th</sup> percentile instead of the last quantile [106].

In addition, in this thesis the problem was simplified by considering the power to be uniformly spread across the gamma band. With this assumption, the power becomes a function of only one parameter (time), which greatly simplifies further calculations. More advanced analysis involve a detection of gamma bursts as local maxima in the two-dimensional time-frequency plane [26]. With this method, it is possible to detect separately two bursts occurring at the same time but at different frequency ranges such as high and low gamma. This is especially useful when the gamma band is broad. On monkeys for instance, it can range up to 100 Hz. In our recording on mice, the band is very narrow (30-40 Hz), making it difficult and less important to distinguish burst frequency ranges.

Furthermore, using more advanced models can lead to estimate burst characteristics more accurately. For instance, a paper [105] proposes to recognize oscillatory bursts as epochs during individual trials when the power exceeds a threshold value in a specific frequency band. Another step is then added: a spectrogram is computed in the burst neighborhood and a two-dimensional Gaussian function is fitted to this map time-frequency map. Burst duration can be defined more accurately as the interval during which average instantaneous power is higher than half of the Gaussian local maximum.

Some researchers even work with more than the two dimensions time and frequency, for instance by considering the spatial location of recording sites. Gamma bursts can be detected as local maxima of a 4-D function (time, frequency, and position of recording sites in a plane) [23]. The rationale behind is that gamma bursts would be caused by a sustained activity of neurons at a specific location. If this activity is observed at two distant locations, then it can be considered as two distinct bursts. This would have been difficult to implement with our data as both the number of recording sites and the information about their spatial location were limited. This approach is more adapted for other

recording techniques such as silicon probes which can distinguish more than 30 different channels with accurate depth location [107].

If the definition of gamma bursts as a peak is quite intuitive, some more abstract methods involving complex mathematical models were also proposed. In Sirota et al. [23], gamma bursts were defined based on several criteria including the covariance of the spectral power between recording site (space variations) and frequency bins.

In addition, Burns et al. [108] tried to distinguish noisy bursts that might occur by chance from bursts related to the network properties, referred to as auto-coherent bursts. They are defined as persistent bursts of gamma activity with a phase bounded in a narrow band. They were detected by first computing spectrograms. Then, classic burst detection based on the deviation from the mean being greater than two standard deviations was applied for all frequencies. When a burst was detected, the time-dependent phase of the corresponding frequency was calculated in order to add a second criterion. If the burst phase wandered further than a limit angle of  $45^\circ$ , the burst was considered not to be auto-coherent.

### 5.3 Is it bursts that were detected?

As explained in the introduction and in the background chapters (chapter 1 and 2), many publications in the literature let think that bursts could be occurring during attention in the gamma band in the PFC. Indeed, the importance of gamma bursts was underlined for cognitive processes such as working memory [26], but also in a labyrinth orientation task [23] or simply in the visual cortex of awake animals [106].

However, none of the results obtained during this thesis really supports the idea that meaningful bursts were detected. The most important point is that no clear difference with the surrogate dataset was shown. In addition, none of the working hypothesis could be validated. The burst characterization was the same in correct, incorrect and omission trials, implying that the tested burst characteristics are not meaningful as regards quality of attention allocation. Finding an underlying mechanism of bursts such as neural correlates would have supported that they are more than simple network fluctuations. However, the assumption of increased spiking activity during bursts could not be validated neither. To sum up, the detected bursts are similar in real and control dataset, do not change according to attention level and no neural correlates were identified.

As the assumptions made from literature study are not supported by the obtained results, two main explanations can be proposed. The first one is that bursts are occurring, like previous works let think. Indeed, this hypothesis cannot be rejected only from the results of this study. For instance, the burst model might present too many limitations to highlight differences with control data or between trial types. Even if the model was perfectly reliable, the phase might not be correlated with bursts. This would make the phase-randomized signals an inappropriate control dataset and would explain the similar characterization in real and surrogate data. Furthermore, the absence of difference in burst characterization between trial types do not necessarily imply that there are no bursts; it means that the events detected as bursts are not modulated by the success or failure of the task for the tested characteristics. As regards the burst occurrence not being correlated with an increased spiking activity, not identifying the underlying mechanism does not presage of bursts presence.

However, the possibility that no meaningful gamma bursts happen during attention

in the PFC should also be considered. In that case, the activity detected as bursts would simply be the power fluctuations that can be expected in any oscillatory signal. The main clue in favor of this is that none of the approaches provided results supporting the presence of meaningful bursts in the signal. This obviously leads to questioning the existence of these bursts, especially as the exact nature of information processing during the 3-CSRTT and more generally in attention is largely unknown. It is not even sure if sustained attention is an active cognitive process. Therefore, hypothesizing that signal properties identified in other processes such as bursts would apply to attention is speculative and could be totally wrong. Even if bursts were actually happening during attention, the 3-CSRTT is only an experimental model believed to reproduce accurately the sustained attention process. Many aspects of the test such as the training, the task specificity and repetitiveness or the reward system could mix the cognitive process of attention with others. This might erase or hide from our recordings bursting activity related specifically to attention.

## 5.4 Limitations

This analysis presents several limitations. First of all, many different algorithms can be used for detecting bursts, but only one of them was fully applied. Several assumptions were made, which could lead to miss some properties. For instance, the power was considered to be time dependent instead of time-frequency dependent [26]. This could mix together bursts that are actually distinct because happening in different frequency ranges. Furthermore, the spatial location was not considered at all. Instead, tetrodes were assumed to provide independent recordings. This is a strong hypothesis, as the four tetrodes are placed close to each others and are recording simultaneously.

More complex methods were presented in the section 5.2. They can be used for estimating the burst characterization (2D Gaussian fitting in the time-frequency plane for instance) or even detecting bursts (covariance of spectral power [23]) and might have provided different results.

As regards the overlapping value defined for evaluating burst pattern repeatability, this method would require some validation. This could be done by creating or finding a dataset with known patterns and look at how representative of the repetitiveness is the overlapping.

While in the first analysis of these data published in Kim et al. [1] the firing rate was normalized, no normalization was applied during this thesis. The observation of increased spiking activity of the FS-PV interneurons in correct trials was not reproduced. This indicate that the approach during this work might not be advanced enough in order to highlight any interesting effect.

Apart from the analysis that was run, the task accomplished during recording sessions also presents many limitations. The 3-CSRTT and its variants are commonly used in cognitive neuroscience to assess attention. However, mice usually need more than 30 days of learning in order to execute the task properly. Each of these learning sessions lasts around one hour. This heavy training could make the attention process during the task differ from a more natural and spontaneous attention happening outside of an experiment. Furthermore, the experimental conditions are very restrictive. The cue is expected in time (the pseudo-random delay between trial start and cue onset never exceeds 5 seconds), in space (only three holes can get activated) and nature (a one second en-

lightenment). In addition, using moving animals can lead to many contamination in the signals, especially when mice happen to bump their head into the box walls. This could end into compromising some of the signal properties.

## 5.5 Ethics and sustainability

Even though I did not work directly with animals myself, the data used during the thesis came from animal experiments. It is therefore important to think about the ethical questions this raises. In my opinion, a major point to underline is that animal experiments are strictly regulated, both by Swedish and European legislations. As explained in section 3.1.1.2, the experiments conducted by the Carlén lab were done according to the Guidelines of the Stockholm municipal committee for animal experiments. The Karolinska Institutet imposes to all the staff to pass a specific course before handling animals, which in addition to practical handling also involves theory classes and especially insists on the 3R principle: replace animal experiments when possible, refine methods and procedures to reduce pain and discomfort, reduce the number of used animals to what is strictly necessary [109].

In neuroscience, animals are used because there is usually no satisfying alternative for experimenting. It is actually very constraining to use animals, not only because of regulations. Animals can get sick, they have limited life expectancy, they need training, they need to be fed and require expensive care. As scientist have to face all of these constraints, using animals is most of the time more a necessity than a preference. When doing cognitive neuroscience like in the Carlén Lab, no satisfying model exist at the time to replace living organisms. However, characterizing neural phenomena is a first step toward modeling them. When the models are accurate enough and well integrated with experiments, they have the potential to reduce the need for animal experimentation.

As animal experiments could not be avoided for collecting the data, and as it is very regulated and controlled, I believe that this whole study is ethically acceptable. Even though I consider that scientific curiosity is enough to justify animal experiment as long as it is realized in a painless and respectful manner, one could also raise the point that neuroscience discoveries will hopefully lay the groundwork for new medications and treatments. Much hope is pinned on the identification of the underlying mechanisms of brain-related diseases in order to develop target-specific drugs that would be more effective and cause less side effects. Therefore, animal sacrificed for neuroscience research do not only contribute to improving mankind knowledge, they could also more pragmatically help to heal patients in the future. Some people might consider this to be a more legit reason for justifying animal experiments than pure scientific curiosity, even though I believe this is a very poor idea to split science according to its supposed usefulness as nobody can anticipate the potential discoveries.

As regards the sustainability, this analysis is based on reusing data that were already published before for another purpose. This prevents from unnecessarily conducting a new set of recordings. It also spares the time and energy required to collect the data, raise and train new animals.

## Chapter 6

# Conclusion

In this study, several methods were tested to detect and characterize gamma bursts. Based on preliminary results, one of them was fully implemented and applied on the LFP recordings of mice during 3-CSRTT. It consists in applying the Hilbert transform on the band-pass filtered signal in order to extract the gamma power. A threshold is then set to detect bursts.

Even though the method detected events considered as bursts, this study did not manage to prove that they are more than simple signal fluctuations. Bursts could not be explained by a specific distribution of the gamma phase. The characteristics that were tested were not dependent on whether the mouse successfully responded to stimuli. In other words, correct and incorrect responses as well as omissions could not be predicted from LFP gamma bursting patterns prior to the mouse's response. The firing rate of pyramidal cells and FS-PV interneurons was not increased during bursts.

Further investigations could be conducted by implementing more advanced approaches. Bursts detection might for instance be more accurate when working in the time-frequency plane and by fitting a two-dimensional Gaussian on them, as performed in [26]. One could also look at spatial distribution of bursts with a higher number of recording channels. Some improvements could be done for the spiking activity analysis as the chosen approach did not reproduce the results of Kim et al. [1].

# Bibliography

- [1] Hoseok Kim, Sofie Åhrlund-Richter, Xinming Wang, Karl Deisseroth, and Marie Carlén. Prefrontal parvalbumin neurons in control of attention. *Cell*, 164(1):208–218, 2016.
- [2] DP Pelvig, Henning Pakkenberg, AK Stark, and Bente Pakkenberg. Neocortical glial cell numbers in human brains. *Neurobiology of aging*, 29(11):1754–1762, 2008.
- [3] David A Drachman. Do we have brain to spare? *Neurology*, 64(12):2004–2005, 2005.
- [4] Robert Desimone and John Duncan. Neural mechanisms of selective visual attention. *Annual review of neuroscience*, 18(1):193–222, 1995.
- [5] R Walter Heinrichs and Konstantine K Zakzanis. Neurocognitive deficit in schizophrenia: a quantitative review of the evidence. *Neuropsychology*, 12(3):426, 1998.
- [6] Earl K Miller and Timothy J Buschman. Cortical circuits for the control of attention. *Current opinion in neurobiology*, 23(2):216–222, 2013.
- [7] Tirin Moore and Katherine M Armstrong. Selective gating of visual signals by microstimulation of frontal cortex. *Nature*, 421(6921):370–373, 2003.
- [8] Oscar Marín. Interneuron dysfunction in psychiatric disorders. *Nature Reviews Neuroscience*, 13(2):107–120, 2012.
- [9] Roberto Cabeza and Lars Nyberg. Imaging cognition ii: An empirical review of 275 pet and fmri studies. *Journal of cognitive neuroscience*, 12(1):1–47, 2000.
- [10] George Bush, Phan Luu, and Michael I Posner. Cognitive and emotional influences in anterior cingulate cortex. *Trends in cognitive sciences*, 4(6):215–222, 2000.
- [11] George Bush, Eve M Valera, and Larry J Seidman. Functional neuroimaging of attention-deficit/hyperactivity disorder: a review and suggested future directions. *Biological psychiatry*, 57(11):1273–1284, 2005.
- [12] Earl K Miller and Jonathan D Cohen. An integrative theory of prefrontal cortex function. *Annual review of neuroscience*, 24(1):167–202, 2001.
- [13] Maurizio Corbetta and Gordon L Shulman. Control of goal-directed and stimulus-driven attention in the brain. *Nature reviews neuroscience*, 3(3):201–215, 2002.

- [14] Andreas K Engel, Pascal Fries, and Wolf Singer. Dynamic predictions: oscillations and synchrony in top-down processing. *Nature Reviews Neuroscience*, 2(10):704–716, 2001.
- [15] Thomas Gruber, Matthias M Müller, Andreas Keil, and Thomas Elbert. Selective visual-spatial attention alters induced gamma band responses in the human eeg. *Clinical neurophysiology*, 110(12):2074–2085, 1999.
- [16] Markus Bauer, Robert Oostenveld, Maarten Peeters, and Pascal Fries. Tactile spatial attention enhances gamma-band activity in somatosensory cortex and reduces low-frequency activity in parieto-occipital areas. *Journal of Neuroscience*, 26(2):490–501, 2006.
- [17] Juan R Vidal, Maximilien Chaumon, J Kevin O’Regan, and Catherine Tallon-Baudry. Visual grouping and the focusing of attention induce gamma-band oscillations at different frequencies in human magnetoencephalogram signals. *Journal of Cognitive Neuroscience*, 18(11):1850–1862, 2006.
- [18] Jochen Kaiser and Werner Lutzenberger. Human gamma-band activity: a window to cognitive processing. *Neuroreport*, 16(3):207–211, 2005.
- [19] Pascal Fries. Neuronal gamma-band synchronization as a fundamental process in cortical computation. *Annual review of neuroscience*, 32:209–224, 2009.
- [20] Ole Jensen, Jochen Kaiser, and Jean-Philippe Lachaux. Human gamma-frequency oscillations associated with attention and memory. *Trends in neurosciences*, 30(7):317–324, 2007.
- [21] Attila I Gulyás, Gergely G Szabó, István Ulbert, Noémi Holderith, Hannah Monyer, Ferenc Erdélyi, Gábor Szabó, Tamás F Freund, and Norbert Hájos. Parvalbumin-containing fast-spiking basket cells generate the field potential oscillations induced by cholinergic receptor activation in the hippocampus. *Journal of Neuroscience*, 30(45):15134–15145, 2010.
- [22] HJ Luhmann and DA Prince. Postnatal maturation of the gabaergic system in rat neocortex. *Journal of Neurophysiology*, 65(2):247–263, 1991.
- [23] Anton Sirota, Sean Montgomery, Shigeyoshi Fujisawa, Yoshikazu Isomura, Michael Zugaro, and György Buzsáki. Entrainment of neocortical neurons and gamma oscillations by the hippocampal theta rhythm. *Neuron*, 60(4):683–697, 2008.
- [24] RD Traub, MA Whittington, SB Colling, GXJJG Buzsaki, and JG Jefferys. Analysis of gamma rhythms in the rat hippocampus in vitro and in vivo. *The Journal of physiology*, 493(Pt 2):471, 1996.
- [25] Mikael Lundqvist, Pawel Herman, and Anders Lansner. Theta and gamma power increases and alpha/beta power decreases with memory load in an attractor network model. *Journal of cognitive neuroscience*, 23(10):3008–3020, 2011.
- [26] Mikael Lundqvist, Jonas Rose, Pawel Herman, Scott L Brincat, Timothy J Buschman, and Earl K Miller. Gamma and beta bursts underlie working memory. *Neuron*, 90(1):152–164, 2016.

- [27] Clayton E Curtis and Mark D'Esposito. Persistent activity in the prefrontal cortex during working memory. *Trends in cognitive sciences*, 7(9):415–423, 2003.
- [28] Joaquin M Fuster, Garrett E Alexander, et al. Neuron activity related to short-term memory. *Science*, 173(3997):652–654, 1971.
- [29] Shintaro Funahashi, Charles J Bruce, and Patricia S Goldman-Rakic. Mnemonic coding of visual space in the monkey's dorsolateral prefrontal cortex. *Journal of neurophysiology*, 61(2):331–349, 1989.
- [30] Tatiana Pasternak and Mark W Greenlee. Working memory in primate sensory systems. *Nature Reviews Neuroscience*, 6(2):97–107, 2005.
- [31] Yair Pinto, Andries R van der Leij, Ilja G Sligte, Victor AF Lamme, and H Steven Scholte. Bottom-up and top-down attention are independent. *Journal of Vision*, 13(3):16–16, 2013.
- [32] Martin Sarter, Ben Givens, and John P Bruno. The cognitive neuroscience of sustained attention: where top-down meets bottom-up. *Brain research reviews*, 35(2):146–160, 2001.
- [33] Russell A Barkley. Behavioral inhibition, sustained attention, and executive functions: constructing a unifying theory of adhd. *Psychological bulletin*, 121(1):65, 1997.
- [34] Richard J Perry and John R Hodges. Attention and executive deficits in alzheimer's disease: A critical review. *Brain*, 122(3):383–404, 1999.
- [35] RG Brown and CD Marsden. Internal versus external cues and the control of attention in parkinson's disease. *Brain*, 111(2):323–345, 1988.
- [36] Richard J McNally. Mechanisms of exposure therapy: how neuroscience can improve psychological treatments for anxiety disorders. *Clinical psychology review*, 27(6):750–759, 2007.
- [37] Cameron S Carter, Deanna M Barch, Robert W Buchanan, Ed Bullmore, John H Krystal, Jonathan Cohen, Mark Geyer, Michael Green, Keith H Nuechterlein, Trevor Robbins, et al. Identifying cognitive mechanisms targeted for treatment development in schizophrenia: an overview of the first meeting of the cognitive neuroscience treatment research to improve cognition in schizophrenia initiative. *Biological psychiatry*, 64(1):4–10, 2008.
- [38] Kerry J Ressler and Helen S Mayberg. Targeting abnormal neural circuits in mood and anxiety disorders: from the laboratory to the clinic. *Nature neuroscience*, 10(9):1116, 2007.
- [39] Antoine Bechara, Hanna Damasio, Antonio R Damasio, and Gregory P Lee. Different contributions of the human amygdala and ventromedial prefrontal cortex to decision-making. *Journal of Neuroscience*, 19(13):5473–5481, 1999.
- [40] Joaquin M Fuster. Prefrontal cortex. In *Comparative neuroscience and neurobiology*, pages 107–109. Springer, 1988.

- [41] Earl K Miller. The prefrontal cortex and cognitive control. *Nature reviews. Neuroscience*, 1(1):59, 2000.
- [42] Steven W Anderson, Antoine Bechara, Hanna Damasio, Daniel Tranel, and Antonio R Damasio. Impairment of social and moral behavior related to early damage in human prefrontal cortex. *Nature neuroscience*, 2(11):1032–1037, 1999.
- [43] Daniel Tranel, Antoine Bechara, and Natalie L Denburg. Asymmetric functional roles of right and left ventromedial prefrontal cortices in social conduct, decision-making, and emotional processing. *Cortex*, 38(4):589–612, 2002.
- [44] Michael E Hasselmo. A model of prefrontal cortical mechanisms for goal-directed behavior. *Journal of cognitive neuroscience*, 17(7):1115–1129, 2005.
- [45] Andrew F Rossi, Luiz Pessoa, Robert Desimone, and Leslie G Ungerleider. The prefrontal cortex and the executive control of attention. *Experimental Brain Research*, 192(3):489–497, 2009.
- [46] Michael J Kane and Randall W Engle. The role of prefrontal cortex in working-memory capacity, executive attention, and general fluid intelligence: An individual-differences perspective. *Psychonomic bulletin & review*, 9(4):637–671, 2002.
- [47] Philip J Bushnell. Behavioral approaches to the assessment of attention in animals. *Psychopharmacology*, 138(3):231–259, 1998.
- [48] Philip J Bushnell and Barbara J Strupp. Assessing attention in rodents. 2009.
- [49] Claire Wardak, Etienne Olivier, and Jean-René Duhamel. A deficit in covert attention after parietal cortex inactivation in the monkey. *Neuron*, 42(3):501–508, 2004.
- [50] Karl Deisseroth. Optogenetics. *Nature methods*, 8(1):26–29, 2011.
- [51] COBIE Brinkman. Supplementary motor area of the monkey’s cerebral cortex: short-and long-term deficits after unilateral ablation and the effects of subsequent callosal section. *Journal of Neuroscience*, 4(4):918–929, 1984.
- [52] Emilio Salinas and Terrence J Sejnowski. Correlated neuronal activity and the flow of neural information. *Nature reviews neuroscience*, 2(8):539–550, 2001.
- [53] Pascal Fries, John H Reynolds, Alan E Rorie, and Robert Desimone. Modulation of oscillatory neuronal synchronization by selective visual attention. *Science*, 291(5508):1560–1563, 2001.
- [54] Markus Siegel, Tobias H Donner, Robert Oostenveld, Pascal Fries, and Andreas K Engel. Neuronal synchronization along the dorsal visual pathway reflects the focus of spatial attention. *Neuron*, 60(4):709–719, 2008.
- [55] Conrado A Bosman, Jan-Mathijs Schoffelen, Nicolas Brunet, Robert Oostenveld, Andre M Bastos, Thilo Womelsdorf, Birthe Rubehn, Thomas Stieglitz, Peter De Weerd, and Pascal Fries. Attentional stimulus selection through selective synchronization between monkey visual areas. *Neuron*, 75(5):875–888, 2012.

- [56] Pascal Fries. A mechanism for cognitive dynamics: neuronal communication through neuronal coherence. *Trends in cognitive sciences*, 9(10):474–480, 2005.
- [57] Michael C Bushnell, Michael E Goldberg, and David L Robinson. Behavioral enhancement of visual responses in monkey cerebral cortex. i. modulation in posterior parietal cortex related to selective visual attention. *Journal of neurophysiology*, 46(4):755–772, 1981.
- [58] John H Reynolds, Tatiana Pasternak, and Robert Desimone. Attention increases sensitivity of v4 neurons. *Neuron*, 26(3):703–714, 2000.
- [59] Marisa Carrasco, Sam Ling, and Sarah Read. Attention alters appearance. *Nature neuroscience*, 7(3):308–313, 2004.
- [60] Marlene R Cohen and John HR Maunsell. Attention improves performance primarily by reducing interneuronal correlations. *Nature neuroscience*, 12(12):1594–1600, 2009.
- [61] Charles E Connor, Dean C Preddie, Jack L Gallant, and David C Van Essen. Spatial attention effects in macaque area v4. *Journal of Neuroscience*, 17(9):3201–3214, 1997.
- [62] Charles M Gray, Peter König, Andreas K Engel, Wolf Singer, et al. Oscillatory responses in cat visual cortex exhibit inter-columnar synchronization which reflects global stimulus properties. *Nature*, 338(6213):334–337, 1989.
- [63] Andreas K Kreiter and Wolf Singer. Stimulus-dependent synchronization of neuronal responses in the visual cortex of the awake macaque monkey. *Journal of neuroscience*, 16(7):2381–2396, 1996.
- [64] Catherine Tallon-Baudry and Olivier Bertrand. Oscillatory gamma activity in humans and its role in object representation. *Trends in cognitive sciences*, 3(4):151–162, 1999.
- [65] Catherine Tallon-Baudry, Olivier Bertrand, Franck Peronnet, and Jacques Pernier. Induced  $\gamma$ -band activity during the delay of a visual short-term memory task in humans. *Journal of Neuroscience*, 18(11):4244–4254, 1998.
- [66] Marc W Howard, Daniel S Rizzuto, Jeremy B Caplan, Joseph R Madsen, John Lisman, Richard Aschenbrenner-Scheibe, Andreas Schulze-Bonhage, and Michael J Kahana. Gamma oscillations correlate with working memory load in humans. *Cerebral cortex*, 13(12):1369–1374, 2003.
- [67] Catherine Tallon-Baudry, Olivier Bertrand, Claude Delpuech, and Jacques Pernier. Oscillatory  $\gamma$ -band (30–70 hz) activity induced by a visual search task in humans. *Journal of Neuroscience*, 17(2):722–734, 1997.
- [68] Georgia G Gregoriou, Andrew F Rossi, Leslie G Ungerleider, and Robert Desimone. Lesions of prefrontal cortex reduce attentional modulation of neuronal responses and synchrony in v4. *Nature neuroscience*, 17(7):1003–1011, 2014.
- [69] Maria V Sanchez-Vives and David A McCormick. Cellular and network mechanisms of rhythmic recurrent activity in neocortex. *Nature neuroscience*, 3(10):1027, 2000.

- [70] I Soltesz and M Deschenes. Low-and high-frequency membrane potential oscillations during theta activity in ca1 and ca3 pyramidal neurons of the rat hippocampus under ketamine-xylazine anesthesia. *Journal of neurophysiology*, 70(1):97–116, 1993.
- [71] György Buzsáki and Andreas Draguhn. Neuronal oscillations in cortical networks. *science*, 304(5679):1926–1929, 2004.
- [72] Patricia S Goldman-Rakic. Cellular basis of working memory. *Neuron*, 14(3):477–485, 1995.
- [73] Albert Compte, Nicolas Brunel, Patricia S Goldman-Rakic, and Xiao-Jing Wang. Synaptic mechanisms and network dynamics underlying spatial working memory in a cortical network model. *Cerebral Cortex*, 10(9):910–923, 2000.
- [74] Jason A Cromer, Jefferson E Roy, and Earl K Miller. Representation of multiple, independent categories in the primate prefrontal cortex. *Neuron*, 66(5):796–807, 2010.
- [75] Mark G Stokes, Makoto Kusunoki, Natasha Sigala, Hamed Nili, David Gaffan, and John Duncan. Dynamic coding for cognitive control in prefrontal cortex. *Neuron*, 78(2):364–375, 2013.
- [76] Gianluigi Mongillo, Omri Barak, and Misha Tsodyks. Synaptic theory of working memory. *Science*, 319(5869):1543–1546, 2008.
- [77] Rufin VanRullen, Leila Reddy, and Christof Koch. Attention-driven discrete sampling of motion perception. *Proceedings of the National Academy of Sciences of the United States of America*, 102(14):5291–5296, 2005.
- [78] Max Garagnani, Yury Y Shtyrov, and Friedemann Pulvermüller. Effects of attention on what is known and what is not: Meg evidence for functionally discrete memory circuits. *Frontiers in human neuroscience*, 3:10, 2009.
- [79] Niko A Busch and Rufin VanRullen. Spontaneous eeg oscillations reveal periodic sampling of visual attention. *Proceedings of the National Academy of Sciences*, 107(37):16048–16053, 2010.
- [80] Todd S Braver, Jonathan D Cohen, Leigh E Nystrom, John Jonides, Edward E Smith, and Douglas C Noll. A parametric study of prefrontal cortex involvement in human working memory. *Neuroimage*, 5(1):49–62, 1997.
- [81] Lief Fenno, Ofer Yizhar, and Karl Deisseroth. The development and application of optogenetics. *Annual review of neuroscience*, 34:389–412, 2011.
- [82] V Reinhardt, C Liss, and C Stevens. Restraint methods of laboratory non-human primates: A critical review. *Animal Welfare*, 4(3):221–238, 1995.
- [83] Nuffield Council on Bioethics. The ethics of research involving animals.
- [84] Adam Michael Stewart, Oliver Braubach, Jan Spitsbergen, Robert Gerlai, and Allan V Kalueff. Zebrafish models for translational neuroscience research: from tank to bedside. *Trends in neurosciences*, 37(5):264–278, 2014.

- [85] Rainer W Friedrich, Christel Genoud, and Adrian A Wanner. Analyzing the structure and function of neuronal circuits in zebrafish. *Frontiers in neural circuits*, 7, 2013.
- [86] André Valente, Kuo-Hua Huang, Ruben Portugues, and Florian Engert. Ontogeny of classical and operant learning behaviors in zebrafish. *Learning & Memory*, 19(4): 170–177, 2012.
- [87] Bart Ellenbroek and Jiun Youn. Rodent models in neuroscience research: is it a rat race? *Disease Models & Mechanisms*, 9(10):1079–1087, 2016.
- [88] T Robbins. The 5-choice serial reaction time task: behavioural pharmacology and functional neurochemistry. *Psychopharmacology*, 163(3):362–380, 2002.
- [89] Andrea Bari, Jeffrey W Dalley, and Trevor W Robbins. The application of the 5-choice serial reaction time task for the assessment of visual attentional processes and impulse control in rats. *Nature protocols*, 3(5):759–767, 2008.
- [90] C Lustig, R Kozak, M Sarter, JW Young, and TW Robbins. Cntrics final animal model task selection: control of attention. *Neuroscience & Biobehavioral Reviews*, 37(9):2099–2110, 2013.
- [91] Jakob Voigts, Joshua H Siegle, Dominique L Pritchett, and Christopher I Moore. The flexdrive: an ultra-light implant for optical control and highly parallel chronic recording of neuronal ensembles in freely moving mice. *Frontiers in systems neuroscience*, 7:8, 2013.
- [92] Robert Oostenveld, Pascal Fries, Eric Maris, and Jan-Mathijs Schoffelen. Fieldtrip: open source software for advanced analysis of meg, eeg, and invasive electrophysiological data. *Computational intelligence and neuroscience*, 2011:1, 2011.
- [93] Chronux official website. URL <http://chronux.org/>.
- [94] Partha Mitra. *Observed brain dynamics*. Oxford University Press, 2007.
- [95] Mario A Rosero and María L Aylwin. Sniffing shapes the dynamics of olfactory bulb gamma oscillations in awake behaving rats. *European Journal of Neuroscience*, 34(5):787–799, 2011.
- [96] Quentin Perrenoud, Cyriel MA Pennartz, and Luc J Gentet. Membrane potential dynamics of spontaneous and visually evoked gamma activity in v1 of awake mice. *PLoS biology*, 14(2):e1002383, 2016.
- [97] Songwon Seo. *A review and comparison of methods for detecting outliers in univariate data sets*. PhD thesis, University of Pittsburgh, 2006.
- [98] Christophe Leys, Christophe Ley, Olivier Klein, Philippe Bernard, and Laurent Licata. Detecting outliers: Do not use standard deviation around the mean, use absolute deviation around the median. *Journal of Experimental Social Psychology*, 49(4): 764–766, 2013.
- [99] Jeff Miller. Reaction time analysis with outlier exclusion: Bias varies with sample size. *The quarterly journal of experimental psychology*, 43(4):907–912, 1991.

- [100] Barry W Connors and Michael J Gutnick. Intrinsic firing patterns of diverse neocortical neurons. *Trends in neurosciences*, 13(3):99–104, 1990.
- [101] Zachary F Mainen, Terrence J Sejnowski, et al. Influence of dendritic structure on firing pattern in model neocortical neurons. *Nature*, 382(6589):363–366, 1996.
- [102] Tristan Cenier, Corine Amat, Philippe Litaudon, Samuel Garcia, Pierre Lafaye de Micheaux, Benoît Liquet, Stéphane Roux, and Nathalie Buonviso. Odor vapor pressure and quality modulate local field potential oscillatory patterns in the olfactory bulb of the anesthetized rat. *European Journal of Neuroscience*, 27(6):1432–1440, 2008.
- [103] James Theiler, Stephen Eubank, André Longtin, Bryan Galdrikian, and J Doyne Farmer. Testing for nonlinearity in time series: the method of surrogate data. *Physica D: Nonlinear Phenomena*, 58(1-4):77–94, 1992.
- [104] Gail M Sullivan and Richard Feinn. Using effect size—or why the p value is not enough. *Journal of graduate medical education*, 4(3):279–282, 2012.
- [105] Mikael Lundqvist, Pawel Herman, Melissa R Warden, Scott L Brincat, and Earl K Miller. Gamma and beta bursts during working memory read-out suggest roles in its volitional control. *bioRxiv*, page 122598, 2017.
- [106] Eelke Spaak, Mathilde Bonnefond, Alexander Maier, David A Leopold, and Ole Jensen. Layer-specific entrainment of gamma-band neural activity by the alpha rhythm in monkey visual cortex. *Current Biology*, 22(24):2313–2318, 2012.
- [107] Jozsef Csicsvari, Darrell A Henze, Brian Jamieson, Kenneth D Harris, Anton Sirota, Péter Barthó, Kensall D Wise, and György Buzsáki. Massively parallel recording of unit and local field potentials with silicon-based electrodes. *Journal of neurophysiology*, 90(2):1314–1323, 2003.
- [108] Samuel P Burns, Dajun Xing, and Robert M Shapley. Is gamma-band activity in the local field potential of v1 cortex a “clock” or filtered noise? *Journal of Neuroscience*, 31(26):9658–9664, 2011.
- [109] Karolinska Institutet. Animal research at karolinska institutet, 2017. URL <http://ki.se/en/research/animal-research-at-karolinska-institutet>.

# Appendix A

## Experimental setup

Level	Delay (s)	Cue (s)	Max response time (s)	Progression criteria
1	2	30	30	≥ 30 correct trials
2	2	20	20	
3	5	10	10	≥ 40 correct trials
4	5	5	5	≥ 50 correct trials ≥ 80% accuracy
5	{3,4,5}	2	5	≥ 50 correct trials ≥ 80% accuracy ≤ 20% omissions
6	{3,4,5}	1	5	
Recordings	{3,4,5}	1	5	

Figure A.1: Animal training program used in Kim et al. [1]. For all levels, the progression criteria had to be met for two consecutive days before progressing to the next level.



Figure A.2: Schematic representation of a mouse after surgery, with recording setup on the head. Source: Open Ephys.

## Appendix B

# Signal analysis

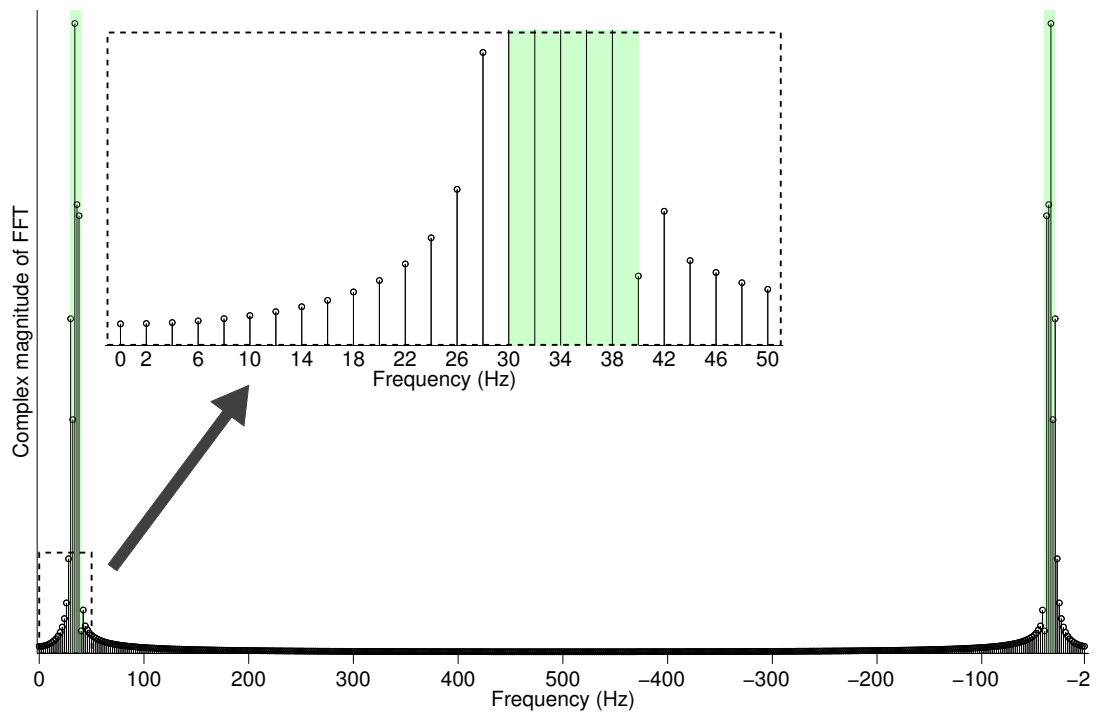


Figure B.1: Example of a spectrum obtained after FFT. Main figure represents the whole FFT. It is zoomed between 0 and 50 Hz in the dashed rectangle. Initial signal is 500 ms long, gamma-filtered and sampled at 1 kHz. Therefore, transformed signal is also made of 500 data points with a space of  $F_s/N = 1000/500 = 2$  Hz between them. Green rectangles are the 30 to 40 Hz gamma band, in both positives and negatives frequencies. As the FFT algorithm returns a sequence of complex values, the spectrum corresponds to the complex magnitude of these values. Because the initial sequence is made of real numbers, the Hermitian symmetry is respected. Most of the power can logically be found in the gamma band as the signal is filtered.

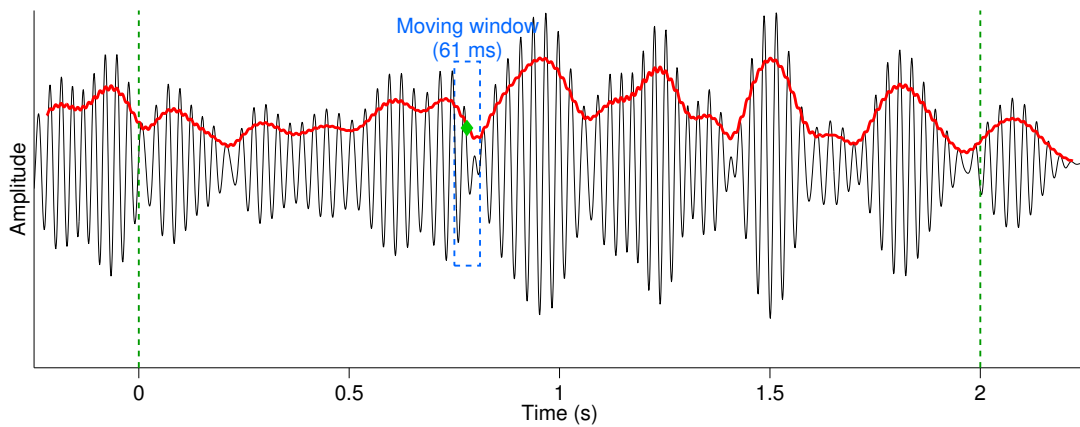


Figure B.2: Raw RMS signal, no smoothing. Moving window is 61 ms wide. Blue dashed rectangle is the moving window at time point 780 ms, ranging from 750 to 811 ms. Green diamond is the 780 ms data point at which RMS is computed. Green dashed vertical lines are limitations of attention period. RMS cannot be computed in the first and last 30 ms of the sequence because of the lack of data (moving window would go out of the sequence).

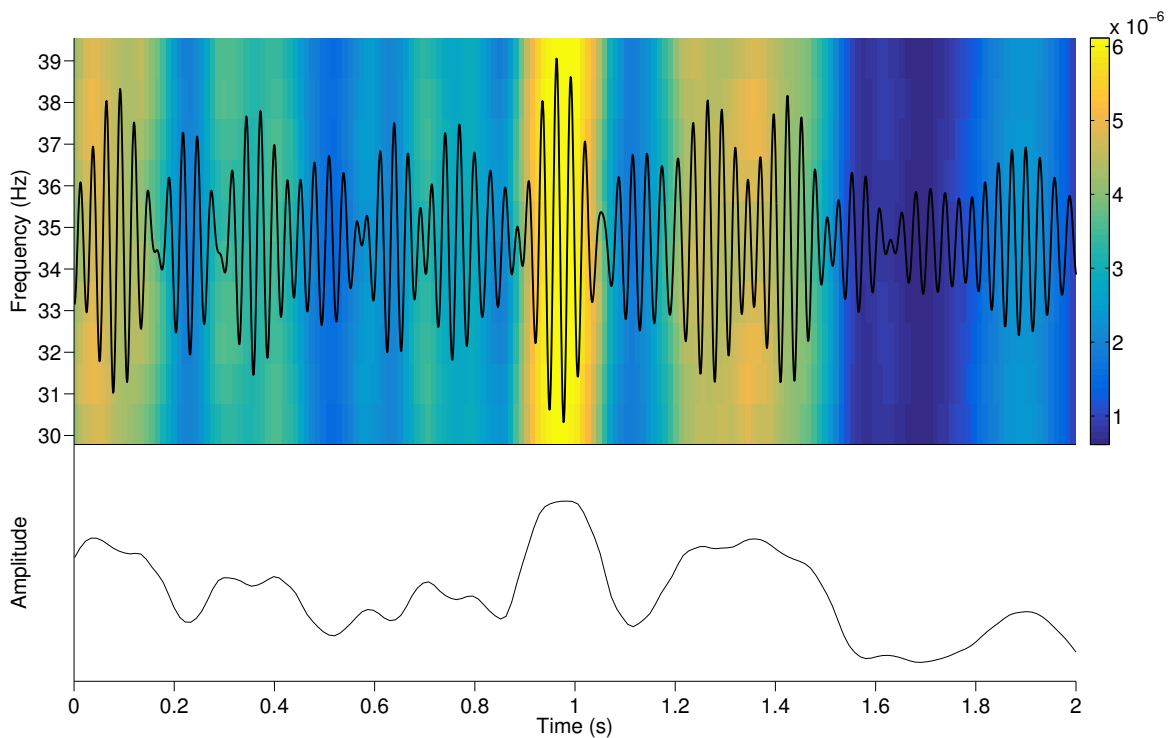


Figure B.3: Defining power trough spectrogram approach during attention period. Spectrogram activity is synchronized with gamma oscillations (black signal). On the bottom, the power is averaged over all frequency bins for every time bin. This reduces the spectrogram into a one parameter function: amplitude depending on time. Computed with multitapers approach (time-bandwidth product = 3, tapers = 5, padding = 2, time window = 175 ms, time bin = 11.66 ms).

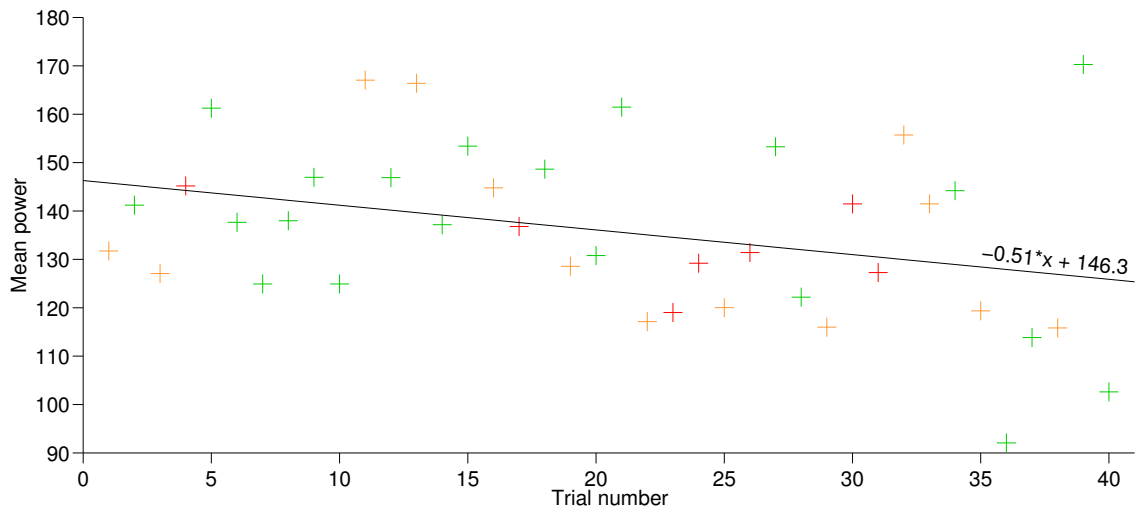


Figure B.4: Mean trial amplitude in one tetrode, ordered by trial occurrence. Green, orange and red cross respectively stand for correct, omission and incorrect trials. Linear regression shows an overall decreasing tendency:  $y = -0.51 * x + 146.3$ . Coefficient of correlation is -0.33.

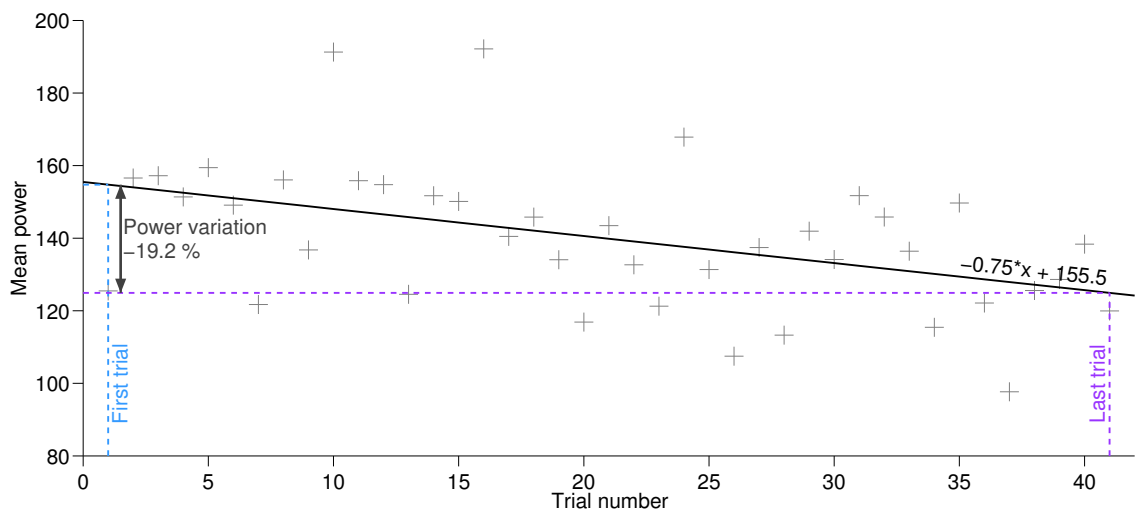


Figure B.5: Estimation of power loss for one tetrode based on linear regression. First, linear regression is computed. Then initial power is obtained by looking at the regression value for the first trial. Power at the end of recording session is obtained in the same way by looking at the last trial. Power variation is the difference of these two values normalized by initial power.

## Appendix C

### Supplementary results

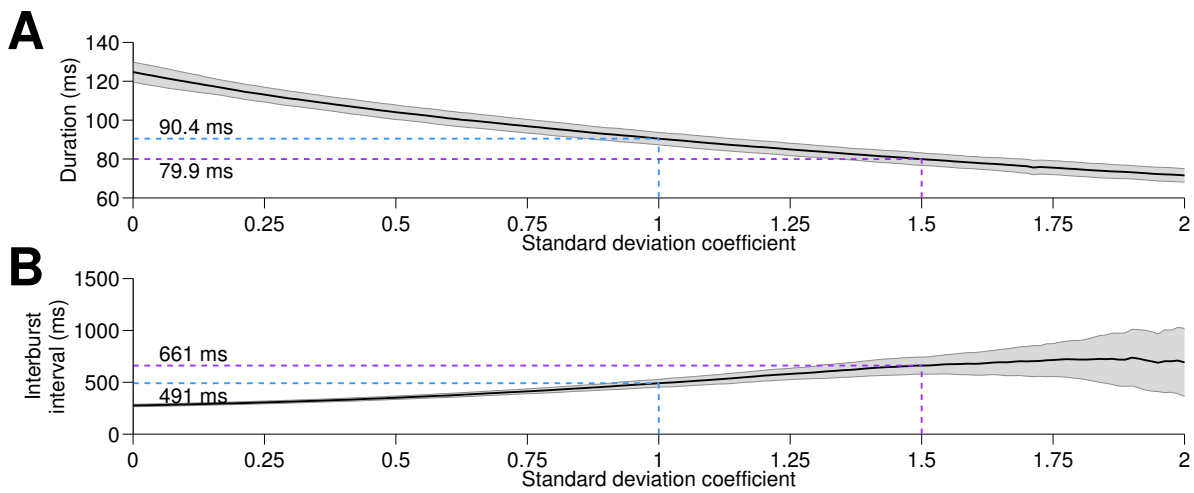


Figure C.1: Burst characteristics averaged over whole dataset. **(A.)** Duration, decreases when the coefficient increases, as the threshold gets higher and therefore the signals stays less time above it. **(B.)** Interburst intervals, becomes bigger with coefficient as less bursts are detected, and therefore the gap between them increases.

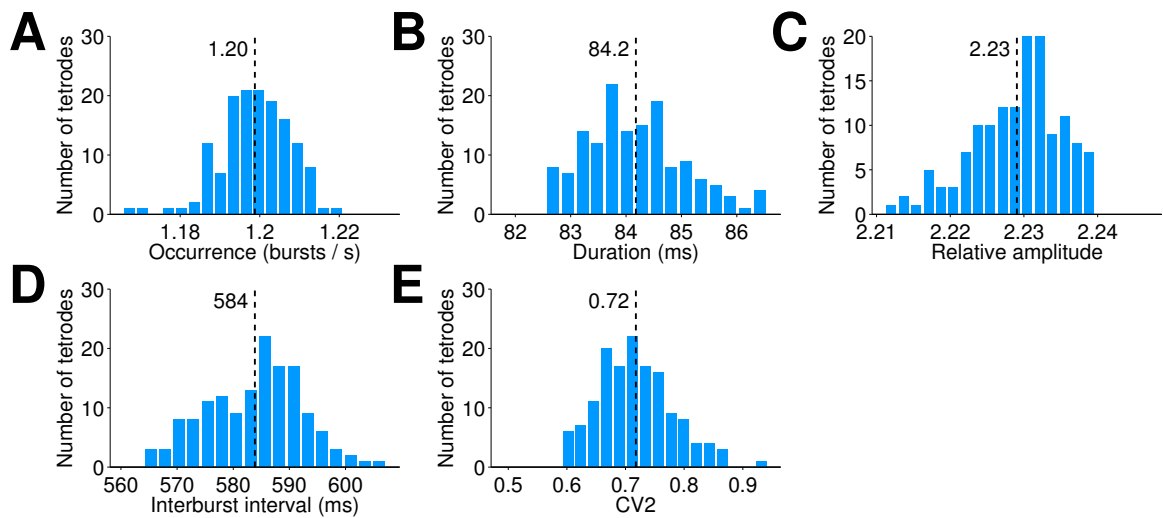


Figure C.2: Distribution of several characteristics across surrogate tetrodes. Dashed lines represent the mean value. Lilliefors test is run on the five distributions with the null hypothesis that the characteristics distribution belongs to the normal family. In none of the distribution can the null hypothesis be rejected at the 5 % significance level.

- A. Occurrence rate**  $p > 0.5$
- B. Duration**  $p = 0.24$
- C. Relative amplitude**  $p = 0.055$
- D. Interburst interval**  $p = 0.088$
- E. CV<sub>2</sub>**  $p > 0.5$

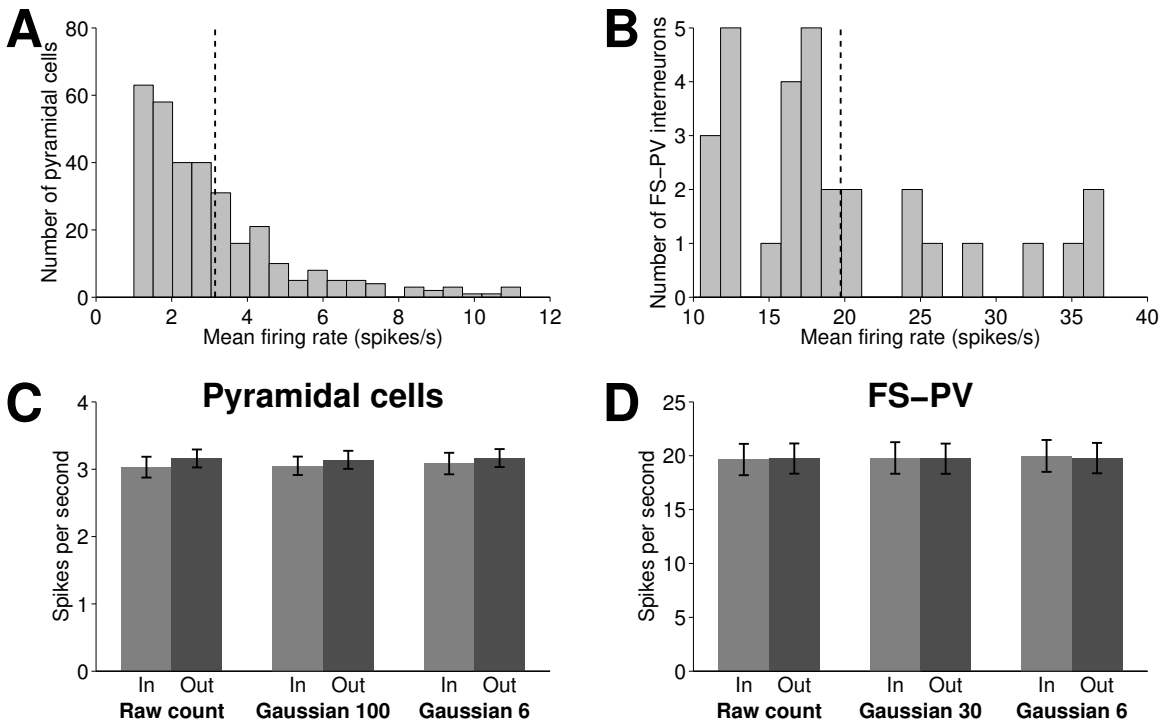


Figure C.3: Firing rates of pyramidal and FS-PV cells

**A. Pyramidal cells firing rate distribution:** Firing rate during whole attention period, inside and outside bursts. Null hypothesis of normality is rejected by the Lilliefors test,  $p < 1e - 3$

**B. FS-PV firing rate distribution:** Firing rate during whole attention period, inside and outside bursts. Null hypothesis of normality is rejected by the Lilliefors test,  $p = 6e - 3$

**C. Pyramidal cells - inside VS outside bursts:** Alternative methods are compared for estimating firing rate. Raw count: counting spikes without convolving, Gaussian 100: using a gaussian kernel with 100 ms of standard deviation, Gaussian 6: using of 30 ms gaussian window with 6 ms standard deviation.

**D. FS-PV - inside VS outside bursts:** Alternative methods are compared for estimating firing rate. Raw count: counting spikes without convolving, Gaussian 30: using a gaussian kernel with 30 ms of standard deviation, Gaussian 6: using of 30 ms gaussian window with 6 ms standard deviation.





